Doctoral (Ph.D.) Dissertation

Free Radical-Initiated Unfolding of Peptide Secondary Structure Elements

By: Michael Christopher Owen, M.Sc.

Supervisor: Béla Viskolcz

Chemistry Doctoral School
Department of Chemical Informatics

2012
Szeged, Hungary

TABLE OF CONTENTS.....1
ABSTRACT.....2
1.0 INTRODUCTION.....5
2.0 PURPOSE AND AIM.....10
3.0 METHODS.....13
3.1 Computing the Potential Energy Surfaces.....13
3.2 Computing the Unfolding of the Pentapeptides.....16
3.3 Parameterization of the Gly• and Ala• Force Fields.....18
3.4 Molecular Dynamics Simulations of the Ala Heptapeptide.....20
4.0 RESULTS.....23
4.1 General Features of the Amino Acid Potential Energy Surfaces.....23
4.2 Hydrogen Abstraction from Monopeptides.....27
4.2.1 The Potential Energy Surfaces.....27
4.2.2 Hydrogen Abstraction Reaction Coordinates.....29
4.3 Structural Analysis of the Pentapeptides.....41
4.3.1 Comparison of the G5 to the G5 Peptide Radicals.....42
4.3.2 Comparison of the A5 to the A5 Peptide Radicals.....48
4.4 Thermodynamic Analysis of the Pentapeptides.....54
4.4.1 Hydrogen Atom Abstraction from G5.....55
4.4.2 Unfolding of $G5_{HEL}$.....56
4.4.3 Reactions of G5 with the Reactive Oxygen Species.....57
4.4.4 Hydrogen Atom Abstraction from A5.....58
4.4.5 Unfolding of $A5_{HEL}$.....61
4.4.6 Reactions of A5 with the Reactive Oxygen Species.....62
4.5 Molecular Dynamics Simulations of Heptapeptides.....64
5.0 DISCUSSION.....67
5.1 Consequences of C_α Radical Formation on Monopeptide Confomers.....67
5.2 Hydrogen Abstraction from the Monopeptides.....68
5.3 Deviations from the G5 and A5 Structures.....74
5.4 Thermodynamic Analysis.....77
5.4.1 Hydrogen Abstraction Energy and Peptide Radical Stability.....77
5.4.2 Helical Unfolding.....78
5.4.3 Reactions of G5 and A5 with Reactive Oxygen Species.....79
5.4.4 Thermodynamic Cycles of Hydrogen Abstraction.....80
5.5 Comparing the Unfolding of G5 to A5.....84
5.5.1 Geometric Analysis.....84
5.5.2 Thermodynamic Analysis.....85
5.6 Comparing the MD Simulation to the Potential Energy Surfaces.....85
6.0 CONCLUSIONS.....88
7.0 REFERENCES.....91
8.0 ACKNOWLEDGEMENTS.....95
APPENDIX A – PUBLICATION LIST.....96

ABSTRACT

The present thesis investigates the effect of radical formation on peptide secondary structure elements, and analyses the changes such radical formations can induce.

To determine if the pro-L hydrogen on C_α of the glycyl residues are more prone to hydrogen abstraction by $^{\bullet}OH$ than the respective hydrogen in Ala, the pre-reaction van der Waals complexes, transition states, and post-reaction van der Waals complexes of H abstraction from Ala and Gly were computed. To evaluate the conformational effect of H abstraction, different conformers (β_L, γ_L, γ_D, α_L and α_D) of these residues were studied. These calculations were carried out at the MPWKCIS1K/6-311++G(3df,2p)//BHandHLYP/6-311+G(d,p) level of theory.

To study the effect of hydrogen abstraction on peptide secondary structures, model pentapetides were also studied. Helical unfolding (as shown in **Figure 1**) was investigated by computing the thermodynamic functions of the radical-initiated unfolding of a helix. A hydrogen atom was extracted from the C_α and amide nitrogen of Gly^3, and the C_α, C_β and amide nitrogen of Ala^3, of the respective G5 (*N*-Ac-GGGGG-NH_2) and A5 (*N*-Ac-AAAAA-NH_2) homo-peptides. The $HO^{\bullet}$, $HO_2^{\bullet}$ and $O_2^{-\bullet}$ radicals were used in each case, and the thermodynamic functions were computed using the B3LYP density functional. The changes in potential energy, standard enthalpy, Gibbs free energy and entropy during these reactions were computed with G5 and A5 in the 3_{10}-helical and fully-extended conformations. These computations were carried out in the gas phase and the effect of solvent was mimicked with the C-PCM implicit water model.

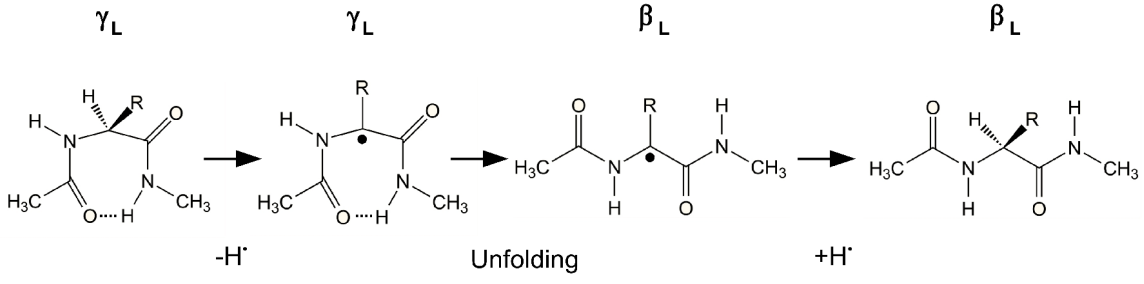

Figure 1. A schematic representation of the radical-initiated unfolding of an amino acid residue.

To enable the effects of C_α-centered radicals to be studied in longer peptides and proteins over greater time intervals with molecular dynamics (MD), force field parameters for the C_α-centered Ala radical were developed for use with the OPLS force field. This was done by minimizing the sum of squares deviation between the quantum chemical and OPLS-AA energy hypersurfaces. These parameters were used to determine the effect of the C_α-centered Ala radical on the structure of a hepta-alanyl peptide in molecular dynamics simulations.

A dramatic change in conformation is observed in the Gly and Ala conformers after converting to Gly$^\bullet$ and Ala$^\bullet$, respectively, and this change can be monitored along the minimal energy pathway by computing the intrinsic reaction coordinate for the conformers of each residue. The β_L conformer of Gly and Ala form the lowest-lying transition states, whereas the side-chain of Ala strongly destabilizes the α conformers compared to the γ conformers. The energies of the α to γ transition in Gly are more similar than those of Ala. This effect shown in Ala could inhibit the abstraction of hydrogen from the chiral amino acid residues in the helices. The energy of a subsequent hydrogen abstraction reactions between Ala$^\bullet$ and Gly$^\bullet$ and H_2O_2 remains approximately 90 kJ mol^{-1} below the entrance level of the $^\bullet$OH reaction, indicating that the $^\bullet$OH radical can initiate an α to β transition in an amino acid. However, a molecule such as H_2O_2 must provide the hydrogen atom necessary to reform the Gly and Ala residues.

As shown in the G5 and A5 peptides, hydrogen abstraction is the most favorable at the C_α, followed by the C_β, then amide nitrogen. The secondary structure has a strong influence on the bond dissociation energy of the H-C_α, but a negligible effect on the dissociation energy of the H-CH_2 and H-N bonds. The HO$^\bullet$ radical is the strongest hydrogen abstractor, followed by $HO_2^\bullet$ and finally $O_2^{-\bullet}$. Secondary structure elements, like H-bonds in the 3_{10}-helix, protect the peptide from radical attack by hindering the potential electron delocalization at the C_α which is present when the peptide is in the extended conformation. The C_α-centered pentapeptide radicals have a *significantly higher* propensity to unfold than the closed shell pentapeptides. Furthermore, only the HO$^\bullet$ radical can initiate the unfolding of the pentapeptides to an extended pentapeptide radical, and the unfolding of the C_α-centered G5 is

more favorable than the unfolding of the C_α-centered A5.

A negligible sum-of-squares energy deviation was observed in the stretching parameters, and the newly-developed OPLS-AA torsional parameters showed a good-agreement with the LMP2/cc-pVTZ(-f) hypersurface. The MD simulations showed planar conformations of the residue with the radical on its alpha carbon (Alr) are preferred and these conformations increase the formation of γ- α- and π-turn structures depending on the position in the turn occupied by the Alr residue. Higher-ordered structures are destabilized by Alr except when this residue occupies position "i + 1" of the 3_{10}-helix.

These results offer new insight in to the protein-misfolding mechanisms initiated by H-abstraction from the C_α of peptide and protein residues.

1.0 INTRODUCTION

1.1 General Implication of Oxidative Stress

O_2 is the terminal electron acceptor in the oxidation of carbon fuels to generate ATP by oxidative phosphorylation. However, the physiological role of O_2 is not limited to energy metabolism. The metabolism of sterols, indoles, alkaloids, antibiotics and some detoxifying pathways are also O_2-dependent.[1] The metabolic analysis of 70 genomes suggested that O_2 is directly or indirectly associated with over a thousand metabolic reactions not associated with anaerobes.[2] In aerobic organisms, the synthesis of mono-unsaturated fatty acids, tyrosine and nicotinic acid are O_2-dependent.[3]

A general consequence of O_2-dependent biosynthesis and aerobic respiration is the production of reactive oxygen species (ROS). When the amount of ROS in the body reaches an elevated state, significant structural modification can be observed in biological macromolecules. This state is known as 'oxidative stress', and result in loss of function and degradation. Oxidative stress is a common feature in the mechanisms that cause carcinogenesis, tumor promotion, Parkinson's disease, Alzheimer's disease and is also implicated in the ageing process.[4-9]

The superoxide radical anion ($O_2^{-\bullet}$), the perhydroxyl radical ($HO_2^{\bullet}$) and the hydroxyl radical ($^{\bullet}OH$) comprise the biologically relevant oxygen radicals.[10] Hydrogen peroxide (H_2O_2) is another biologically active oxygen species. Superoxide is formed when the ground-state O_2 molecule accepts a single electron into one of its π^* anti-bonding orbitals and is formed in almost all aerobic cells.[11] The addition of the subsequent electron forms the

peroxide ion (O_2^{2-}) which has no unpaired electron and is not a radical, and readily accepts two protons to form H_2O_2. Homolytic cleavage of the O-O bond in H_2O_2 produces two hydroxyl radicals. It has been shown that $^{\bullet}OH$ can be produced by heat, ionization radiation or in several reactions with Fe^{2+}.[12] The hydroxyl radical reacts at an extremely high rate with carbohydrates, amino acids, phospholipids, DNA bases and organic acids.[12] $HO_2^{\bullet}$ is produced in reactions between $H^{\bullet}$ and O_2, however $HO_2^{\bullet}$ has a pK_a of 4.8, therefore the biological significance of this radical may be limited.[11]

Reactive oxygen species can oxidize lipids or DNA, and form glycation end-products. However, proteins form by far the largest mass of oxidizable organic components of living matter.[13-16] Free radicals have been shown to induce the formation of bi-tyrosine induced protein aggregates, increase the rate of protein fragmentation and increase the susceptibility of proteins to degradation.[10,17] The formation of protein carbonyls has become the marker used to identify proteins that have been damaged by oxidative stress.[18,19] All amino acids are susceptible to modification by both $^{\bullet}OH$ and $^{\bullet}OH + O_2^{-\bullet}$, however tryptophan, tyrosine, histidine and cysteine showed greater sensitivity and the rate of oxidation depended on the concentration of the ROS. Moreover, it was suggested that $^{\bullet}OH$ is the primary radical responsible for all amino acid modifications and that O_2^- and O_2 can further transform the products of $^{\bullet}OH$ reactions.[18,20-22] A decrease in protein solubility, used as a measure of protein unfolding, was also shown in the presence of $^{\bullet}OH$ in a dose-dependent manner, which was also exacerbated in the presence of O_2 and O_2^-.[23]

1.2. Basic Structural Properties of Peptides

Ab initio and DFT methods, once limited to small molecules, are becoming practical for use on peptides and peptide analogues. The use of *N*-Ac- and -NHMe protection groups for the N and C termini, respectively, allows an amino acid residue to be studied in a local environment comparable to that of a peptide.[23] This method can be used to accurately calculate the relative energies of two or more systems, allowing the relative stabilities of different secondary structures to be determined.

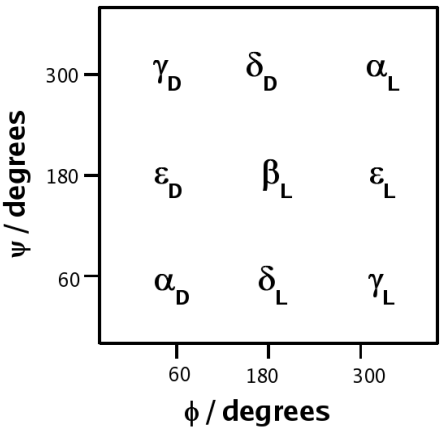

Figure 2. The symbols used to describe the conformations of an amino acid residue and their corresponding ϕ and ψ angles.

The conformation of an amino acid residue can be described by its ϕ and ψ angles. The relationship between ϕ and ψ angles and conformation are described in **Figure 2**. The Greek letters originate from an older nomenclature, involving α, β, γ, and ε for an α-helix, β-sheet, γ-turn, and ε for the polyproline II conformations, respectively, while the L and D subscripts indicate the conformations favored by the L and D configurations of amino acids.[25] This scheme will be used to describe the conformations of the peptide structures in this work.

In the search of a subset of the protein data bank, it was observed that the 3_{10}-helix occurs less frequently than the α-helix in regions that are greater than 5 residues, but is more

prevalent in regions containing 5 residues or less.[26,27] Also, 3_{10}-helices are considered to be sequential type III β-turns, therefore the occurrence of these structures can be underestimated.[28,29] These short 3_{10}-helices can be crucial motifs which mediate the conformational transitions of proteins.[30-32] It has been observed that 3_{10}-helices are an intermediate structure in the conversion of α-helices to β-sheets in amyloid fibrils, and this has been shown to be initiated by free radicals.[33] The aim of this study is to understand how free radicals initiate the unfolding of the 3_{10}-helix to an extended conformation.

1.3 Parameterization of the Gly˙ and Ala˙ Force Fields

The OPLS-AA force field is a Class I force-field according to the generally accepted force-field classification criteria and is widely accepted for simulations of structures of peptides and proteins in solution.[34-36] The energy of a molecule at a particular geometry can be described with the OPLS-AA/L force field using **Equation 1**. The energy of the same

$$E_i^{MM} = \sum_{bonds} K_r (r - r_0)^2 + \sum_{angles} K_\Theta (\Theta - \Theta_0)^2 + \sum_{torsions} \left(\frac{V_1^k}{2}[1+\cos(\phi_i)] + \frac{V_2^k}{2}[1-\cos(2\phi_i)] + \frac{V_3^k}{2}[1+cos(3\phi_i)]\right) + \sum_{k<l} \left(\frac{q_k q_l e^2}{r_{kl}} + 4\epsilon_{kl}\left(\frac{\sigma_{kl}^{12}}{r_{kl}^{12}} - \frac{\sigma_{kl}^{6}}{r_{kl}^{6}}\right)\right) \quad (1)$$

molecule at the same geometry can be computed using quantum mechanics and yield the E_i^{QM} energy described in **Equation 2**, where $\hat{H}$ is the molecular Hamiltonian and $\boldsymbol{\Psi}$ is the wave function:

$$\hat{H}_i \Psi = E_i^{QM} \Psi \quad (2)$$

The quantum mechanical energy can be used to develop molecular mechanical parameters by fitting the mechanical hyper-surface to the values obtained using quantum mechanics, as initially described by Lifson and Warshel.[37] In this method, the molecular mechanics parameter-dependent sum of squares distances between the selected points on these two hyper-surfaces are minimized. In this work, the experimental values were replaced with the computed energy values as a function of the geometrical parameters.

2.0 PURPOSE AND AIM

The presence of the methyl side chain of the alanyl (Ala, A) residue could be the reason for the difference in the kinetics of hydrogen abstraction reactions between ˙OH and the respective glycyl (Gly, G) and Ala residues. To see if this is the case, the influence of the methyl side chain of Ala on the stability of the Gly-˙OH and Ala-˙OH pre-reaction complexes, transition states, and post-reaction complexes will be determined. This will reveal the extent to which steric hindrance inhibits hydrogen abstraction and also determines which conformations enable or inhibit the progress of the reaction. Moreover, the structural perturbations induced by hydrogen abstraction from two model pentapeptides will be investigated. The B3LYP density functional will be used to compare the geometries of *N*-Ac-AAAAA-NH_2 and *N*-Ac-GGGGG-NH_2 peptides with radicals centered at the C_α, C_β and amide nitrogen atoms of the third Ala residue (Ala^3), and the C_α and amide nitrogen of the third Gly residue (Gly^3) to that of the respective third residue of the closed-shell peptides.

Density functionals have been shown to lead to accurate predictions for the energetics of H-atom abstraction reactions and have also been shown to compute geometries that are in good agreement with experimentally determined values.[38,39] The penta-alanyl helix was chosen because Ala is the smallest amino acid residue that is able to stabilize the conformations preferred by L-amino acids, and its small size causes a small entropy loss during helix formation.[40] On the basis of X-ray crystallographic data, the frequency at which Gly is found at the 3rd position of the type-III β-turns is among the highest of all the amino acid residues.[41] Since Gly is the only achiral amino acid residue used for protein synthesis, it

is important to investigate the unfolding properties of this residue.

Quantum chemical calculations have been shown to elucidate mechanisms of free radical-initiated oxidation of amino acids and peptide analogues.[24,42-47] One of many peptide radical structures and reaction intermediates, the C_α-centered radical is of particular interest because it is common to all of the amino acid residues and is stabilized by the capto-dative effect.[48-50] In quantum chemical studies of pentapeptides, it has been determined that peptides with C_α-centered radicals have a higher propensity to unfold to the β conformation.[51,52] The number of atoms in the pentapeptide is near the upper limit for quantum chemical studies, and this technique is best-applied near potential energy critical points, using time-independent techniques. In order to determine the effect of C_α-centered radicals on the structure of large and dynamic systems, force-field parameters for C_α-centered Gly and Ala radicals will be developed. The use of these systems will enable it to be

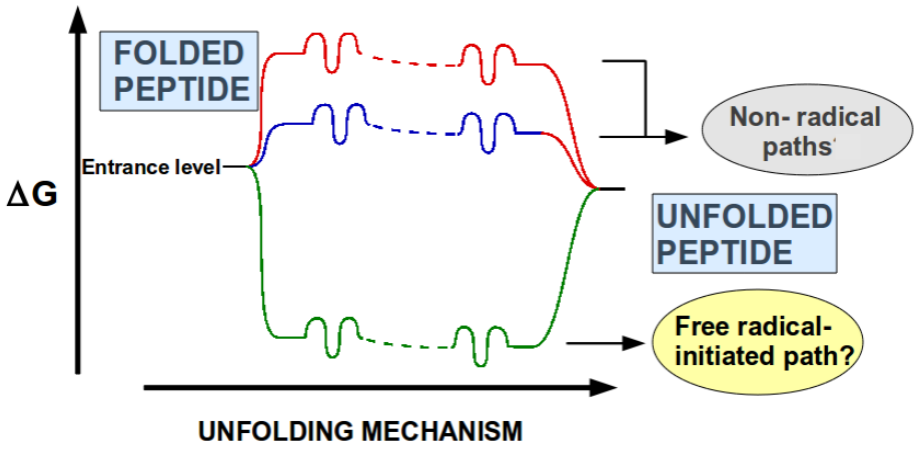

Figure 3. The central question of this work: does radical initiated unfolding of peptides occur through a lower energy path than unfolding without free radical initiation?

determined whether a free radical can initiate the unfolding of a peptide. This scheme is

illustrated in **Figure 3**. The changes to the structure of these peptides will be determined using the methods described in the subsequent section.

3.0 METHODS

3.1 Computing the Potential Energy Surfaces

3.1.1 Determining the General Features of the Potential Energy Surfaces

The Jaguar 5.5® software package was used to determine the general features of the potential energy surfaces. The *N*-Ac-Gly-NHMe and *N*-Ac-Gly•-NHMe molecules were constructed using a previously described Z-matrix method.[25] To generate a PES, ϕ and ψ angles were independently constrained at 30° intervals starting at ϕ and $\psi = 0°$, and all other variables were fully relaxed during geometry optimization. This procedure generated 144 conformers on each PES. Geometry optimizations, using the *ab initio* method at the HF/3-21G and then HF/6-31G(d,p) levels of theory, provided the input structures for the final optimization using DFT at the B3LYP/6-31G(d,p) level of theory, both *in vacuo* and in a simulated aqueous environment. The aqueous environment was mimicked with a self-consistent reaction field method, using a Poisson-Boltzmann solver as incorporated in Jaguar 5.5®.[53,54] Water was represented with a dielectric constant of 80.37 and a probe radius of 1.40 Å.

3.1.2 Obtaining the Conformers of Gly, Gly•, Ala, Ala• for the H Abstraction Reaction Coordinates

The subsequent computations were completed with the Gaussian 09 program package.[55] The ϕ and ψ angles of *N*-Ac-Ala-NHMe (Ala), *N*-Ac-Ala•-NHMe (Ala•), *N*-Ac-Gly-NHMe (Gly) and *N*-Ac-Gly•-NHMe (Gly•) were rotated in 30° increments to produce 144 conformations for each residue, which were then energy minimized using the Becke three-

parameter Lee-Yang-Parr (B3LYP) density functional, with the 6-31G(d) basis set.[56-58] The potential energy values as a function of the ϕ and ψ angles were plotted to construct the potential energy surfaces of Ala, Ala•, Gly and Gly• diamides (**Figure 4**).

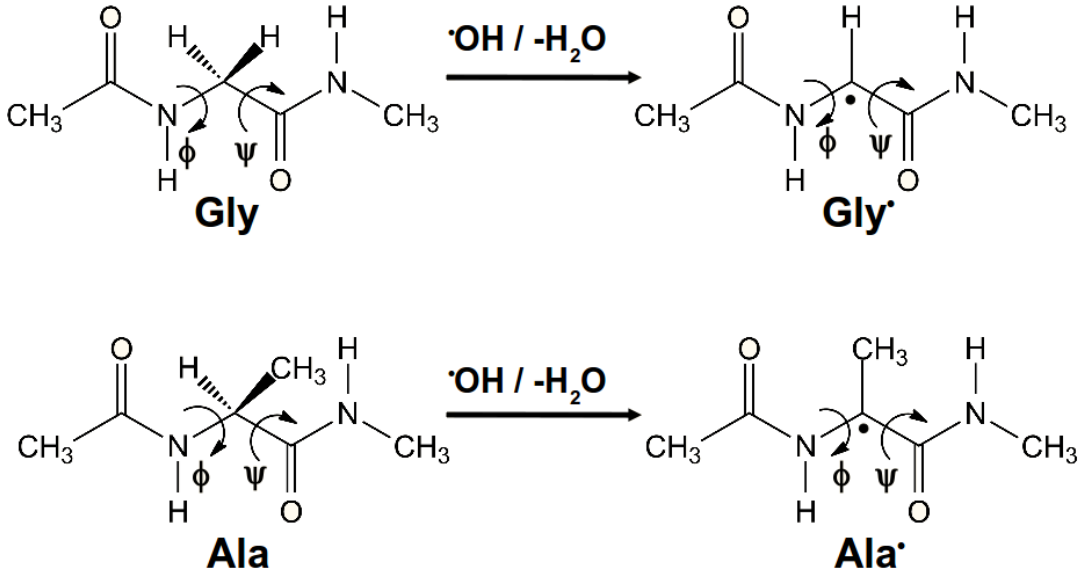

Figure 4. The Gly, Gly•, Ala and Ala• diamide structures. The ϕ and ψ angles which were the dependent variables for the potential energy surfaces are also shown.

Each of the minima of the potential energy surfaces were subsequently optimized using the Berny algorithm at the BHandHLYP/6-311+G(d,p) level of theory and were confirmed as such by asserting that none of the calculated frequencies were imaginary.[59,60] The standard free energy correction (G^o), enthalpy correction (H^o) and entropy (S^o) were also computed at this level of theory. The MPWKCIS1K/6-311++G(3df,2p) level of theory was used to compute the potential energy of the structures.[61] The pre-reaction and post-reaction complexes were found by minimizing the transition state structure along the intrinsic reaction coordinate in the reverse and forward directions, respectively. The ability of the MPWKCIS1K and BHandHLYP functionals to reproduce the activation energies computed

with the G3MP2B3 method was compared by using the 6-311+G(d,p) and 6-311++G(3df,2p) basis sets.[62] An implicit solvent using the conductor-like polarizable continuum model (C-PCM) for water with a dielectric constant of ε = 78.39 was used for all calculations to mimic an aqueous solvent and all of the optimizations were fully relaxed.[63]

The main disadvantage of the self-consistent reaction field (SCRF) method is the absence of explicit water molecules. In an attempt to account for this simplification, the dielectric coefficient is used to account for the "average" of the ensemble of possible hydrogen bonds between the solvent and solutes and to account for the different electrostatic environments that can surround a peptide when exposed to water. Previous benchmark calculations indicate that the BHandHLYP functional yields geometries and energy values that are in good agreement with results obtained by experiment and high level (G3MP2B3) *ab initio* methods, which in turn give results that are in excellent agreement with experimentally-derived results in radical systems.[38,65-67] Moreover, the MPWKCIS1K functional yields hydrogen abstraction barrier height energy values that are in excellent agreement with G3MP2B3 *ab initio* methods.[68] Several transition states involving Gly, Gly$^{\bullet}$, Ala and Ala$^{\bullet}$ with $^{\bullet}$OH and H_2O_2 were computed in this study. The ability of the MPWKCIS1K and BHandHLYP functionals to reproduce the activation energies computed with the with the G3MP2B3 method was compared by using the 6-311+G(d,p) and 6-311++G(3df,2p) basis sets. The results of this comparison are discussed in *Section 3.1*. The use of the SCRF with these functionals should yield acceptable results in the systems studied herein.

The relative energy values of the structures will be discussed throughout, whereas the

temperature dependent parameters, ΔG^o, ΔH^o and ΔS^o will be presented for comparison. This will enable the temperature-independent results obtained herein to be compared to larger systems, with more degrees of freedom.

3.2 Computing the Unfolding of the Pentapeptides

The Gaussian 09 program package was used to optimize the *N*-Ac-GGGGG-NH_2 (G5) and *N*-Ac-AAAAA-NH_2 (A5) geometries. The G5 and A5 structures were optimized in the gas phase and in an implicit solvent using the unrestricted B3LYP density functional method, with the 6-31G(d) and 6-311+G(d,p) basis sets.[56-58] The implicit solvent was represented by a conductor-like polarizable continuum model (C-PCM) for water, with a dielectric constant (ε) of 78.39.[69] The fully-extended conformations ($G5_{EXT}$, $A5_{EXT}$) were formed using initial ϕ and ψ angles of 180°, whereas the helical conformations ($G5_{HEL}$, $A5_{HEL}$) were stabilized by hydrogen bonds between the respective amide hydrogen and carbonyl oxygen of residues "i" and "i + 2". The geometry of both structures was subsequently optimized and their frequencies were computed to confirm that they were minima. **Figure 5** illustrates the definition of the ϕ, ψ and "i" symbols used to specify the sequence number of the amino acid residues in the peptides. The thermodynamic functions were calculated using the unscaled frequencies. A hydrogen atom was removed from the C_α and amide nitrogen of Gly^3 and Ala^3 in G5 and A5 to construct the G5($C_\alpha^\bullet$), A5($C_\alpha^\bullet$), G5($N^\bullet$), A5($N^\bullet$) peptide radicals, whereas a hydrogen atom was also removed from the methyl group of Ala^3 to form the A5($CH_2^\bullet$) peptide radical. The geometries of the peptide radicals were subsequently optimized in the doublet electron configuration using the levels of theory, conformations and environments used to

optimize G5 and A5. The bond lengths, ϕ and ψ dihedral angles pertaining to Gly^3 and Ala^3, hydrogen bond distances and root-mean-squared deviations

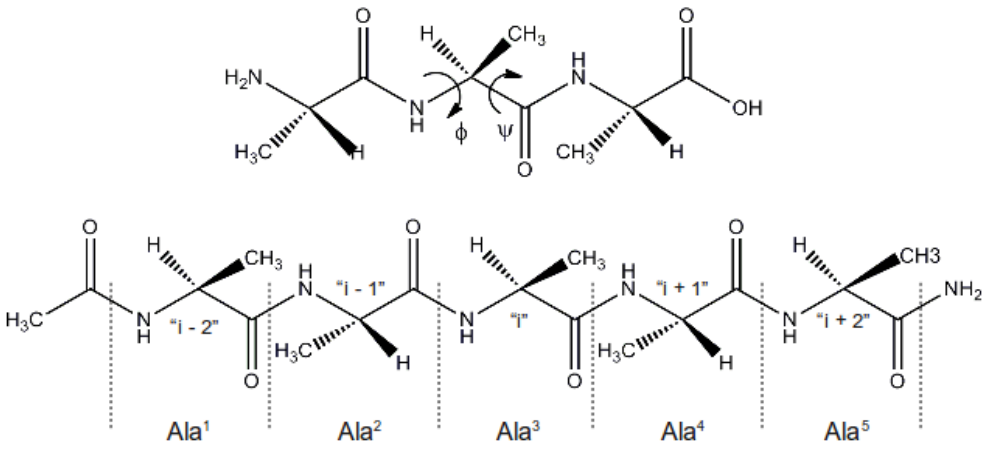

Figure 5. Representations of the ϕ and ψ nomenclature for the peptide dihedral angles (top) and the "i – 1", "i", and "i + 1" nomenclature of amino acid residues of A5 (*N*-Ac-AAAAA-NH_2). The same nomenclature was used for the G5 peptide (*N*-Ac-GGGGG-NH_2).

(RMSD) of peptide backbone atoms of the peptide radicals were compared to those of the respective G5 and A5 peptides. A diagram that schematically outlines these peptides can be

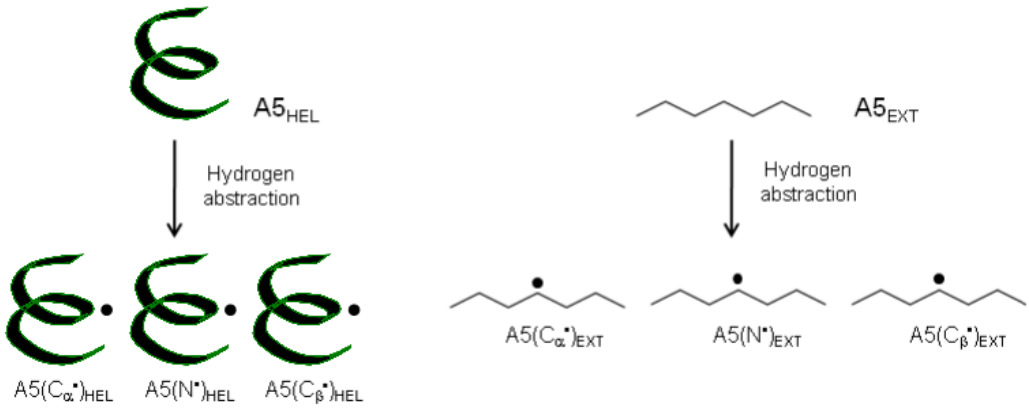

Figure 6. A schematic representation of the peptides computed in this study. The structures of the $A5_{HEL}$ and $A5_{EXT}$ peptides are to be compared to the structures of the respective peptide radicals after hydrogen abstraction. The G5, G_{EXT} and G_{HEL} peptides were compared in a similar way.

found in **Figure 6**.

The ΔH^o, ΔG^o and ΔS^o for the reactions with $^{\bullet}OH$, $HO_2^{\bullet}$ and $O_2^{-\bullet}$ that resulted in the formation of the peptide radicals were measured using the previously described gas phase and implicit solvent conditions. The relative stability and the ΔH^o, ΔG^o and ΔS^o of the unfolding of the peptide radicals were also computed in these conditions.

3.3 Parameterization of the Gly$^{\bullet}$ and Ala$^{\bullet}$ force-fields

3.3.1 Force-field Parameterization of Gly$^{\bullet}$

The parameter fitting of Gly was accomplished by calculating the OPLS-AA/L energy and the analytical energy first derivatives with respect to the molecular mechanical parameters. The point-charge parameters for *N*-Ac-Gly$^{\bullet}$-*N*-Me-amide were fitted to the electrostatic potential using the restrained electrostatic potential (RESP) methodology and the RESP program from the AMBER8 program package.[70-73] The partial charges on the *N*-Acetyl and *N*-Methyl groups were kept the same as they were in the original OPLS-AA/L force field, to conserve the electroneutrality of the core Gly$^{\bullet}$ radical structure. The electrostatic potentials at nine geometries, with independent $\pm 15.0^o$ fluctuations of φ and ψ from the planar equilibrium geometry, were calculated.

3.3.2 Force-field Parameterization of Ala$^{\bullet}$

A new atom type was defined for the carbon atom at the radical center (CRA), being different from that at the glycyl radical in order to allow more flexible parameter derivation. However, the van der Waals parameters were chosen to be identical for both of them. The atomic partial charges were generated from RESP HF/6-31G(d) calculation, as in the case of

Gly.[60]

During parameterization only small perturbations were allowed for all but the torsion internal coordinates. Only the C-N-CRA-CT, H-N-CRA-CT, N-C-CRA-CT, O-C-CRA-CT, N-CRA-CT-H and the C-CRA-CT-H torsion parameters were developed. Rigid rotor approach was used to scan the torsion potential energy surface. The N-CRA-C-O, N-CRA-C-N, C-N-CRA-C, H-N-CRA-C, CT1-C-N-CRA, O-C-N-CRA, H-N-C-CRA and CT1-N-C-CRA torsion parameters were adopted from the glycyl radical force field.

The proper torsion parameters were derived from LMP2/cc-pVTZ(-f) computations as proposed by Kaminski et al. using a rigid rotor approach from the MP2/6-31+G(d,p) equilibrium geometry.[36] All the other force field parameters were obtained with the use of MP2/6-31+G(d,p) calculations.

The geometry of *N*-Ac-Ala•-NHMe was fully optimized at the MP2/6-31+G(d,p) level of theory. In order to derive the parameters, the potential energy of a series of geometries of *N*-Ac-Ala•-NHMe was computed and the variations thereof are shown in **Table 1**.

Table 1. The variation in bond lengths, bond angles and torsional angles used to parameterize the N-*N*-Ac-Ala•-Me amide.

Parameter	Atoms	Variations
Bond Lengths	C-CR CR-CT CR-N	+/- (0.01°, 0.02°, 0.03°, 0.04°, 0.05°, 0.06°, 0.07°, 0.08°, 0.1°, 0.12°, 0.15°)
Bond Angles	CR-CT-H C-CR-CT N-C-CT	+/- (1.0°, 2.0°, 3.0°, 4.0°, 5.0°, 6.0°, 7.0°, 8.0°, 9.0°, 10.0°, 12.0°, 14.0°, 16.0°, 20.0°)
Torsional Angles	T1 T2 T3	15.0° increments

Quantum chemical calculations were performed with the Gaussian09 software package, while the parameter fitting was carried out by Professor István Komáromi, at the University of Debrecen.[74]

3.4 Molecular Dynamics Simulations of the Ala Heptapeptides

Using the newly developed alanyl radical parameters described in *Section 2.1*, the conformational space of two heptapeptides was investigated with molecular dynamics simulations. The peptides were solvated with 2360 TIP4P water molecules in a cubic box of 41.7 Å × 41.7 Å × 41.7 Å.[75] The two model heptaalanyl peptides were used: *N*-Ac_1-Ala_2-Ala_3-Ala_4-Ala_5-Ala_6-Ala_7-Ala_8-Nma_9 (ALA) and *N*-Ac_1-Ala_2-Ala_3-Ala_4-Alr_5-Ala_6-Ala_7-Ala_8-Nma_9 (ALR), where the central alanine (Ala_5) of the latter peptide was modified manually into the radical form (Alr_5) by deleting the hydrogen from the C_α atom (**Figure 7**).

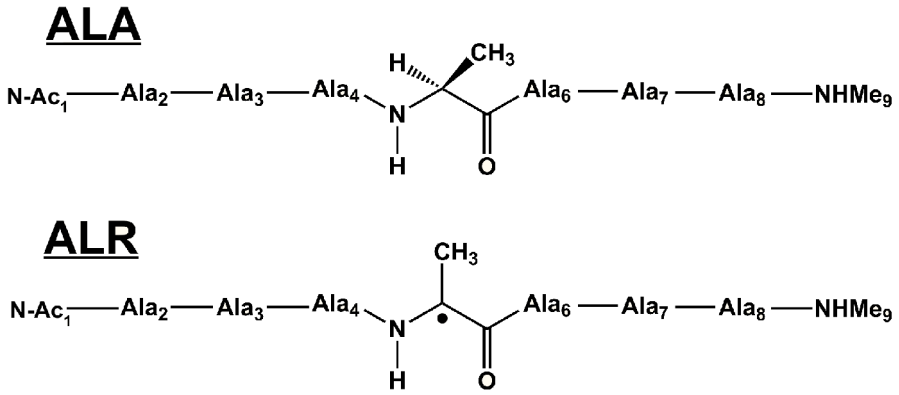

Figure 7. A schematic representation of the ALA and ALR heptapeptides. The force field for the ALR peptide contains the newly-developed alanyl radical parameters.

The system was pre-equilibrated with the provided protocol followed by a 96 ns simulation under NPT conditions (T = 310 K, P = 1.01325 bar), using the Martyna-Tobias-Klein pressure and temperature control.[76] A 2 fs integration step was used, while the cutoff for the short-range non-bonded interactions was 9 Å and was updated every second step. Long-range electrostatic interactions were treated with the particle mesh Ewald method, containing 32 Fourier mesh points along each axis, and were updated every third integration

step.[77] The structures were saved every 4.8 ps, which established a trajectory of 20,000 structures.

Table 2. Definitions of the Secondary Structure Elements (SSE). Higher order structures consist of repeating turn structures.

SSE	Definition
Turn Structures	
δ-turn:	2 consecutive residues with a hydrogen bond between NH_i and CO_{i+1}
γ-turn:	3 consecutive residues with a hydrogen bond between CO_i and NH_{i+2}
inverse γ-turn:	3 consecutive residues with a hydrogen bond between NH_i and CO_{i+2}
β-turn:	4 consecutive residues with less than 7 Å between the C_α of residue "i" and residue "i + 3", in the absence of a helix.
α-turn:	5 consecutive residues with less than 7 Å between the C_α of residue "i" and residue "i + 4", in the absence of a helix.
π-turn:	6 consecutive residues with less than 7 Å between the C_α of residue "i" and residue "i + 5", in the absence of a helix.
Higher-Order Structures	
3_{10}-helix:	2 or more consecutive β-turns and stabilized by hydrogen bonds.
α-helix:	2 or more consecutive α-turns, stabilized by hydrogen bonds.
π-helix:	2 or more consecutive π-turns hydrogen bonds.

The density Ramachandran map was used to analyze the conformational space sampled by the Ala_5 or Alr_5 residues. The Ramachandran space was divided into 30° × 30° boxes, and the percentage of the structures in which Ala_5 or Alr_5 had ϕ and ψ angles values that fit within each box was recorded. The number of secondary structure elements that were found in the discrete regions of the heptapeptides containing the Ala_5 or Alr_5 residues was quantified using secondary structure analysis (**Table 2**).

The secondary structure elements consisted of individual β-, γ- δ-, α-, and π-turns as described by Chou, and also higher-order secondary structure elements (SSE), which are composed of individual turns that combine to form helices.[78] The definition of the each secondary structure element can be found in **Table 2**.

An H bond was assigned to the peptide residues if the distance between the amide N and the carbonyl oxygen was less than 3.5 Å and the angle, α(N-H···O), was greater than 100º.

4.0 RESULTS

4.1 General Features of the Amino Acid Potential Energy Surfaces

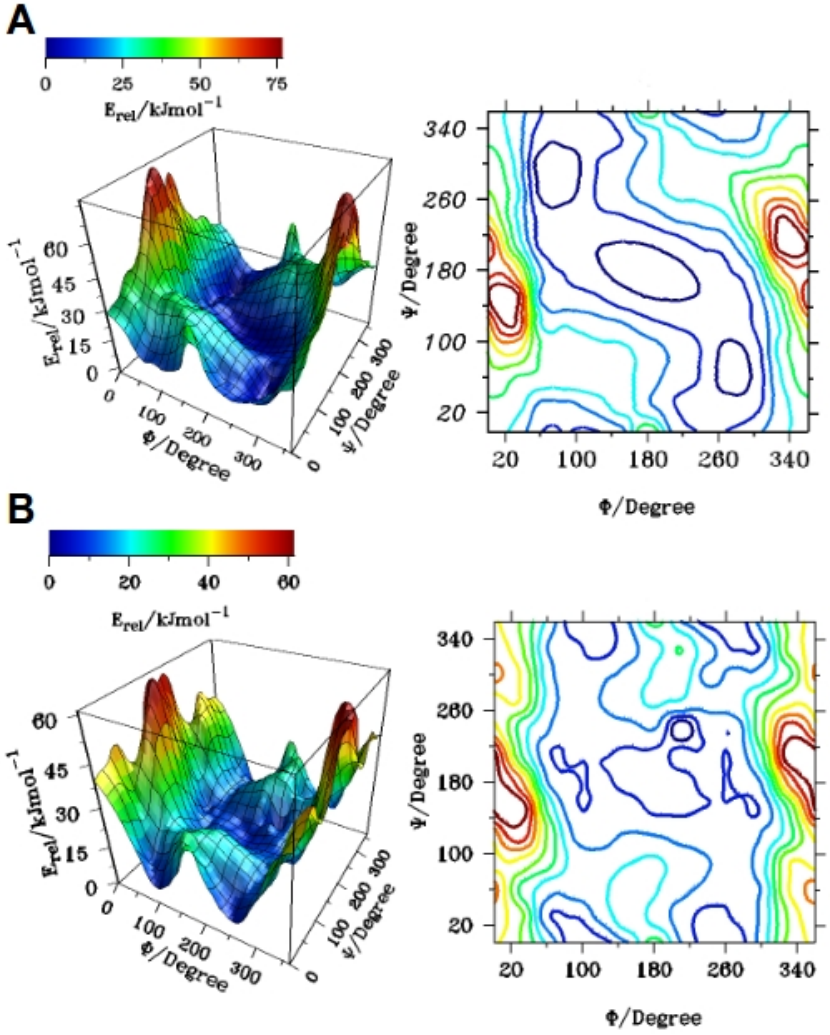

Figure 8. PES and contour plot for *N*-Ac-Gly-NHMe in the gas phase (A) and in solution (B).

The PES of *N*-Ac-Gly-NHMe in the gas phase was predominantly flat, except for a maximum at $\phi = 0^{o}$ and $\psi = 180^{o}$ (**Figure 8A**). A large and broad valley connected several conformations of Gly. When ϕ was between 30^{o} and 120^{o} and ψ between 150^{o} and 300^{o}, the system was in a low energy state. This was also the case when ϕ was between 90^{o} and 270^{o} and ψ was between 150^{o} and 210^{o}, and when ϕ was between 270^{o} and 300^{o} and ψ was

between 30° and ψ 180°. These three regions were connected and contained low-energy conformers with minima located in the γ_D, β_L and γ_L conformations. The PES of *N*-Ac-Gly-NHMe in a simulated aqueous environment (**Figure 8B**) was similar to that of the gas phase PES, indicating the same stable conformations as that of the gas phase model (**Figure 8A**).

The C_α-centered *N*-Ac-Gly•-NHMe lacked the conformational flexibility of the closed-shell model. The PES of this model indicated that the β_L conformation was the global minimum (**Figure 9A**).

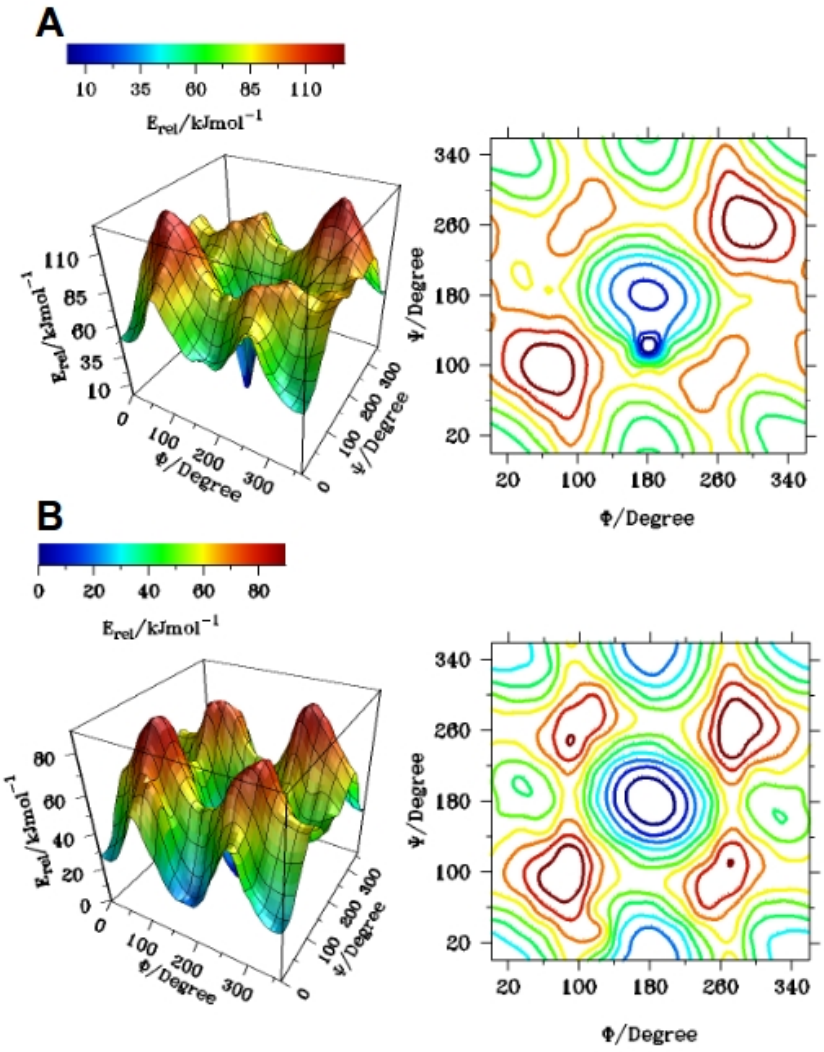

Figure 9. PES and contour plot for *N*-Ac-Gly•-NHMe in the gas phase (A) and in solution (B).

This minimum had a high energy barrier of about 80 kJ mol^{-1} extending in a 90° radius from the geometry with ϕ of 180°, ψ of 180°. Other minima were present in the δ_L, δ_D, and ϕ = 0°, ψ = 0° geometry, which also includes the α_D, α_L, γ_D, γ_L conformations. Two maxima were located at ϕ = 60°, ψ = 90° and ϕ = 300°, ψ =270°, and were 127 kJ mol^{-1} less stable than the global minimum. The aqueous environment induced a qualitatively similar PES (**Figure 3B**) to that in the gas phase. The global minimum was still present in the β_L conformation with a barrier of 60 kJ mol^{-1}, restricting this conformation. The minima found in the gas phase also were found in the solvent. In addition, the solvent stabilized ε_D and ε_L conformations. The unstable conformers in the aqueous environment had the same geometry as those in the gas phase, but the structures were 88 kJ mol^{-1} less stable than the global minimum.

4.1.1 Comparison of the MPWKCIS1K and BHandHLYP functionals

Activation energies of Gly-$^{\bullet}$OH, Ala-$^{\bullet}$OH, Gly$^{\bullet}$-H_2O_2 and Ala$^{\bullet}$-H_2O_2 transition states using the BHandHLYP/6-311+G(d,p), BHandHLYP/6-311++G(3df,2p), MPWKCIS1K/6-311+G(d,p), MPWKCIS1K/6-311++G(3df,2p) methods were calculated on geometries obtained by the BHandHLYP/6-311+G(d,p) level of theory. This was done to compare the accuracy of the respective method. The G3MP2/BHandHLYP/6-311G(d,p) calculations were used as a reference and the results of the comparison are shown in Table 3.[38,68] The maximum absolute deviation (MAD) and average absolute deviation (AAD) of the BhandHLYP/6-311+G(d,p) energies from the reference values is 19.4 and 14.5 kJ mol^{-1}, respectively, showing that the use of this functional with the smaller basis set is unsuitable for computing

Table 3. Single point activation energies of Gly-˙OH, Ala-˙OH, Gly˙-H_2O_2 and Ala˙-H_2O_2 calculated with the BHandHLYP and MPWKCIS1K functionals. The G3MP2 method was used as a reference. The maximum absolute deviation (MAD) and average absolute deviation (AAD) are reported, and the deviations pertaining to the Gly-˙OH and Ala-˙OH transition states are in parenthesis.

Transition State	Conf	Activation Energy (ΔE^o) / kJ mol^{-1}				
		BHandHLYP/ 6-311+G(d,p)	BHandHLYP/ 6-311++G(3df,2p)	G3MP2	MPWKCIS1K /6-311+G(d,p)	MPWKCIS1K/ 6-311++G(3df,2p)
Gly-˙OH	β_L	12.2	-5.3	-2.9	0.2	-0.3
	γ_L	18.1	0.1	2.2	4.5	3.8
	γ_D	15.1	-4.2	5.7	1.0	0.3
	α_L	22.2	4.2	3.4	7.9	7.0
	α_D	19.9	1.1	7.5	6.6	5.6
Ala-˙OH	β_L	11.0	-6.4	-6.3	-1.3	-1.6
	γ_L	14.0	-3.7	-3.1	2.1	1.6
	γ_D	19.1	0.4	0.6	3.8	2.9
	α_L	15.2	-3.0	-4.2	2.7	1.8
	α_D	20.4	2.4	5.9	9.6	8.6
Gly˙-H_2O_2	β_L	57.3	51.8	44.9	45.8	51.2
Ala˙-H_2O_2	β_L	35.1	47.6	31.9	41.4	47.8
MAD		19.4 (19.4)	15.7 (9.9)	0.0 (0.0)	9.5 (6.9)	15.9 (6.0)
AAD		14.5 (15.8)	4.2 (2.7)	0.0 (0.0)	4.2 (4.0)	4.8 (3.6)

transition state energies, given the overestimation of the activation energies. The use of the BHandHLYP/6-311++G(3df,2p) (MAD = 15.7 kJ mol^{-1}, AAD = 4.2 kJ mol^{-1}),MPWKCIS1K/6-311+G(d,p) (MAD = 9.5 kJ mol^{-1}, AAD = 4.2 kJ mol^{-1}) and MPWKCIS1K/6-311++G(3df,2p) (MAD = 15.9 kJ mol^{-1}, AAD = 6.0 kJ mol^{-1}) functionals yielded results that are close to the experimental error, given that the AAD values are 6.0 kJ mol^{-1} or less.

The use of either basis set with the MPWKCIS1K functional and the larger basis set with the BHandHLYP functional is suitable for these systems. When the reactions involving OH are combined with that of H_2O_2 to regenerate Gly or Ala, the Gly-˙OH and Ala-˙OH transition

states were shown to be the rate limiting step. Therefore, the accuracy of the Gly-˙OH and Ala-˙OH barrier height energies are crucial for determining the minimum energy path for the ˙OH-initiated unfolding of Gly and Ala. When the conformers of the Gly-˙OH and Ala-˙OH transition states are considered, the MAD and AAD obtained from the MPWKCIS1K/6-311++G(3df,2p) combine to be the lowest of the three methods (MAD = 6.0 kJ mol^{-1}, AAD = 3.6 kJ mol^{-1}), therefore this method was chosen for the remainder of the calculations. The efficiency of this computational method makes it suitable for use in larger systems in future studies.

4.2 Hydrogen Abstraction from the Monopeptides

The conformers of the Gly, Gly˙, Ala and Ala˙ potential energy surfaces were identified from the respective potential energy surface. The pre-reaction complexes, transition states, post-reaction complexes and a general description of the H abstraction reaction coordinate with ˙OH are presented in the subsequent sections.

4.2.1 The Potential Energy Surfaces

Figure 10 shows the Gly and Ala potential energy surfaces. The subsequent optimization of the minima of the PES of Gly and Ala each yielded five minima: β_L, γ_L , γ_D, α_L and α_D. The β_L conformation is the global minimum in the case of Gly, whereas the α_L conformation is the global minimum of the Ala PES. The ϕ and ψ angles and energy values for all of the minima can be found in **Table 4**. In Ala, the D-configurations are less favorable and are more than 10 kJ mol^{-1} higher in energy than the respective L-configurations. Conversely, the α_L and γ_L conformations have energy values that are similar to their

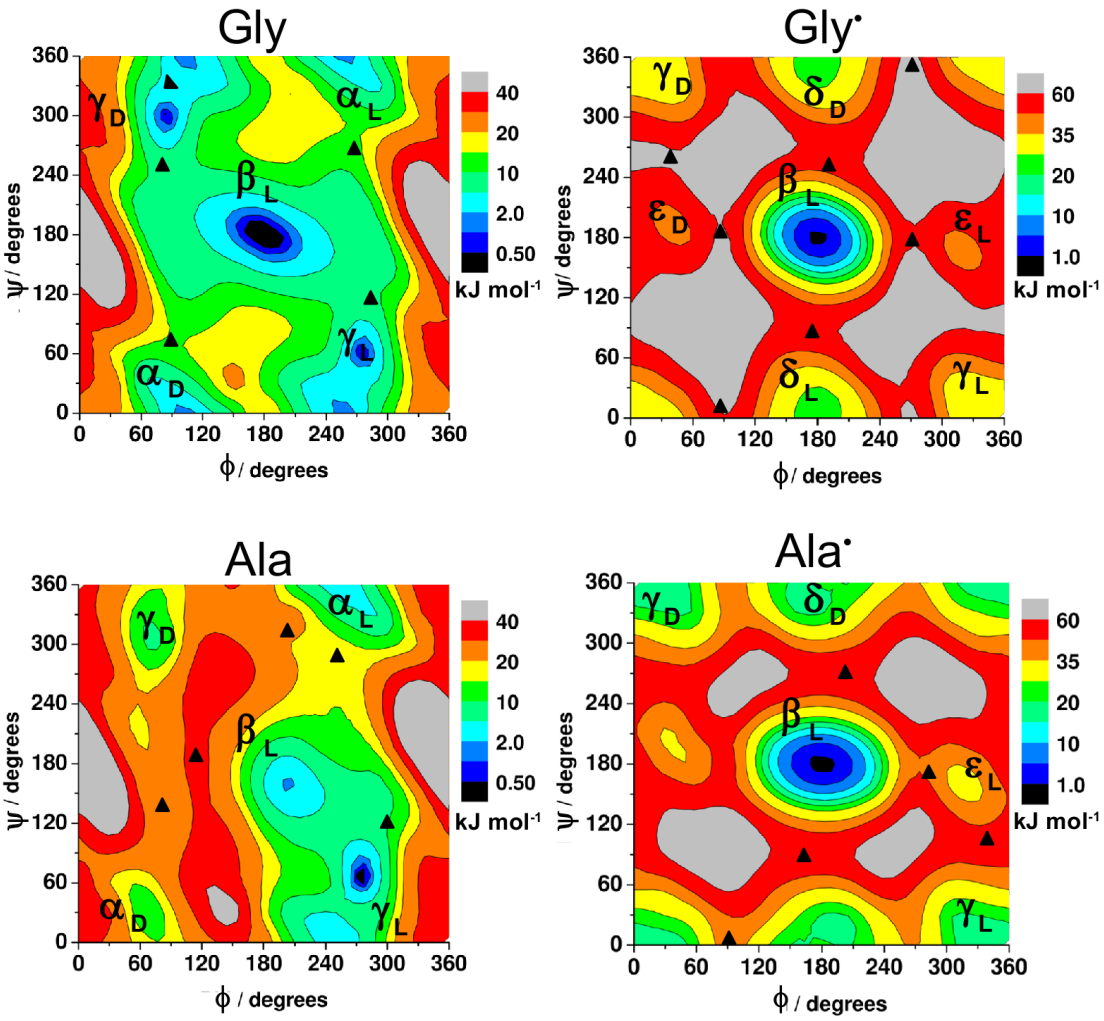

Figure 10. The potential energy surfaces of the Gly, Gly•, Ala, and Ala• amino acid diamides. The minima are labeled by their respective conformation whereas the transition states are labeled with triangles.

respective α_D and γ_D conformations in Gly.

The β_L conformation is the global minimum of both the Ala• and the Gly• potential energy surfaces. These conformations have the lowest relative free energy and enthalpy, and also the most entropy. In contrast to the closed-shell Gly and Ala potential energy surfaces, the other minima in the Gly• and Ala• surfaces are less stable than their respective global minimum. The higher-energy minima of Gly• are greater than the global minimum by 20 kJ

mol^{-1}, whereas energy of the the Ala$^{\bullet}$ minima are 15 kJ mol^{-1} higher in energy than the global minimum. Moreover, to convert from the global minima of the Gly$^{\bullet}$ and Ala$^{\bullet}$ structures to any of the other minima requires at least 50 kJ mol^{-1} of energy to overcome the ϕ and ψ rotational barriers. Therefore, the Gly$^{\bullet}$ and Ala$^{\bullet}$ peptide radicals are prone to convert to the β_L conformer. This increased barrier height can be attributed to the increased electron delocalization and increased influence of the capto-dative effect shown in the β_L conformation. This barrier constrains the conformation of the Gly and Ala structures and increases the propensity of these molecules to be in the β-conformation. The first-order saddle points of the potential energy surfaces listed in **Table 4** show the relative flexibility of the Gly Gly$^{\bullet}$, Ala and Ala$^{\bullet}$ residues. The difference in energy between the minima and first-order saddle points of Gly (17 kJ mol^{-1}) is less than that of Ala (33 kJ mol^{-1}), indicating that Gly is more flexible than Ala. The relative energy of the transition states (first-order saddle points) of the Gly$^{\bullet}$ PES is similar to those of Ala and Ala$^{\bullet}$, suggesting that the peptide radicals have a similar flexibility. The ΔH^o values corresponded well with the electronic energy values (ΔE). The ΔG^o values were usually more elevated than the ΔE values and this increase was usually coupled to an increase in the negativity of the ΔS^o value. The ΔS^o values of the transition states were generally lower than those of the minima, due to the extra intrinsic degree of freedom of the transition state structures.

4.2.2 The Hydrogen Abstraction Reaction Coordinates

The structures and relative energies of the different Gly and Ala conformers in complexes with $^{\bullet}$OH will be presented in the subsequent sections.

Table 4. Conformation (Conf), ϕ and ψ angles, intra-residue hydrogen bond [(N)H···O(=C)] and the ΔE^{o}_{rel}, ΔG^{o}_{rel}, ΔH^{o}_{rel}, ΔS^{o}_{rel} of the lowest energy conformations and transition state structures of Gly, Gly•, Ala and Ala•.

Struct.	Conf.	ϕ, ψ / degrees	(N)H···O(=C) / Å	ΔE^{o}_{rel} / kJ mol^{-1}	ΔG^{o}_{rel} / kJ mol^{-1}	ΔH^{o}_{rel} / kJ mol^{-1}	ΔS^{o}_{rel} / J mol^{-1} K^{-1}
Gly	β_L	-179.9, 179.9	2.18	0.0	0.0	0.0	0.0
	γ_L	-83.9, 60.4	2.06	3.8	9.5	5.2	-14.6
	γ_D	83.9, -60.4	2.06	3.8	9.5	5.2	-14.6
	α_L	-92.5, -5.8	3.37	0.1	-0.1	0.7	2.9
	α_D	92.6, 5.6	3.37	0.1	-0.1	0.7	2.8
[Gly]‡	γ_D <–> α_D	88.0, -6.70	3.19	2.8	5.4	-1.1	-21.8
	β_L <–> γ_L	-77.4, -115.2	2.78	11.5	16.8	8.1	-29.3
	β_L <–> γ_D	77.4, 115.2	2.78	11.5	16.8	8.1	-29.2
	β_L <–> α_L	-95.3, -74.2	3.97	16.4	20.3	12.7	-25.4
	β_L <–> α_D	95.2, 74.2	3.97	16.4	20.3	12.7	-25.4
Gly•	β_L	-179.9, -180.0	2.3	0.0	0.0	0.0	0.0
	γ_L	-20.4, 4.6	1.81	31.0	31.8	31.9	0.5
	γ_D	20.2, -4.8	1.81	30.9	32.5	31.9	-2.0
	δ_L	-172.8, 12.4	3.87	39.3	40.3	38.4	-6.3
	δ_D	172.8, -12.4	3.87	21.0	23.9	21.0	-9.7
	ε_L	-47.2, 165.9	3.73	39.3	40.3	38.4	-6.3
	ε_D	47.2, -165.9	3.73	39.3	40.3	38.4	-6.3
[Gly•]‡	γ_L <–> δ_D	10.7, -94.1	3.07	61.8	63.9	57.0	-23.1
	δ_L <–> γ_D	-95.5, -2.2	3.35	57.2	53.2	50.2	-10.0
	δ_D <–> γ_L	95.5, 2.2	3.35	57.2	53.2	50.2	-10.1
	β_L <–> δ_L	165.1, 97.5	3.21	54.2	54.7	49.4	-17.9
	β_L <–> δ_D	-165.2, -97.5	3.21	54.2	54.7	49.4	-17.8
	β_L <–> ε_L	-86.0, 178.4	3.16	59.1	55.7	52.3	-11.2
	β_L <–> ε_D	86.0, -178.4	3.16	59.1	55.7	52.3	-11.2

Table 4. Continued

Struct.	Conf.	ϕ, ψ / degrees	(N)H···O(=C) / Å	ΔE^{o}_{rel} / kJ mol^{-1}	ΔG^{o}_{rel} / kJ mol^{-1}	ΔH^{o}_{rel} / kJ mol^{-1}	ΔS^{o}_{rel} / J mol^{-1} K^{-1}
Ala	β_L	-154.3, 156.7	2.23	0.0	0.0	0.0	0.0
	γ_L	-85.8, 70.5	2.09	1.3	4.0	1.8	-7.3
	γ_D	74.4, -52.6	1.93	10.5	16.3	11.7	-15.4
	α_L	-83.0, -17.6	3.36	-0.7	0.4	-0.3	-2.4
	α_D	63.7, 34.1	3.21	9.6	12.3	9.7	-8.8
[Ala]‡	β_L <–> α_L	-96.7, -75.3	3.92	15.8	16.0	10.4	-18.7
	β_L <–> γ_L	-76.4, 117.6	2.88	7.5	8.6	2.4	-20.8
	α_D <–> γ_D	81.5, 155.4	3.24	25.5	28.2	26.0	-21.5
	β_L <–> γ_D	117.4, -150.4	2.32	33.5	36.7	29.0	-25.7
	α_L <–> γ_D	-157.6, -61.1	3.50	19.6	20.5	14.1	-21.5
Ala$^{\bullet}$	β_L	-171.9, 176.8	2.09	0.0	0.0	0.0	0.0
	γ_L	-46.7, 10.8	1.85	18.3	22.0	18.0	-13.5
	γ_D	46.7, -10.7	1.85	18.3	22.0	18.0	-13.6
	ε_L	-48.8, 159.5	4.28	24.0	26.8	22.8	-13.4
	δ_D	155.5, -15.0	3.75	15.5	20.7	15.3	-18.2
[Ala$^{\bullet}$]‡	β_L <–> δ_L	-13.5, 96.1	3.03	45.5	48.5	39.8	-29.2
	β_L <–> δ_L	95.7, 2.6	3.32	30.8	28.9	23.1	-19.7
	β_L <–> δ_L	-84.3, 172.7	3.04	40.2	37.4	32.7	-15.6
	β_L <–> δ_L	-177.3, 99.9	2.95	53.2	54.1	47.8	-21.4
	β_L <–> δ_L	177.3, -99.9	2.95	53.2	54.1	47.8	-21.4

4.2.2.1 Pre-Reaction van der Waals complexes

In each Gly van der Waals complex, the hydrogen atom of the ˙OH radical formed a hydrogen bond with a carbonyl oxygen that was between 1.73 Å and 1.80 Å (**Table 4**). The structures of the van der Waals complexes are shown in **Figure 11**. In the γ_D and α_D conformations, the hydrogen atom formed a hydrogen bond with the carbonyl residue of the i^{th} residue, whereas the oxygen atom of the ˙OH radical was equidistant to the both the pro-L and pro-D hydrogen atoms. This was also true in the β_L conformation, however the hydroxyl

Table 5. The distances between the Gly and Ala diamide and the •OH radical along the reaction coordinate. The C···H(-O) bond is between the C_α and the hydrogen (to be abstracted); the (C-)H···O bond is between the abstracted hydrogen and the oxygen of the hydroxy group and the H···O(=C) bond is between the hydroxy oxygen and the carbonyl carbon of the amino acid diamide.

Struct.	Conf.	Distances / Å		
		C···H(-O)	(C-)H···O	H···O(=C)
Gly-•OH pre-reaction complex	β_L	1.087	3.161	1.733
	γ_L	1.085	3.052	1.770
	γ_D	1.084	3.630	1.803
	α_L	1.082	2.915	1.754
	α_D	1.084	3.634	1.727
[Gly···•OH]‡	β_L	1.200	1.347	2.114
	γ_L	1.216	1.316	2.111
	γ_D	1.209	1.330	2.170
	α_L	1.226	1.292	2.059
	α_D	1.209	1.329	2.169
Gly-H_2O post-reaction complex	β_L	2.268	-	1.841
	γ_L	1.892	-	1.899
	γ_D	4.676	-	1.803
	α_L	2.997	-	1.946
	α_D	4.680	-	1.803
Ala-•OH pre-reaction complex	β_L	1.084	2.934	1.731
	γ_L	1.084	2.536	-
	γ_D	1.081	3.018	1.719
	α_L	1.084	3.252	1.726
	α_D	1.086	2.453	5.188
[Ala···•OH]‡	β_L	1.206	1.339	2.015
	γ_L	1.207	1.332	2.063
	γ_D	1.225	1.272	2.077
	α_L	1.207	1.334	2.162
	α_D	1.200	1.338	4.026
Ala-H_2O post-reaction complex	β_L	5.156	-	1.845
	γ_L	3.800	-	1.886
	γ_D	4.361	-	1.805
	α_L	3.180	-	1.913
	α_D	1.91	-	1.913

hydrogen formed a hydrogen bond with the carbonyl carbon of residue "i – 1". The γ_L and α_L Gly complexes were the least stable, in spite of the fact that the distance between the hydroxy oxygen and the pro-D hydrogen was the shortest in these structures. The β_L and α_D conformations of Gly were the most stable van der Waals complexes. The relative energy of the pre-reaction complexes are listed in **Table 2**, whereas the complex-formation energy values are listed in **Table 5**. The γ_L conformation formed the least-stable pre-reaction complex.

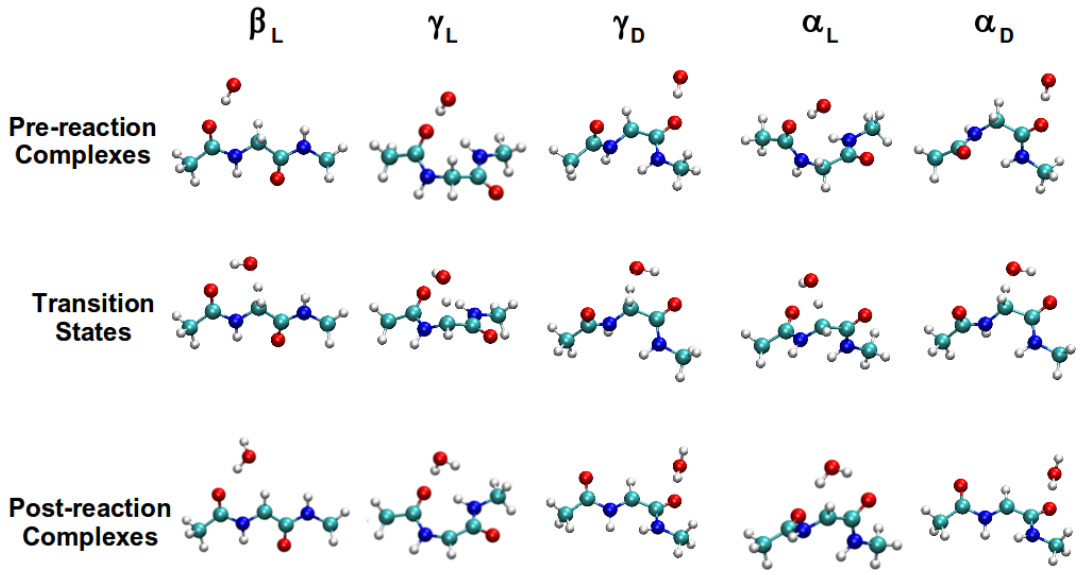

Figure 11. The pre-reaction van der Waals complexes, transition states and post-reaction complexes for the hydrogen abstraction from Gly by •OH. The distances between the •OH/H_2O molecule and each conformation of the Gly/Gly• diamide are shown in **Table 5**.

In the Ala α_D pre-reaction complex the carbonyl oxygens of residues "i" and "i – 1" were too far from the pro-D hydrogen to enable a hydrogen bond to form with the hydrogen atom of the hydroxy radical. This is shown in **Figure 12**. As such, this van der Waals complex was the least stable. The hydrogen atom of the hydroxy radical formed a hydrogen bond with the residue "i" carbonyl carbon of γ_D and α_L, however the α_L van der Waals complex was the

most stable. The β_L van der Waals complex formed a 9-membered ring, linking the carbonyl oxygen of residue "n – 1" to the amide hydrogen of residue "n + 1". A hydrogen bond within residue "i" remained intact.

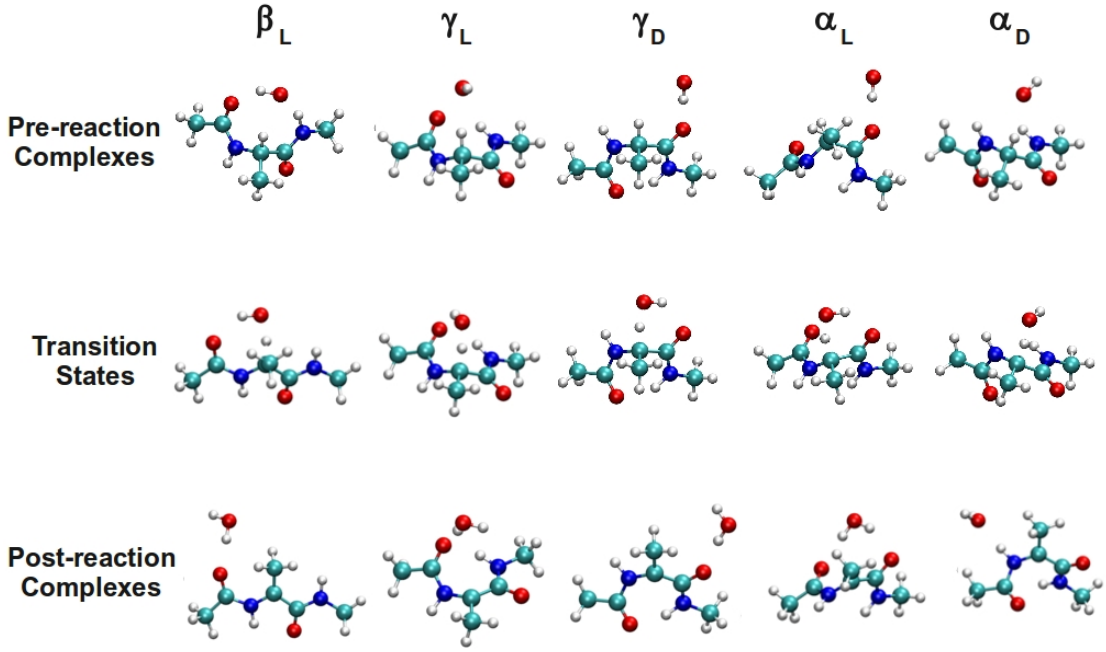

Figure 12. The pre-reaction van der Waals complexes, transition states and post-reaction complexes for the hydrogen abstraction from Ala by ˙OH. The distances between the ˙OH/H_2O molecule and each conformation of the Ala/Ala˙ diamide are shown in **Table 2**.

4.2.2.2 The Transition State Structures

The hydrogen atom of the ˙OH radical formed a hydrogen bond with the carbonyl carbon of the "i – 1" residue of Gly in the transition state when Gly was in the β_L, γ_L and α_L conformations. The structure of the transition states are shown in **Figure 11**. The β_L conformation was the lowest-lying transition state, whereas the γ_L and α_L conformations had the highest energy. The ˙OH radical completed a seven-membered ring formed a bridge between the "i – 1" carbonyl and the C_α hydrogen atom. Conversely, the hydroxyl oxygen formed a hydrogen bond of the "i"th carbonyl carbon, and therefore formed a six-membered

Table 6. The ϕ and ψ angles, relative potential energy, free energy, enthalpy, entropy for each of the Gly and Ala pre-reaction and post-reaction complexes and transition states with the ˙OH radical. The β_L conformation was the reference conformation for each structure.

Struct.	Conf.	ϕ, ψ / degrees	ΔE / kJ mol^{-1}	ΔG^o / kJ mol^{-1}	ΔH^o/ kJ mol^{-1}	ΔS^o / J mol^{-1} K^{-1}
Gly-˙OH pre-reaction complex	β_L	178.3, -176.9	0.0	0.0	0.0	0.0
	γ_L	-85.1, 50.7	10.4	11.2	9.4	-6.2
	γ_D	94.1, 4.0	0.8	2.8	14.0	37.8
	α_L	-92.2, -4.0	2.7	3.2	2.6	-2.0
	α_D	93.4, 5.0	-0.9	-2.5	-0.9	-5.4
[Gly···˙OH]‡	β_L	-174.4, -170.8	0.0	0.0	0.0	0.0
	γ_L	-76.2, 46.5	10.9	12.8	11.0	-7.1
	γ_D	140.4, -25.1	7.5	5.9	7.5	0.7
	α_L	-75.7, -11.3	10.7	10.7	10.1	0.2
	α_D	140.4, -25.1	7.5	5.9	7.5	7.1
Gly post-reaction complex	β_L	-179.7, -179.9	0.0	0.0	0.0	0.0
	γ_L	-35.4, 5.0	35.7	35.6	20.1	-52.0
	γ_D	172.7, -13.2	16.5	19.3	18	-4.4
	α_L	-51.0, -27.4	39.1	37.1	22.8	-47.8
	α_D	172.6, -12.9	16.6	12.9	0.9	-40.4
Ala-˙OH pre-reaction complex	β_L	-155.7, 156.9	0.0	0.0	0.0	0.0
	γ_L	-85.8, 69.0	5.7	-3.8	-10.3	-21.8
	γ_D	74.0, -55.1	9.0	-1.7	9.4	37.6
	α_L	-80.2, -21.5	-0.5	-11.8	-16.2	-14.9
	α_D	64.7, 33.2	32.5	15.9	31.3	51.7
[Ala···˙OH]‡	β_L	-160.5, 175.9	0.0	0.0	0.0	0.0
	γ_L	-78.4, 52.2	4.8	5.7	4.7	-3.4
	γ_D	78.1, -58.2	3.6	2.7	3.8	-3.6
	α_L	-58.4, -38.4	22.3	15.1	20.7	-18.6
	α_D	64.9, 32.6	20.6	19.1	19.9	2.9
Ala post-reaction complex	β_L	-170.2, 176.8	0.0	0.0	0.0	0.0
	γ_L	-53.5, 9.9	20.6	27.0	4.0	-77.3
	γ_D	45.5, -14.0	16.1	26.6	15.3	-37.8
	α_L	-58.2, -25.1	22.9	22.1	21.0	-3.7
	α_D	56.8, 18.6	14.7	19.8	14.5	-17.9

ring in the transition state when the Gly residue was in the γ_D and α_D conformations. The transition states that formed six-membered rings were more stable than those that were seven-membered rings. The relative stabilities of the transition states are reported in **Table 6**.

Six-membered rings were formed in the α_L and γ_D conformations of the transition state between the •OH radical and Ala. However, the α_L transition state was more stable, and this is probably due to the hydrogen bond that formed between the "i – 1" carbonyl oxygen and "i + 1" amide hydrogen. The structures of the Ala transition states are also shown in **Figure 12**. The steric hindrance caused by the methyl group of Ala prevented the formation of ring structures for the α_D transition state. The hydrogen of the •OH radical may be interacting with the amide nitrogen in the case of the α_D and conformation, since the distance between these atoms is approximately 3.4 Å. These values can be found in **Table 5**. The β_L transition state was the lowest-lying Ala transition state, whereas the α_D and α_L were the highest in energy.

4.2.2.3 The Post-Reaction Complexes

The water molecule that forms after the hydrogen atom is abstracted from Gly• forms a hydrogen bond between 1.80 Å and 1.95 Å in length with a carbonyl carbon. These values are listed in **Table 5**. The γ_D and α_D transition states formed the same van der Waals complex, with ϕ and ψ angels close to 173° and -13°, respectively, and their conformation is similar to that of the γ_D conformation observed in the Gly• in the absence of H_2O. The relative energy of these van der Waals complex (16.5 kJ mol^{-1}, **Table 6**) is also similar to that of the γ_D conformation of the Gly• (21.0 kJ mol^{-1}, **Table 4**), indicating that the H_2O molecule has a

small effect on the relative stabilities of the complexes. Both the relative energies and ϕ and ψ angles of the van der Waals complexes are shown in **Table 6**. However, the γ_L and α_L transition states (35.7 kJ mol^{-1} and 39.1 kJ mol^{-1}, respectively) converged to van der Waals complexes that were similar in structure to the γ_L conformation of Gly$^{\bullet}$. The β_L van der Waals complex was the most stable and the ϕ and ψ angles of the Gly$^{\bullet}$ were -179.7^o and -179.9^o, respectively. The water molecule in the Gly$^{\bullet}$ complexes stabilized the α_L and α_D conformations more than the others.

The β_L post reaction van der Waals complex of Ala$^{\bullet}$ was the most stable. The ϕ and ψ angles of the complex were -170.2^o and 176.8^o, respectively, which deviated slightly from the ϕ and ψ angles of Ala$^{\bullet}$ in the absence of water, (-171.9^o and 176.7^o). The γ_L and α_L conformations were similar in energy, whereas the γ_D and α_D conformations were similar to each other in energy, and more stable than the γ_L and α_L conformations. This energy difference can be attributed to the orientation of the water molecule. One of the hydrogen atoms of H_2O was 2.08 Å above the "i + 1" amide nitrogen, which was hydrogen bonded to the amide nitrogen. However, this water orientation was also observed in the β_L conformation, which was the most stable. The closest distance between the oxygen of the water molecule and the carbon of the Ala side chain is 3.62 Å and 3.64 Å, in the α_L and γ_D conformations, respectively.

4.2.2.4 Relative Energies of Gly and Ala H-Abstraction Reactions

Table 7 contains the energy of the pre-reaction van der Waals complex, transition state and post-reaction complex for each of the conformations of Gly, Gly$^{\bullet}$, Ala and Ala$^{\bullet}$. The

energy values are relative to the sum of the energies of the respective Gly and Ala conformation and an infinitely separated ˙OH radical. The relative energy of the pre-reaction van der Waals complexes of Gly was between -19.0 kJ mol^{-1} and -29.4 kJ mol^{-1}, whereas the Ala values were between -1.4 kJ mol^{-1} and -25.9 kJ mol^{-1}. The formation of the γ_D pre-reaction complex of Gly was the most favorable. Moreover, the γ_D and α_D conformations of the Gly pre-reaction complexes were more stable than the respective γ_L and α_L conformations.

Table 7. The ΔE and ΔG^o of the pre-reaction complexes, transition states, and post-reaction complexes relative to the those of the reactants of the hydrogen abstraction reactions from Gly and Ala by ˙OH and the subsequent abstraction of hydrogen from H_2O_2 by Gly˙ and Ala˙.

Reaction	Conf	ΔE^o (ΔG^o) / kJ mol^{-1}			
		Pre-reaction complex	**Transition State**	**Post-reaction complex**	**Products**
Gly + ˙OH → Gly˙ + H_2O	β_L	-24.5 (9.2)	-0.8 (32.9)	-159.8 (-124.0)	-144.7 (-148.0)
	γ_L	-19.0 (10.9)	6.2 (36.2)	-127.9 (-98.0)	
	γ_D	-29.4 (2.5)	2.8 (29.3)	-147.1 (-118.8)	
	α_L	-21.4 (12.5)	9.8 (43.7)	-120.7 (-86.9)	
	α_D	-25.5 (6.9)	6.5 (38.9)	-143.3 (-110.9)	
Ala + ˙OH → Ala˙ + H_2O	β_L	-24.4 (19.6)	-1.1 (32.4)	-156.4 (-128.3)	-141.7 (-148.8)
	γ_L	-19.9 (11.8)	2.4 (34.1)	-137.1 (-105.3)	
	γ_D	-25.9 (23.2)	8.9 (35.2)	-152.3 (-124.8)	
	α_L	-24.1 (7.4)	3.1 (34.7)	-139.6 (-102.2)	
	α_D	-1.4 (23.1)	11.6 (35.2)	-143.1 (-118.5)	
Gly˙ + H_2O_2 → Gly + HO_2˙	β_L	-23.3 (9.3)	55.6 (94.8)	-53.3 (-2.1)	-15.9 (-11.1)
Ala˙ + H_2O_2 → Ala + HO_2˙	β_L	-23.1 (18.5)	50.8 (101.7)	-55.9 (-5.1)	-18.8 (-10.3)

The γ_L and α_D pre-reaction complexes of Ala were the least stable.

The β_L conformations of Gly and Ala were the lowest-lying transition states, which were

approximately 1 kJ mol^{-1} lower in energy than the respective conformation of the reactant and the $^{\bullet}OH$ radical. All of the other transition states had positive activation energies. The α_L transition state of Ala and the γ_D transition state of Gly were the next lowest-lying of the respective structures, and were within 3 kJ mol^{-1} of the β_L energies. The β_L conformation of Gly$^{\bullet}$ post-reaction complex was the most stable, which was approximately 11 kJ mol^{-1} more stable than that of the γ_D conformation, which had the second highest relative stability. Inter-residue comparison shows that the β_L post-reaction complex of Gly$^{\bullet}$ was only 2.4 kJ mol^{-1} more stable than the β_L conformation of the Ala$^{\bullet}$ post-reaction complex, which had the highest relative stability for Ala$^{\bullet}$.

Given the relative stability of the β_L conformation of Gly$^{\bullet}$ and Ala$^{\bullet}$ in the absence of H_2O, the sum of the energy of the respective structures in the β_L conformation and that of H_2O was used to represent the energy of the dissociated products, which was -144.7 kJ mol^{-1} for Gly$^{\bullet}$ + H_2O and -141.7 kJ mol^{-1} for Ala$^{\bullet}$ + H_2O. The β_L, and γ_D van der Waals complexes are more stable than the dissociated Gly$^{\bullet}$ and H_2O, whereas the γ_L, α_L and α_D complexes are not. In the case of Ala$^{\bullet}$, the β_L, α_D and γ_D complexes are more stable than the dissociated Ala$^{\bullet}$ and H_2O, whereas the γ_L and α_L were less stable than the dissociated Ala$^{\bullet}$ and H_2O.

4.2.2.6 Reforming Gly and Ala through Hydrogen Abstraction from H_2O_2

After being chemically activated by the $^{\bullet}OH$ radical, the formation of Gly$^{\bullet}$ and Ala$^{\bullet}$ radicals from the Gly and Ala residues resulted in 144.7 kJ mol^{-1} and 141.7 kJ mol^{-1} to be released in the case of Gly and Ala, respectively. The formation of the Gly$^{\bullet}$-H_2O_2 and Ala$^{\bullet}$-H_2O_2 pre-reaction complexes released 24.8 kJ mol^{-1} of energy in the case of Gly$^{\bullet}$ and 23.3 kJ

mol^{-1} for Ala$^{\bullet}$. These values can be found in **Table 7**. The transition state also had similar relative energies; however, the Ala transition state was approximately 5 kJ mol^{-1} higher than that of Gly. The geometry of the Ala$^{\bullet}$ and Gly$^{\bullet}$ transition state structures are shown in **Figure 13**. An eight-membered ring was formed between H_2O_2 and Ala$^{\bullet}$. A similar structure was observed for the Gly residue, however, the distance between the carbonyl carbon and H_2O_2 molecule was 0.9 Å larger in the Gly transition state. Moreover, the post-reaction Ala van der Waals complex (-2.6 kJ mol^{-1}) and the infinitely separated Ala and $HO_2^{\bullet}$ (-2.9 kJ mol^{-1}) were more stable than the respective Gly structures by 2.6 kJ mol^{-1} and 2.9 kJ mol^{-1}, respectively. The post-reaction van der Waals structures of both Gly and Ala were more stable than the respective non-interacting products.

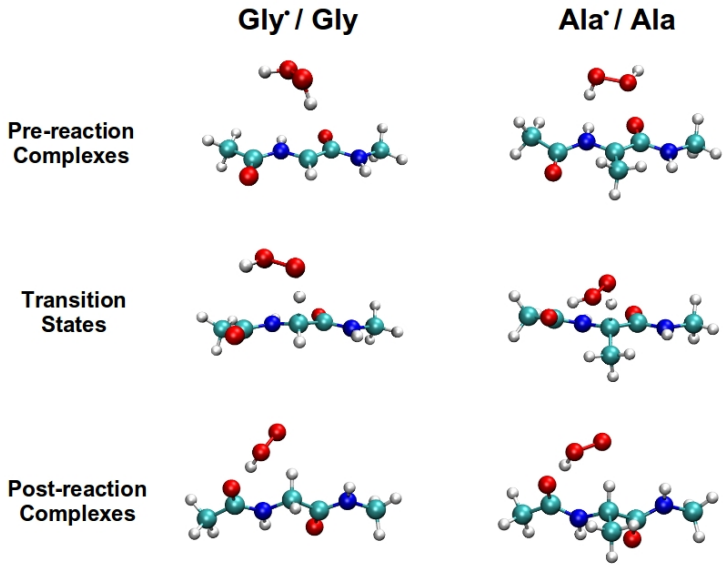

Figure 13. The pre-reaction van der Waals complexes, transition states and post-reaction complexes for the hydrogen abstraction from H_2O_2 by Gly$^{\bullet}$ and Ala$^{\bullet}$.

During the reaction in which H_2O_2 regenerates Gly, the energy stays well below the energy of the entrance level, which is the sum of the energy of $^{\bullet}$OH and the Gly residue. This

is shown in **Figure 14**. The transition state of the hydrogen abstraction reaction between Gly• and H_2O_2 is approximately 90 kJ mol^{-1} lower in energy than the energy of the entrance level, which suggests that the subsequent reaction with H_2O_2 can take place following activation by •OH.

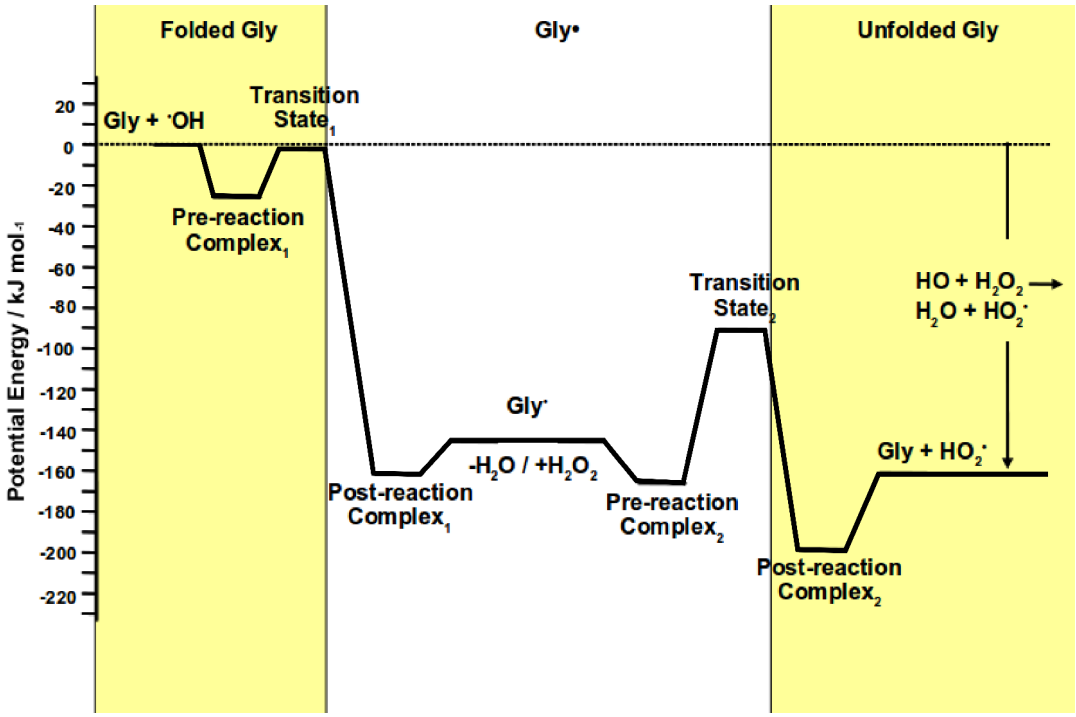

Figure 14. The reaction coordinate diagram showing the E_{pot} of the hydrogen abstraction from Gly in the β_L conformation by •OH and the subsequent hydrogen abstraction from H_2O_2 by Gly• and Ala• in the β_L conformation. The sum of the energy of Gly and •OH is used as a reference, which shows that energy of the two reactions stays below the energy of the entrance level.

4.3 Structural analysis of the Pentapeptides

The structures of the G5(C_α•) and G5(N•) peptides will be compared to the G5 peptide in the subsequent sections. **Figure 15** shows a schematic diagram of G5, and the positions from which hydrogen atoms were removed to yield the peptide radicals.

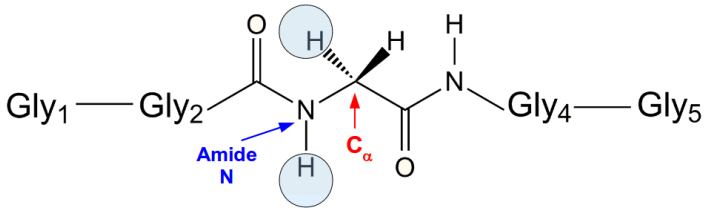

Figure 15. A schematic representation of the G5 peptide and the position of the hydrogen atoms before abstraction.

4.3.1 Comparison of G5 to the G5 Peptide Radicals

4.3.1.1 The G5 Structure

The extended conformation of the G5 peptide was conserved during the optimizations at both levels of theory and in both the gas phase and the simulated aqueous environment. A list of geometric parameters can be found in **Table 8** and **Table 9**. The ϕ and ψ angles were within 0.4° of 180.0°, indicating that the peptide remained fully extended, and also caused the peptide to remain flat, as shown in **Figure 15**. This structure was stabilized with hydrogen bonds between the amide nitrogen and carbonyl oxygen of neighboring residues.

In the case of the 3_{10} helix, the hydrogen bonds between "i" and "i +2" residues remained intact during the optimizations at both levels of theory and in both environments, thus conserving the 3_{10} helical conformation.

4.3.1.2 Deviations from the G5 Structure

The structural perturbations resulting from H-Abstraction from the C_α and amide nitrogen of residue 3 in G5 will be described in the subsequent sections.

4.3.1.3 The Effect of H-Abstraction from the C_α of G5

The removal of a hydrogen atom from the C_α decreased the length of the bonds between

the C_α and the amide nitrogen, C_α hydrogen and carbonyl carbon atoms in the gas phase by 0.079 Å, 0.016 Å and 0.077 Å, respectively, (**Table 8**) when G5 is in the extended conformation. The length of the amide bond between Gly^3 and Gly^2 increased by 0.025 Å, whereas the length of the bond between Gly^3 and Gly^4 increased by 0.011 Å. The respective amide bonds increased by 0.030 Å and 0.015 Å when the structures were optimized in the implicit solvent.

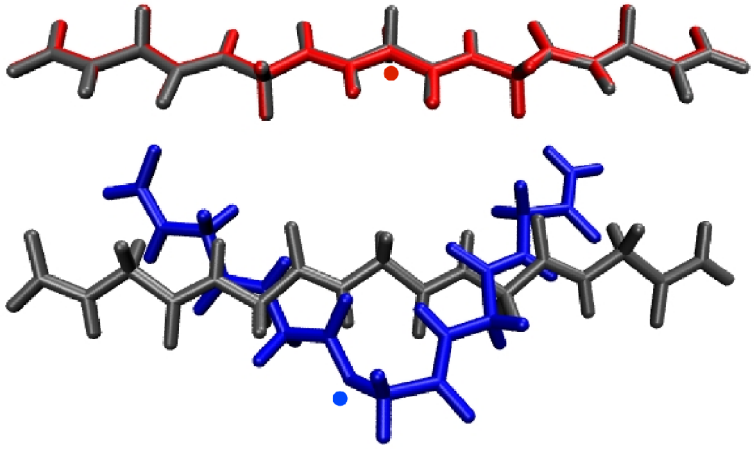

Figure 16. Structural alignment of the G5 peptide and the G5 peptide radicals in the extended conformation. The structures were obtained at the B3LYP/6-311+G(d,p) level of theory in the gas phase. The G5($C_\alpha^{\bullet}$) peptide is shown in red, the G5($N^{\bullet}$) is shown in blue and the G5 peptide is shown in gray.

Hydrogen atom abstraction from the C_α of Gly^3 also increased the length of the bond between the C_α and the amide nitrogen, C_α hydrogen and carbonyl carbon atoms in the helical conformation, as shown in **Figure 16**. The length of these bonds increased by 0.071 Å, 0.011 Å and 0.074 Å, respectively. The length of the amide bond between Gly^2 and Gly^3 increased by 0.017 Å, whereas the length of the amide bond between Gly^3 and Gly^4 increased by 0.010 Å. The respective amide bond lengths increased by 0.028 Å and 0.012 Å in the implicit

Table 8. Bond lengths in Gly^3 of G5, A($C_\alpha^\bullet$) and A($N^\bullet$) in the extended and helical conformations. The bond lengths were computed at the B3LYP/6-31G(d) and B3LYP/6-311+G(d,p) (shown in parentheses) levels of theory, both and in the gas phase and implicit solvent.

Peptide	Environment	Bond Length / Å						
		"n – 1" amide	N-C_α	N-H	C_α-H	C_α-C	C=O	"n + 1" amide
G_{Ext}	Gaseous	1.349 (1.349)	1.444 (1.445)	1.016 (1.014)	1.098 (1.095)	1.533 (1.53)	1.444 (1.445)	1.349 (1.349)
	Aqueous	1.343 (1.342)	1.446 (1.447)	1.015 (1.013)	1.097 (1.094)	1.532 (1.53)	1.446 (1.447)	1.343 (1.342)
$G(C_\alpha^\bullet)_{Ext}$	Gaseous	1.372 (1.374)	1.367 (1.366)	1.020 (1.018)	1.080 (1.079)	1.454 (1.453)	1.367 (1.366)	1.360 (1.360)
	Aqueous	1.371 (1.372)	1.367 (1.365)	1.019 (1.017)	1.080 (1.078)	1.452 (1.45)	1.367 (1.365)	1.358 (1.357)
$G(N^\bullet)_{Ext}$	Gaseous	1.373 (1.374)	1.428 (1.427)	-	1.090 (1.096)	1.584 (1.581)	1.428 (1.427)	1.344 (1.344)
	Aqueous	1.375 (1.375)	1.433 (1.434)	-	1.091 (1.09)	1.575 (1.567)	1.433 (1.434)	1.342 (1.340)
G_{Hel}	Gaseous	1.355 (1.354)	1.453 (1.454)	1.015 (1.013)	1.093 (1.091)	1.537 (1.535)	1.453 (1.454)	1.355 (1.354)
	Aqueous	1.351 (1.348)	1.450 (1.451)	1.018 (1.016)	1.093 (1.091)	1.533 (1.531)	1.450 (1.451)	1.351 (1.349)
$G(C_\alpha^\bullet)_{Hel}$	Gaseous	1.378 (1.371)	1.387 (1.383)	1.020 (1.019)	1.083 (1.08)	1.463 (1.461)	1.387 (1.383)	1.366 (1.364)
	Aqueous	1.377 (1.376)	1.382 (1.38)	1.023 (1.02)	1.080 (1.081)	1.460 (1.458)	1.382 (1.38)	1.363 (1.361)
$G(N^\bullet)_{Hel}$	Gaseous	1.363 (1.360)	1.431 (1.428)	-	1.097 (1.095)	1.541 (1.54)	1.431 (1.428)	1.351 (1.350)
	Aqueous	1.366 (1.362)	1.432 (1.431)	-	1.104 (1.096)	1.541 (1.535)	1.432 (1.431)	1.347 (1.345)

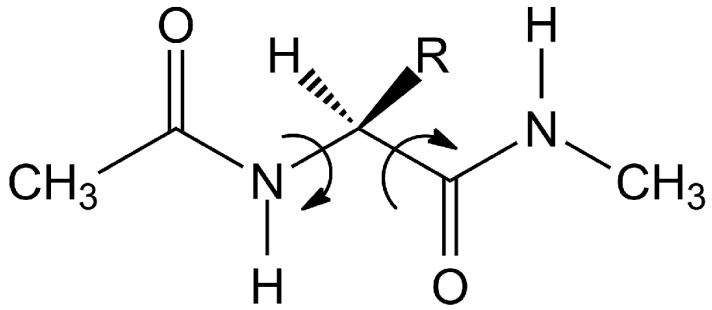

solvent.

The ϕ and ψ angles remained within one degree of full extension (180°) in the gas phase and implicit solvent, and this was also observed when both basis sets were used. The intra-residue hydrogen bond of the extended structure is 0.074 Å and 0.126 Å longer than the corresponding bond in G5 in the gas phase and implicit solvent, respectively, and these bonds were slightly shorter when the 6-31G(d) basis set was used.

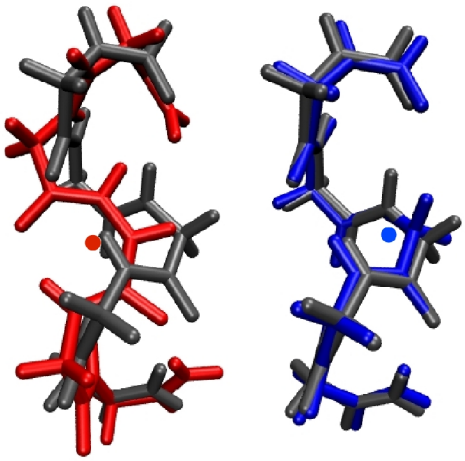

Figure 17. Structural alignment of the G5 peptide and the G5 peptide radicals in the helical conformation. The structures were obtained at the B3LYP/6-311+G(d,p) level of theory in the gas phase. The G5($C_\alpha^\bullet$) peptide is shown in red, the G5($N^\bullet$) is shown in blue and the G5 peptide is shown in gray.

Hydrogen abstraction from the C_α in the helical conformation caused the ϕ and ψ angles to go from -62.91° and -18.53°, to 0.11° and 2.87°, respectively, and an intra-residue hydrogen bond formed between the amide hydrogen and the carbonyl carbon of 2.221 Å. These results are shown in **Figure 17**. Hydrogen abstraction caused the ϕ angle to decreased

by approximately 20^{o} in the implicit solvent, whereas the change in the ψ angle was negligible. Moreover, the hydrogen bond between the amide nitrogen of Gly^{3} and carbonyl carbon of Gly^{1} dissociated and the intra-residue hydrogen bond of 2.221 Å formed between the amide hydrogen and carbonyl oxygen. The hydrogen bond between the amide nitrogen of Gly^{3} and carbonyl oxygen of Gly^{1} and that between the carbonyl oxygen of Gly^{3} and the amide nitrogen of Gly^{5} were conserved in the aqueous phase and when the smaller basis set was used. The RMSD of the peptide backbone atoms of the C_{α} peptide radical from those of G5 was 0.0725 Å and 0.132 Å in the gas phase and implicit solvent, respectively. The corresponding deviations in the helical conformation were 0.322 Å and 0.279 Å.

4.3.1.4 The Effect of H-Abstraction from the Amide Nitrogen of G5

The removal of the hydrogen atom from the amide nitrogen of the extended G5 caused the length of the bond between the amide N and the C_{α} to decrease by 0.018 Å, whereas the subsequent bond between the C_{α} and the carbonyl carbon increased by 0.051 Å. This data is shown in **Table 9**. In the helical G5(N$^{\bullet}$), the decrease in the N-C_{α} bond length was 0.026 Å and the increase in the C_{α}-C=O bond length was 0.050 Å. In both conformations the length of the amide bonds between Gly^{3} and Gly^{2} and those between Gly^{3} and Gly^{4} increased. The length of the amide bond between Gly^{3} and Gly^{2} increased by 0.026 Å in the extended conformation and 0.006 Å in the helical. The increase in the length of the bond between Gly^{3} and Gly^{4} was 0.005 Å in the extended conformation and 0.004 Å in the helical conformation.

Table 9. The ϕ and ψ dihedral angles and H-bond distances of Gly^3 in G5 and the peptide radicals in the extended and helical conformations. The geometric parameters were computed at the B3LYP/6-31G(d) and B3LYP/6-311+G(d,p) (shown in parentheses) levels of theory, both and in the gas phase and implicit solvent. The RMSD of the backbone atoms for the peptide radicals compared to those of G5 are also shown.

Peptide	Condition	Dihedral Angle		Hydrogen bond length		Backbone RMSD / Å
		ϕ / degrees	ψ / degrees	Amide H	Carbonyl O	
G_{Ext}	Gaseous	179.5 (179.9)	-179.7 (-179.9)	2.11 (2.14)	2.11 (2.14)	0.00 (0.00)
	Aqueous	179.2 (179.7)	-179.4 (-179.4)	2.12 (2.16)	2.12 (2.16)	0.00 (0.00)
$G(C_\alpha^\bullet)_{Ext}$	Gaseous	179.8 (-179.9)	179.9 (-179.9)	2.18 (2.22)	2.18 (2.22)	0.12 (0.072)
	Aqueous	-179.8 (-179.9)	-179.9 (-179.9)	2.24 (2.29)	2.24 (2.29)	0.11 (0.13)
$G(N^\bullet)_{Ext}$	Gaseous	-96.6 (-97.8)	61.1 (60.5)	-	-	2.86 (2.82)
	Aqueous	-99.5 (-102.8)	63.6 (66.9)	-	-	2.80 (2.61)
G_{Hel}	Gaseous	-62.1 (-62.9)	-19.0 (-18.5)	2.07 (2.12)	2.15 (2.12)	0.00 (0.00)
	Aqueous	-60.5 (-61.9)	-21.5 (-20.1)	2.01 (2.08)	2.06 (2.15)	0.00 (0.00)
$G(C_\alpha^\bullet)_{Hel}$	Gaseous	-38.9 (0.1)	-23.8 (2.87)	2.07 (2.05)	2.13 (2.08)	0.38 (1.99)
	Aqueous	-39.9 (-40.7)	–23.3 (–24.1)	2.03 (2.10)	2.04 (2.11)	0.33 (0.32)
$G(N^\bullet)_{Hel}$	Gaseous	-3.4 (-3.3)	-52.5 (-51.8)	-	2.15 (2.22)	0.28 (0.27)
	Aqueous	6.4 (6.4)	-58.2 (-47.3)	-	2.06 (2.13)	0.29 (0.48)

In the extended structure, the absence of the H atom in the amide nitrogen prevents the formation of the intra-residue hydrogen bond; however, a hydrogen bond was formed between the carbonyl oxygen of Gly^2 and the amide nitrogen of Gly^4. It is suspected that this contributes to the ≈ 80° and 120° respective differences between the ϕ and ψ angles of the native G5 peptide in the extended conformation and those of the extended G5($N^\bullet$) (**Table 9**). This change in hydrogen bonding is reflected in the RMSD, which showed that the backbone of the extended G5($N^\bullet$) deviated from the backbone of the G5 peptide by 2.82 Å. In the helical G5($N^\bullet$), H-abstraction from the amide nitrogen eliminated the hydrogen bond with the carbonyl carbon of Gly^1. The loss of the hydrogen bond resulted in a decrease in the ϕ angle of approximately 60°, whereas the ψ angle changed by approximately 10°. These

perturbations in structure was also shown in the RMSD analysis, however this deviation was only 0.279 Å.

4.3.2 Comparison of A5 to the A5 Peptide Radicals

The structures of the A5($C_\alpha^\bullet$), A5($C_\beta^\bullet$) and A5($N^\bullet$) peptides are compared to the A5 peptide in the subsequent sections. **Figure 18** shows a schematic diagram of A5, and the positions from which hydrogen atoms were removed to yield the corresponding peptide radicals.

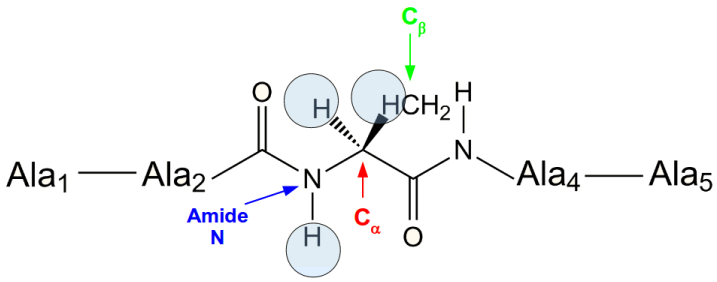

Figure 18. A schematic representation of the A5 peptide and the position of the hydrogen atoms before abstraction.

4.3.2.1 The A5 Pentapeptide

The extended conformation of the A5 peptide was conserved during the optimizations at both levels of theory and in both the gas phase and the simulated aqueous environment. A list of geometric parameters can be found in **Table 10** and **Table 11**. The ϕ and ψ angles were approximately -155° and 160°, respectively, causing the peptide to appear 'pleated', as shown in **Figure 16**. This peptide was not as extended as the G5 peptide was. This structure was stabilized with hydrogen bonds between the amide nitrogen and carbonyl oxygen of neighboring residues.

The hydrogen bonds between "i" and "i + 2" residues of the $A5_{HEL}$ peptide remained

intact during the optimizations at both levels of theory and in both environments, thus conserving the structure of the 3_{10} helix.

The structural perturbations resulting from H-Abstraction from the Ca and amide nitrogen of residue 3 in A5 will be described in the subsequent sections.

4.3.2.2 The Effect of H-Abstraction from the C_α of A5

The removal of the hydrogen atom from the C_α decreased the length of the bonds between the C_α and the amide nitrogen, methyl carbon (C_β) and carbonyl carbon atoms in the

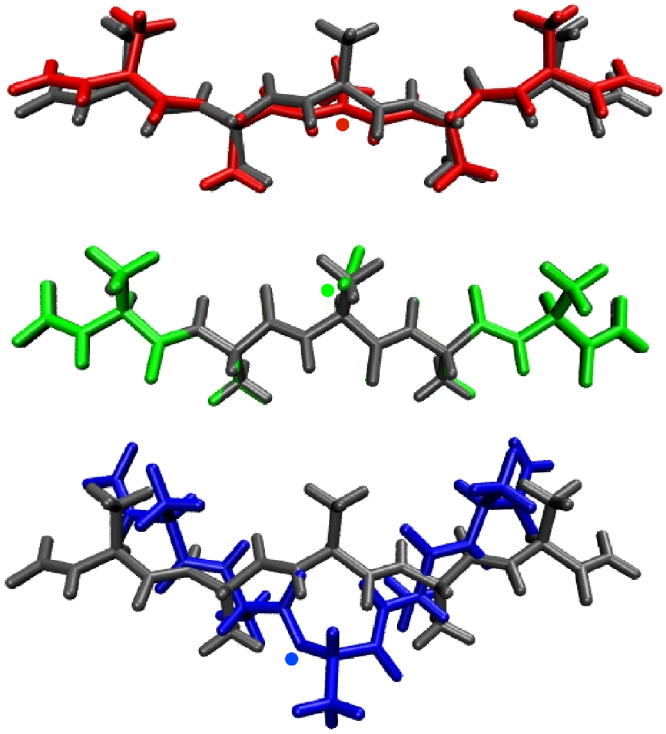

Figure 19. Structural alignment of the A5 peptide and the A5 peptide radicals in the extended conformation. The structures were obtained at the B3LYP/6-311+G(d,p) level of theory in the gas phase. The alignment of A5($C_\alpha^\bullet$) peptide is shown in red (top), that of A5(Me$^\bullet$) is shown in green (middle) and that of A5(N$^\bullet$) is shown in blue (bottom), whereas the A5 peptide is shown in gray. The RMSD of the structural alignments can be found in Table 11.

gas phase by 0.074 Å, 0.049 Å and 0.072 Å, respectively (**Table 10**). The observed decrease

in bond length was slightly less pronounced when the 6-31G(d) basis set was used. The length of the amide bond between Ala^3 and Ala^2 increased by 0.020 Å, whereas the length of the bond between Ala^3 and Ala^4 increased by 0.012 Å. The respective amide bonds increased by 0.024 Å and 0.013 Å when the structures were optimized in the implicit solvent.

The pleats in the A5 peptide in the extended conformation can be shown in **Figure 19**, and is also characterized by ϕ and ψ angles of -157.42° and 164.65°. The removal of the hydrogen atom from the C_α caused the dihedral angles to become more planar, with ϕ and ψ angles of 177.66° and -177.89°, respectively. The increased planarity was observed only at

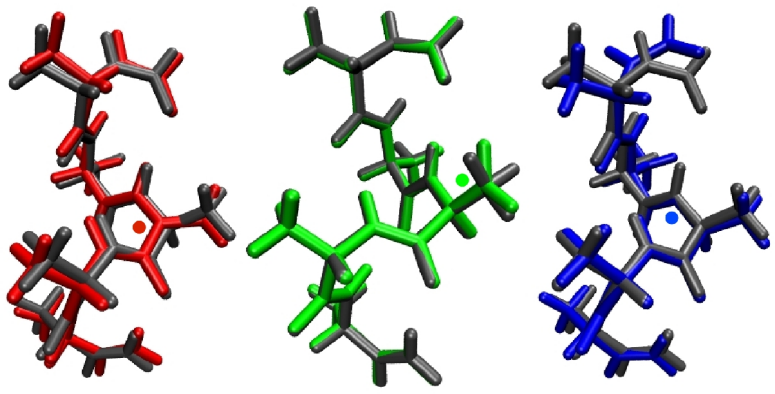

Figure 20. Structural alignment of the A5 peptide and the A5 peptide radicals in the helical conformation. The structures were obtained at the B3LYP/6-311+G(d,p) level of theory in the gas phase. The alignment of A5($C_\alpha^\bullet$) peptide is shown in red (left), that of A5($Me^\bullet$) is shown in green (middle) and that of A5($N^\bullet$) is shown in blue (right), whereas the A5 peptide is shown in gray. The RMSD of the structural alignments can be found in Table 11.

the Ala^3 of the A5($C_\alpha^\bullet$) peptide, whereas the remaining residues retained the pleats shown in the A5 peptide. The intra-residue hydrogen bond between the amide nitrogen and the carbonyl oxygen decreased by 0.083 Å when the 6-311+G(d,p) basis set was used, which is 0.057 Å more than what was computed with the 6-31G(d) basis set. The RMSD of the

peptide backbone containing the C_α radical from that of the A5 peptide was 0.781 Å in the gas phase, and 1.04 Å in the implicit solvent. These results are shown in **Table 11**.

Similar to what was shown in the extended conformation, hydrogen atom abstraction from the C_α of Ala^3 increased the length of the bond between the C_α and the amide nitrogen, C_β and carbonyl carbon atoms in the helical conformation, as shown in **Figure 15**. The length of these bonds decreased by 0.062 Å, 0.042 Å and 0.073 Å, respectively. The length of the amide bond between Ala^2 and Ala^3 increased by 0.019 Å, whereas the length of the amide bond between Ala^3 and Ala^4 increased by 0.013 Å. The respective amide bond lengths increased by 0.021 Å and 0.015 Å in the implicit solvent. Hydrogen abstraction from the C_α in the helical conformation caused the ϕ dihedral angle to adopt a conformation that is moreplanar, as indicated by the ϕ angle changing from of -157.42° to 177.66°, however, the change in the ψ angle was negligible. This data is presented in **Table 11**. The hydrogen bond between the amide nitrogen of Ala^3 and carbonyl carbon of Ala^1 decreased by 0.033 Å, whereas the hydrogen bond between the carbonyl carbon of Ala^3 and the amide nitrogen of Ala^5 decreased by 0.013 Å. Changes in dihedral angles suggest that there is a stronger coupling between C_α and the amide nitrogen than between the C_α and the carbonyl carbon. The RMSD of the C_α peptide radical backbone from the backbone of the A5 peptide was 0.781 Å and 1.04 Å, respectively. This data is shown in **Table 11**.

4.3.2.3 The Effect of H-Abstraction from the C_β of Ala^3

Hydrogen abstraction from the methyl group of A5 in the extended conformation caused increased the length of the bond between C_β and C_α by 0.045 Å This bond decreased by

0.042 Å in the helical conformation as shown in **Table 10**. The remaining bond lengths in Ala^3 changed by less than 0.003 Å in both conformations. Moreover, the length of the amide bond between Ala^2 and Ala^3 decreased by only 0.001 Å, whereas the length of the bond between Ala^3 and Ala^4 decreased by 0.002 Å, with a negligible change shown to the respective bond lengths in optimized in the implicit solvent. The decrease in the intra-residue hydrogen bond distance compared to the extended and helical A5 was also negligible. Also, the ϕ and ψ dihedral angles of the extended and helical A5(N•) deviated from the respective native A5 peptide by less than 5° and the RMSD from the backbone of

Table 11. The ϕ and ψ dihedral angles and H-bond distances of Ala^3 in A5 and the peptide radicals in the extended and helical conformations. The geometric parameters were computed at the B3LYP/6-31G(d) and B3LYP/6-311+G(d,p) (shown in parentheses) levels of theory, both and in the gas phase and implicit solvent. The RMSD of the backbone atoms for the peptide radicals compared to those of A5 are also shown.

Peptide	Environment	Dihedral Angle		Hydrogen bond length		Backbone RMSD / Å
		ϕ / degrees	ψ / degrees	Amide N	Carbonyl C	
A_{Ext}	Gaseous	-160.0 (-157.4)	167.3 (164.6)	2.10 (2.11)	2.10 (2.11)	0.00 (0.00)
	Aqueous	-158.5 (-152.5)	162.1 (157.4)	2.14 (2.22)	2.14 (2.22)	0.00 (0.00)
$A(C_\alpha^\bullet)_{Ext}$	Gaseous	-178.7 (177.6)	-179.5 (-177.8)	2.02 (2.03)	2.02 (2.03)	0.673 (0.781)
	Aqueous	178.1 (172.9)	178.9 (-177.2)	2.04 (2.06)	2.04 (2.06)	0.854 (1.04)
$A(^\bullet CH_3)_{Ext}$	Gaseous	-164.4 (-160.6)	-163.1 (171.5)	2.06 (2.10)	2.06 (2.10)	0.0623 (0.168)
	Aqueous	-163.1 (-159.0)	169.2 (161.0)	2.10 (2.17)	2.10 (2.17)	0.192 (0.143)
$A(N^\bullet)_{Ext}$	Gaseous	-98.2 (-98.6)	66.0 (72.6)	-	-	2.72 (2.53)
	Aqueous	-100.7 (-102.5)	67.0 (69.1)	-	-	2.59 (2.43)
A_{Hel}	Gaseous	-63.2 (-64.6)	-19.9 (-18.4)	2.10 (2.18)	2.15 (2.17)	0.00 (0.00)
	Aqueous	-61.1 (-63.2)	-24.3 (-20.9)	2.06 (2.17)	2.08 (2.11)	0.00 (0.00)
$A(C_\alpha^\bullet)_{Hel}$	Gaseous	-45.5 (-45.9)	-21.6 (-22.4)	2.07 (2.12)	2.13 (2.17)	0.352 (0.345)
	Aqueous	-45.0 (-45.6)	-22.0 (-22.7)	2.03 (2.12)	2.04 (2.08)	0.421 (0.346)
$A(^\bullet CH_3)_{Hel}$	Gaseous	-61.3 (-62.2)	-24.4 (-22.5)	2.11 (2.17)	2.19 (2.21)	0.097 (0.066)
	Aqueous	-59.7 (-60.8)	-26.8 (-24.3)	2.06 (2.15)	2.08 (2.12)	0.054 (0.032)
$A(N^\bullet)_{Hel}$	Gaseous	-80.1 (-81.4)	-11.3 (-12.5)	-	2.26 (2.30)	0.64 (0.524)
	Aqueous	-81.5 (-86.0)	-13.6 (-22.9)	-	2.17 (2.15)	0.65 (1.25)

Table 10. Bond lengths in Ala^3 of A5, $A(C_\alpha^\bullet)$, $A(^\bullet CH_3)$ and $A(N^\bullet)$ in the extended and helical conformations. The bond lengths were computed at the B3LYP/6-31G(d) and B3LYP/6-311+G(d,p) (shown in parentheses) levels of theory, both and in the gas phase and implicit solvent.

Peptide	Environment	Bond Length (Å)						
		"n – 1" amide	N-C_α	N-H	C_α-C_β	C_α-C	C=O	"n + 1" amide
A_{Ext}	Gaseous	1.350 (1.349)	1.452 (1.454)	1.015 (1.013)	1.540 (1.539)	1.539 (1.538)	1.232 (1.227)	1.350 (1.349)
	Aqueous	1.345 (1.344)	1.455 (1.457)	1.015 (1.013)	1.540 (1.539)	1.538 (1.536)	1.236 (1.232)	1.345 (1.344)
$A(C_\alpha^\bullet)_{Ext}$	Gaseous	1.370 (1.369)	1.379 (1.380)	1.023 (1.020)	1.494 (1.490)	1.467 (1.466)	1.247 (1.243)	1.361 (1.361)
	Aqueous	1.369 (1.344)	1.379 (1.380)	1.022 (1.019)	1.494 (1.490)	1.467 (1.465)	1.251 (1.248)	1.357 (1.357)
$A(CH_2^\bullet)_{Ext}$	Gaseous	1.352 (1.351)	1.459 (1.457)	1.016 (1.014)	1.459 (1.494)	1.558 (1.558)	1.231 (1.225)	1.347 (1.347)
	Aqueous	1.347 (1.345)	1.456 (1.457)	1.016 (1.013)	1.496 (1.495)	1.558 (1.556)	1.234 (1.229)	1.344 (1.342)
$A(N^\bullet)_{Ext}$	Gaseous	1.371 (1.371)	1.434 (1.432)	-	1.529 (1.529)	1.593 (1.593)	1.222 (1.216)	1.345 (1.345)
	Aqueous	1.372 (1.371)	1.439 (1.440)	-	1.530 (1.530)	1.585 (1.581)	1.226 (1.223)	1.343 (1.342)
A_{Hel}	Gaseous	1.354 (1.353)	1.460 (1.461)	1.016 (1.014)	1.531 (1.530)	1.543 (1.541)	1.232 (1.227)	1.354 (1.353)
	Aqueous	1.350 (1.349)	1.458 (1.459)	1.019 (1.016)	1.533 (1.531)	1.539 (1.538)	1.239 (1.235)	1.351 (1.348)
$A(C_\alpha^\bullet)_{Hel}$	Gaseous	1.373 (1.372)	1.400 (1.399)	1.020 (1.018)	1.490 (1.488)	1.470 (1.468)	1.242 (1.237)	1.367 (1.366)
	Aqueous	1.371 (1.370)	1.395 (1.395)	1.022 (1.020)	1.490 (1.488)	1.465 (1.463)	1.250 (1.246)	1.364 (1.363)
$A(CH_2^\bullet)_{Hel}$	Gaseous	1.353 (1.352)	1.458 (1.459)	1.015 (1.013)	1.489 (1.488)	1.562 (1.561)	1.229 (1.224)	1.353 (1.351)
	Aqueous	1.350 (1.349)	1.456 (1.456)	1.018 (1.016)	1.491 (1.489)	1.557 (1.489)	1.236 (1.232)	1.350 (1.347)
$A(N^\bullet)_{Hel}$	Gaseous	1.377 (1.372)	1.421 (1.419)	-	1.534 (1.534)	1.589 (1.588)	1.225 (1.219)	1.342 (1.342)
	Aqueous	1.380 (1.374)	1.427 (1.438)	-	1.535 (1.538)	1.574 (1.558)	1.231 (1.226)	1.344 (1.344)

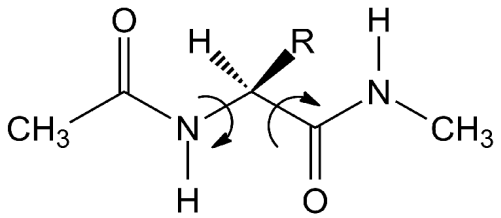

A5 was only 0.168 Å.

4.3.2.4 The Effect of H-Abstraction from the Amide Nitrogen of Ala^3

The removal of the hydrogen atom from the amide nitrogen caused the length of the bond between the amide N and the C_α to decrease by 0.022 Å, whereas the subsequent bond between the C_α and the carbonyl carbon increased by 0.055 Å. In the helical A5($N^\bullet$) the decrease in the N-C_α bond length was 0.042 Å and the increase in the C_α-C=O bond length was 0.047 Å. In both conformations the length of the amide bonds between Ala^3 and Ala^2 and those between Ala^3 and Ala^4 increased. The length of the amide bond between Ala^3 and Ala^2 increased by 0.022 Å in the extended conformation and 0.019 Å in the helical, whereas the change in the length of the amide bond between Ala^3 and Ala^4 was negligible.

In the extended structure, the absence of the H atom prevented the formation of the intra-residue hydrogen bond; however, a hydrogen bond was formed between the carbonyl oxygen of Ala^2 and the amide nitrogen of Ala^4. It is suspected that this contributed to the roughly 60° difference between the ϕ and ψ angles of the native A5 peptide in the extended conformation and those of the extended A5($N^\bullet$). In the helical A5($N^\bullet$), H abstraction from the amide nitrogen cleaved the hydrogen bond with the carbonyl carbon of Ala^1. The loss of the hydrogen bond resulted in a decrease in the ϕ angle by 20°. The ψ angle, deviated by less than 10°. The large perturbations in structure also appears in the RMSD value, which showed a deviation of 2.72 Å from the backbone of the A5 peptide.

4.4 Thermodynamic Analysis of the Pentapeptides

The ΔG^{o}, ΔH^{o} and ΔS^{o} calculated for the H-abstraction from G5 and A5 by the ROS and the subsequent unfolding are described in the subsequent sections.

4.4.1 H-Abstraction from G5.

Gas phase results at the 6-311+G(d,p) basis set shows that the strength of the C_{α}-H bond is less than that of the N-H bond of the amide group, as shown in **Table 12**. Hydrogen abstraction from the C_{α} whilst the peptide is in the extended conformation needs 109.6 kJ mol^{-1} less energy than that released from the amide nitrogen in the same conformation. The difference between BDE of the C_{α}-H bond and that of the N-H bond in the helical conformation is 86.1 kJ mol^{-1}. The BDE values of the C_{α}-H and N-H bonds showed a conformational dependence, as shown by the lower BDE of the peptide in the helical conformation. Hydrogen abstraction from the C_{α} requires 28.4 kJ mol^{-1} less energy in the extended conformation than in the helical conformation, whereas hydrogen abstraction from the amide nitrogen required 4.9 kJ/mol less energy in the extended conformation.

The results obtained in the implicit solvent are within 1% of those obtained in the gas phase. The greatest deviation between the results obtained with the 6-31G(d) basis set and those obtained with the 6-311+G(d,p) basis set was shown in the helical G5($C_{\alpha}^{\bullet}$) peptide computed in the gas phase and the G5($N^{\bullet}$) peptide in the extended conformation, which had deviations of less than 3%.

The bond dissociation energy energy can act as a measure of the relative stability of the peptide radicals since both of the peptides are derived from the same reactant and have the

same co-product, an infinitely separated hydrogen atom. Therefore, the results in the gas phase with the 6-311+G(d,p) basis set indicate that G5(C_α•) is 109.6 kJ mol^{-1} more stable than G5(N•). The relative stabilities computed in the implicit solvent model are within 1% of the gas phase values, and a similar deviation was observed between the two basis sets. When in a helix, G5(C_α•) is 86.1 kJ mol^{-1} more stable than G5(N•). The deviations from the relative stability values in $G5_{Ext}$ were negligible when the implicit solvent and the smaller basis set was used.

Table 12. Reactions of •OH, HO_2• and O_2•$^-$ with G5 in the helical and extended conformations. The bond dissociation energy and helical to extended unfolding are computed at the B3LYP/6-31G(d) and B3LYP/6-311+G(d,p) (in parenthesis).

Peptide	Environment	Bond Dissociation Energy / kJ mol^{-1}		Transition from Helical to Extended		
		Extended	Helix	ΔH^o / kJ mol^{-1}	ΔG^o / kJ mol^{-1}	ΔS^o / J mol^{-1} K^{-1}
G5	Gaseous	-	-	3.3 (-3.6)	-32.7 (-36.2)	62.8 (109.2)
	Aqueous	-	-	20.8 (10.4)	-12.4 (-20.5)	111.6 (104.2)
G5(C_α•)	Gaseous	370.7 (368.6)	411.6 (397.0)	-36.0 (-31.8)	-64.8 (-55.7)	48.1 (80.2)
	Aqueous	370.9 (368.8)	409.2 (407.3)	-15.7 (-26.1)	-44.6 (-52.7)	97.0 (89.1)
G5(N•)	Gaseous	465.6 (478.2)	474.4 (483.1)	-3.4 (-6.3)	-26.5 (-30.3)	65.0 (80.5)
	Aqueous	469.7 (482.4)	484.4 (489.7)	8.2 (5.3)	-13.6 (-16.2)	73.6 (72.3)

4.4.2 Unfolding of $G5_{HEL}$

The change in standard free energy (ΔG^o) calculated with the 6-311+G(d,p) basis set are all negative when computed in the gas phase, and the corresponding gain in entropy under these conditions indicates that the helical unfolding is mainly entropy-driven. The ΔG^o values were also negative for the calculations done in implicit solvent and those computed with the 6-31G(d) basis set, and these results can be found in **Table 12**. The difference in the

ΔG^o measured in the gas phase with the 6-311+G(d,p) basis set indicates that the unfolding of G5(N$^\bullet$) is 5.9 kJ mol^{-1} less favorable than the unfolding of G5. However, calculations in the same conditions indicate that the unfolding of G5($C_\alpha^\bullet$) is more favorable than the unfolding of G5 by -19.5 kJ mol^{-1}. The unfolding of G5($C_\alpha^\bullet$) is 28.2 kJ mol^{-1} more exothermic than the unfolding of G5 and 25.5 kJ mol^{-1} more exothermic than the unfolding of G5(N$^\bullet$), which suggests that increased tendency of G5($C_\alpha^\bullet$) to unfold is enthalpy-driven. Moreover, the unfolding of G5($C_\alpha^\bullet$) and G5(N$^\bullet$) produced less entropy than the unfolding of G5, by 29.0 J mol^{-1}K^{-1} and 28.7 J mol^{-1}K^{-1}, respectively. The unfolding of each peptide is more favorable in the implicit solvent than in the gas phase.

4.4.3 Reactions of G5 with Reactive Oxygen Species

The change in free energy computed in the gas phase with the 6-311+G(d,p) basis set showed that only the reass entropy than the unfolding of G5, by 29.0 J ctions involving the $^\bullet$OH radical and the G5 extended peptide are exergonic. These results can be found in **Table 13**. Reactions with the $^\bullet$OH radical at the C_α of G5 in the gas phase releases 141.5 kJ mol^{-1} of free energy. The reactions with the $HO_2^\bullet$ and $O_2^{-\bullet}$ radicals at the C_α are both endergonic, and require 28.8 kJ mol^{-1} and 81.6 kJ mol^{-1}, respectively, to proceed. These results were qualitatively similar to those computed with G5 in the helical conformation, however hydrogen abstraction from helical $G5_{Hel}$ was less favorable. The ΔG^o with $^\bullet$OH released only 122.0 kJ mol^{-1}, whereas the reaction with $HO_2^\bullet$ requires 48.3 kJ mol^{-1} to proceed and that of the $O_2^{-\bullet}$ requires an influx of 101.1 kJ mol^{-1} into the system. The relative reactivity of the

ROS observed at the amide nitrogen are similar to that observed at the C_α. However hydrogen abstraction from the amide nitrogen is less favorable. The reactions at the amide nitrogen were still exergonic, however the ΔG^o was only -32.8 kJ mol^{-1}. The ΔG^o of the reactions with the $^{\bullet}OH$ radical at the C_α released 108.7 kJ mol^{-1} more free energy than hydrogen abstraction from the amide nitrogen. Moreover, the relative propensity of $HO_2^{\bullet}$ and $O_2^{-\bullet}$ to abstract a hydrogen atom from the C_α is similar to that of $^{\bullet}OH$.

The relative enthalpy of the ROS and that of each H-abstraction reactions was similar to the trends observed for their free energy. The enthalpy change of the reaction with $^{\bullet}OH$ at the C_α in the gas phase using the 6-311+G(d,p) basis set was -140.0 kJ mol^{-1}, whereas the reaction with the $HO_2^{\bullet}$ and $O_2^{-\bullet}$ were both endothermic, requiring 27.2 kJ mol^{-1} and 86.3 kJ mol^{-1} of heat, respectively, to proceed. The enthalpy in the implicit solvent was within 10% of the gas phase values.

A gain in entropy contributed to the gas phase reaction of $^{\bullet}OH$ (4.8 J $mol^{-1}K^{-1}$) and $O_2^{-\bullet}$ (15.6 J $mol^{-1}K^{-1}$) at the C_α when G5 was in the extended conformation whereas entropy was lost in the reaction at the same site with $HO_2^{\bullet}$ (-5.4 J $mol^{-1}K^{-1}$). Entropy was lost during hydrogen abstraction from the $^{\bullet}OH$ (-1.7 J $mol^{-1}K^{-1}$), $HO_2^{\bullet}$ (-12.0 J $mol^{-1}K^{-1}$) during abstraction at the amide nitrogen, whereas 9.0 J $mol^{-1}K^{-1}$ of entropy was gained when a hydrogen atom was abstracted by $O_2^{-\bullet}$. Hydrogen abstraction from the amide nitrogen of the helical G5 caused an increase in entropy for all three ROS.

4.4.4 H-Abstraction from A5.

Gas phase results at the 6-311+G(d,p) basis set shows that the strength of the C_α-H bond

Table 13. The enthalpy, free energy and entropy of the reactions of $^{\bullet}OH$, $HO_2^{\bullet}$ and $O_2^{-\bullet}$ with G5, producing the G($C_\alpha^{\bullet}$) and G($N^{\bullet}$) radicals in the helical and extended conformations. The values were computed in the gas phase and implicit solvent, at the B3LYP/6-31G(d) and B3LYP/6-311+G(d,p) (in parenthesis) levels of theory.

Reactants	Environment	ΔH^o / kJ mol^{-1}		ΔG^o / kJ mol^{-1}		ΔS^o / J mol^{-1} K^{-1}	
		C_α	N	C_α	N	C_α	N
$^{\bullet}OH + G5_{Ext}$	Gaseous	-134.7 (-140.0)	-42.3 (-33.3)	-112.0 (-141.5)	-17.76 (-32.8)	-10.8 (4.8)	-17.1 (-1.7)
	Aqueous	-121.5 (-146.8)	-25.4 (-36.3)	-120.9 (-145.8)	-23.60 (-39.3)	-2.1 (-3.3)	-6.2 (10.1)
$HO_2^{\bullet} + G5_{Ext}$	Gaseous	19.7 (27.2)	112.1 (133.9)	58.3 (28.8)	152.59 (137.5)	-21.2 (-5.4)	-27.6 (-12.0)
	Aqueous	36.1 (10.8)	132.2 (121.3)	39.9 (14.9)	137.28 (121.3)	-12.6 (-13.6)	-16.7 (-0.2)
$O_2^{-\bullet} + G5_{Ext}$	Gaseous	87.2 (86.3)	179.6 (193.0)	87.3 (81.6)	181.62 (190.3)	-0.1 (15.6)	-6.4 (9.0)
	Aqueous	89.0 (87.8)	185.1 (198.3)	86.5 (85.6)	183.86 (192.1)	8.4 (7.3)	4.3 (20.7)
$^{\bullet}OH + G5_{Hel}$	Gaseous	-95.4 (-111.8)	-35.6 (-30.6)	-79.9 (-122.0)	-24.03 (-38.6)	13.6 (33.9)	26.5 (27.0)
	Aqueous	-85.0 (-110.2)	-12.8 (-31.2)	-88.7 (-113.7)	-22.37 (-43.7)	12.4 (11.7)	31.7 (41.9)
$HO_2^{\bullet} + G5_{Hel}$	Gaseous	59.1 (55.3)	118.8 (136.6)	90.3 (48.3)	146.33 (131.6)	3.2 (23.5)	16.0 (16.6)
	Aqueous	72.7 (47.4)	144.8 (126.4)	72.1 (47.0)	138.50 (117.0)	1.9 (1.3)	21.2 (31.6)
$O_2^{-\bullet} + G5_{Hel}$	Gaseous	126.6 (114.4)	186.4 (195.7)	119.3 (101.1)	175.36 (184.4)	24.3 (44.6)	37.1 (37.7)
	Aqueous	125.5 (124.4)	197.7 (203.4)	118.6 (117.8)	185.08 (187.7)	23.0 (22.3)	42.3 (52.6)

was less than that of the C_β-H bond of the Ala side chain and that of the N-H bond of the amide group. As presented in **Table 14,** hydrogen abstraction from the C_α whilst the peptide is in the extended conformation requires 83.5 kJ mol^{-1} and 106.2 kJ mol^{-1} less energy than from C_β and the amide nitrogen, respectively. The difference between BDE of C_α-H bond and those of the C_β-H and N-H bonds in the helical conformation is 58.2 kJ mol^{-1} and 92.7 kJ mol^{-1}, respectively. The BDE values of the C_α-H and N-H bonds showed a conformational dependence, as shown by the lower BDE of the peptide in the helical conformations.

Hydrogen abstraction from the C_α required 23.4 kJ mol^{-1} less energy in the extended conformation than in the helical conformation, whereas hydrogen abstraction from the amide nitrogen required 9.9 kJ mol^{-1} less energy in the extended conformation. The results obtained in the implicit solvent are within 1% of those obtained in the gas phase. The greatest deviation between the results obtained with the 6-31G(d) basis set and those obtained with the 6-311+G(d,p) basis set was shown in the A5(N$^\bullet$) peptide, which had a deviation of less than 3%.

The bond dissociation energy values can act as a measure of the relative peptide radical stability in this case as well. Therefore, the results in the gas phase with the 6-311+G(d,p) basis set indicate that A5($C_\alpha^\bullet$) is 83.5 kJ mol^{-1} more stable than A5($CH_2^\bullet$) and 106.2 kJ mol^{-1} more stable than A5(N$^\bullet$). The relative stabilities computed in the implicit solvent model are within 1% of the gas phase values, and a similar deviation was observed between the two basis sets. When in a helix, A5($C_\alpha^\bullet$) is 58.2 kJ mol^{-1} more stable than A5($^\bullet CH_3$) and 92.7 kJ mol^{-1} more stable than A5(N$^\bullet$). As shown in the extended the conformation, the deviations

Table 14. Reactions of $^{\bullet}OH$, $HO_2^{\bullet}$ and $O_2^{-\bullet}$ with A5 in the helical and extended conformations. The free energy of H abstraction and helical to extended unfolding are computed at the B3LYP/6-31G(d) and B3LYP/6-311+G(d,p) (in parenthesis).

Peptide	Environment	Bond Dissociation Energy / kJ mol^{-1}		Transition from Helical to Extended Conformation		
		Extended	Helix	ΔH^o / kJ mol^{-1}	ΔG^o / kJ mol^{-1}	ΔS^o / J mol^{-1} K^{-1}
A5	Gaseous	-	-	10.8 (2.3)	-7.8 (-17.8)	62.8 (67.9)
	Aqueous	-	-	29.5 (15.2)	9.0 (-7.3)	68.6 (75.5)
A5($C_\alpha^{\bullet}$)	Gaseous	366.4 (367.5)	393.0 (390.9)	-13.4 (-19.0)	-27.7 (-36.4)	48.1 (58.5)
	Aqueous	369.2 (370.4)	390.0 (387.6)	9.2 (0.0)	-14.2 (-18.4)	78.8 (61.6)
A5($^{\bullet}CH_3$)	Gaseous	456.9 (451.0)	455.2 (449.1)	12.7 (4.5)	-6.6 (-16.6)	65.0 (70.8)
	Aqueous	455.6 (449.3)	455.6 (450.1)	29.1 (14.4)	8.5 (-9.1)	68.9 (79.1)
A5($N^{\bullet}$)	Gaseous	461.4 (473.7)	475.9 (483.6)	-2.5 (-6.4)	-13.1 (-19.7)	35.6 (44.7)
	Aqueous	463.8 (476.6)	489.1 (486.6)	4.1 (5.2)	-8.9 (-3.2)	43.7 (28.6)

from the relative stability values were negligible when the implicit solvent and the smaller basis set was used.

4.4.5 Unfolding of $A5_{HEL}$

The change in standard free energy (ΔG^o), calculated with the 6-311+G(d,p) basis set are all negative when computed in the gas phase, and the corresponding gain in entropy under these conditions indicates that this conformational change is mainly entropy-driven. These results can be found in **Table 14**. The ΔG^o for the helix to extended conformational change of A5($CH_2^{\bullet}$) and A5($N^{\bullet}$) are similar to that of the A5 peptide, however, the unfolding of A5($C_\alpha^{\bullet}$) is more favorable than the unfolding of A5 by -18.6 kJ mol^{-1}. The unfolding of A5($C_\alpha^{\bullet}$) is 16.7 kJ mol^{-1} more exothermic than the unfolding of A5, which suggests that increased tendency of A5($C_\alpha^{\bullet}$) to unfold is enthalpy-driven. The unfolding of A5($N^{\bullet}$) is 8.7 kJ mol^{-1} more exothermic than the unfolding of the A5 peptide. Moreover, the unfolding of A5($C_\alpha^{\bullet}$) and A5($N^{\bullet}$) showed smaller increases in entropy than the unfolding of A5, by 9.4 J

$mol^{-1}K^{-1}$ and 23.2 J $mol^{-1}K^{-1}$, respectively. The unfolding of each peptide was less favorable in the implicit solvent than the gas phase.

4.4.6 Reactions of A5 with Reactive Oxygen Species

The change in free energy computed in the gas phase with the 6-311+G(d,p) basis set showed that only the reactions involving the $^{\bullet}OH$ radical and the A5 extended peptide were exergonic. These results can be found in **Table 15**. For reactions at the C_α of A5 in the gas phase, the reactions involving the $^{\bullet}OH$ radical released 167.2 kJ mol^{-1} more free energy than those with the $HO_2^{\bullet}$ radical and 226.3 kJ mol^{-1} more free energy than with the $O_2^{-\bullet}$ radical. The reaction Gibbs free energy values indicate that the C_α is more susceptible than the C_β and amide nitrogen to H-abstraction by the ROS. The reaction of $^{\bullet}OH$ with A5 at the C_α released 79.3 kJ mol^{-1} more free energy than the abstraction from the CH_3 and 102.4 kJ mol^{-1} more energy than the abstraction from the amide nitrogen. The ΔH^o values of the reactions with each of the ROS were similar to those of the ΔG^o values. The H abstraction reactions of each ROS in the gas phase gained entropy, irrespective of the location. Hydrogen abstraction from C_α and the amide nitrogen showed a decrease of enthalpy in the implicit solvent, whereas the reactions with $O_2^{-\bullet}$ radical showed the largest gain in entropy. Results in the gas phase with the 6-311+G(d,p) basis set showed that the reaction of the $O_2^{-\bullet}$ radical at the C_α of the A5 yielded 10.7 $J{\cdot}mol^{-1}K^{-1}$ and 21.1 $J{\cdot}mol^{-1}K^{-1}$ more entropy than the analogous reaction with $^{\bullet}OH$ and $O_2^{-\bullet}$.

The order of the reactivity of the ROS with the helical A5 peptide was qualitatively similar to those with A5 in the extended conformation, however the ΔG^o of each reaction was

Table 15. The enthalpy, free energy and entropy of the reactions of $^{\bullet}OH$, $HO_2^{\bullet}$ and $O_2^{-\bullet}$ with A5, producing the A($C_{\alpha}^{\bullet}$), A($^{\bullet}CH_3$) and A($N^{\bullet}$) radicals in the helical and extended conformations. The values were computed in the gas phase and implicit solvent, at the B3LYP/6-31G(d) and B3LYP/6-311+G(d,p) (in parenthesis) levels of theory.

Reactants	Environment	ΔH^o / kJ mol^{-1}			ΔG^o / kJ mol^{-1}			ΔS^o / J mol^{-1} K^{-1}		
		C_{α}	CH_3	N	C_{α}	CH_3	N	C_{α}	$^{\bullet}CH_3$	N
$^{\bullet}OH$ + $A5_{Ext}$	Gaseous	-138.4 (-140.9)	-52.7 (-61.6)	-47.4 (-38.5)	-123.4 (-145.8)	-40.3 (-69.1)	-32.9 (-44.2)	14.9 (16.6)	23.6 (25.1)	16.8 (19.2)
	Aqueous	-124.0 (-145.0)	-41.7 (-70.7)	-32.4 (-42.4)	-131.6 (-145.3)	-46.8 (-76.4)	-36.6 (-42.4)	25.6 (0.9)	17.2 (19.3)	14.0 (0.1)
$HO_2^{\bullet}$ + $A5_{Ext}$	Gaseous	16.0 (26.3)	101.7 (105.6)	107.0 (128.7)	46.9 (24.4)	130.0 (101.2)	137.4 (126.0)	4.4 (6.2)	13.1 (14.8)	6.3 (8.9)
	Aqueous	33.7 (12.6)	116.0 (87.0)	125.2 (115.2)	29.2 (15.4)	114.0 (84.3)	124.2 (118.3)	15.1 (-9.4)	6.7 (9.0)	3.5 (-10.2)
$O_2^{-\bullet}$+ $A5_{Ext}$	Gaseous	83.5 (85.4)	169.3 (164.7)	174.6 (187.8)	75.9 (77.2)	159.0 (154.0)	166.4 (178.8)	25.6 (27.3)	34.2 (35.9)	27.4 (30.0)
	Aqueous	86.5 (89.6)	168.8 (164.0)	178.1 (192.3)	75.7 (86.2)	160.5 (155.0)	170.7 (189.0)	36.2 (11.5)	27.8 (30.0)	24.5 (10.7)
$^{\bullet}OH$ + $A5_{Hel}$	Gaseous	-114.2 (-119.5)	-54.6 (-63.7)	-34.0 (-29.7)	-103.5 (-127.2)	-41.5 (-70.3)	-27.6 (-42.3)	29.6 (26.0)	21.3 (22.3)	43.9 (42.5)
	Aqueous	-103.7 (-129.7)	-41.3 (-69.9)	-7.0 (-32.4)	-108.3 (-134.1)	-46.3 (-74.6)	-18.6 (-46.4)	15.5 (14.8)	17.0 (15.8)	38.9 (47.0)
$HO_2^{\bullet}$ + $A5_{Hel}$	Gaseous	40.3 (47.7)	99.8 (103.5)	120.5 (137.5)	66.8 (43.0)	128.8 (99.9)	142.7 (127.9)	19.1 (15.7)	10.8 (11.9)	33.5 (32.2)
	Aqueous	54.0 (27.9)	116.4 (87.7)	150.6 (125.2)	52.5 (26.5)	114.5 (86.1)	142.1 (114.3)	5.0 (4.4)	6.5 (5.4)	28.4 (36.6)
$O_2^{-\bullet}$+ $A5_{Hel}$	Gaseous	107.8 (106.8)	167.3 (162.6)	188.0 (196.6)	95.8 (95.8)	157.8 (152.7)	171.7 (180.7)	40.2 (36.8)	32.0 (33.0)	54.6 (53.2)
	Aqueous	106.8 (104.9)	169.3 (164.7)	203.5 (202.2)	99.1 (97.3)	161.0 (156.8)	188.7 (185.0)	26.1 (25.4)	27.6 (26.4)	49.5 (57.6)

slightly less favorable. Moreover, the relative ease at which a hydrogen atom can be abstracted from the of the C_α, C_β and the amide nitrogen was also similar to what was found in the extended conformation.

4.5 Molecular Dynamic Simulations of Heptapeptides

Analysis of the secondary structure elements showed that only γ-, β-, α- and π-turn structures were observed in the ALA and ALR peptides, whereas neither δ- nor inverse γ-turns were detected. These results are shown in **Table 16**.

Table 16. The number of turn structures identified in ALA and ALR, where i is the residue number of the starting amino acid of the turn and Hb identifies the turn structures that were further stabilized by H-bonds.

Secondary Structure Element	No. of Structures		Secondary Structure Element	No. of Structures	
	ALA	ALR		ALA	ALR
γ-turn (i = 3)	1781	1273	β-turn (i = 2)	3858	1730
γ-turn (i = 4)	1493	7936	β-turn (Hb, i = 2)	1953	15
γ-turn (i = 5)	2107	1366	β-turn (i = 3)	3356	2292
π-turn (i = 2)	1266	3645	β-turn (Hb, i = 3)	1693	228
π-turn (Hb, i = 2)	135	44	β-turn (i = 4)	3323	1457
π-turn (i = 3)	1626	8050	β-turn (Hb, i = 4)	2277	8371
π-turn (Hb, i = 3)	1	26	β-turn (i = 5)	3874	4519
-	-	-	β-turn (Hb, i = 5)	1661	1074

More than 4-times more γ-turns (i = 4), β-turns (Hb, i = 4), α-turns (i = 2) and π-turns (i = 3) were observed in ALR than were observed in ALA, as shown in **Table 16**. The Ala_5 residue was one of the two central residues, or the only central residue in each of these structures, indicating that the ALR residue increased the propensity of turn formation when in a central position. The distribution of the distances between $O_i \cdots N_{i+2}$ (i = 3, 4 and 5) was calculated for ALA and ALR, which corresponds to a γ-turn, and is shown in **Figure 21**.

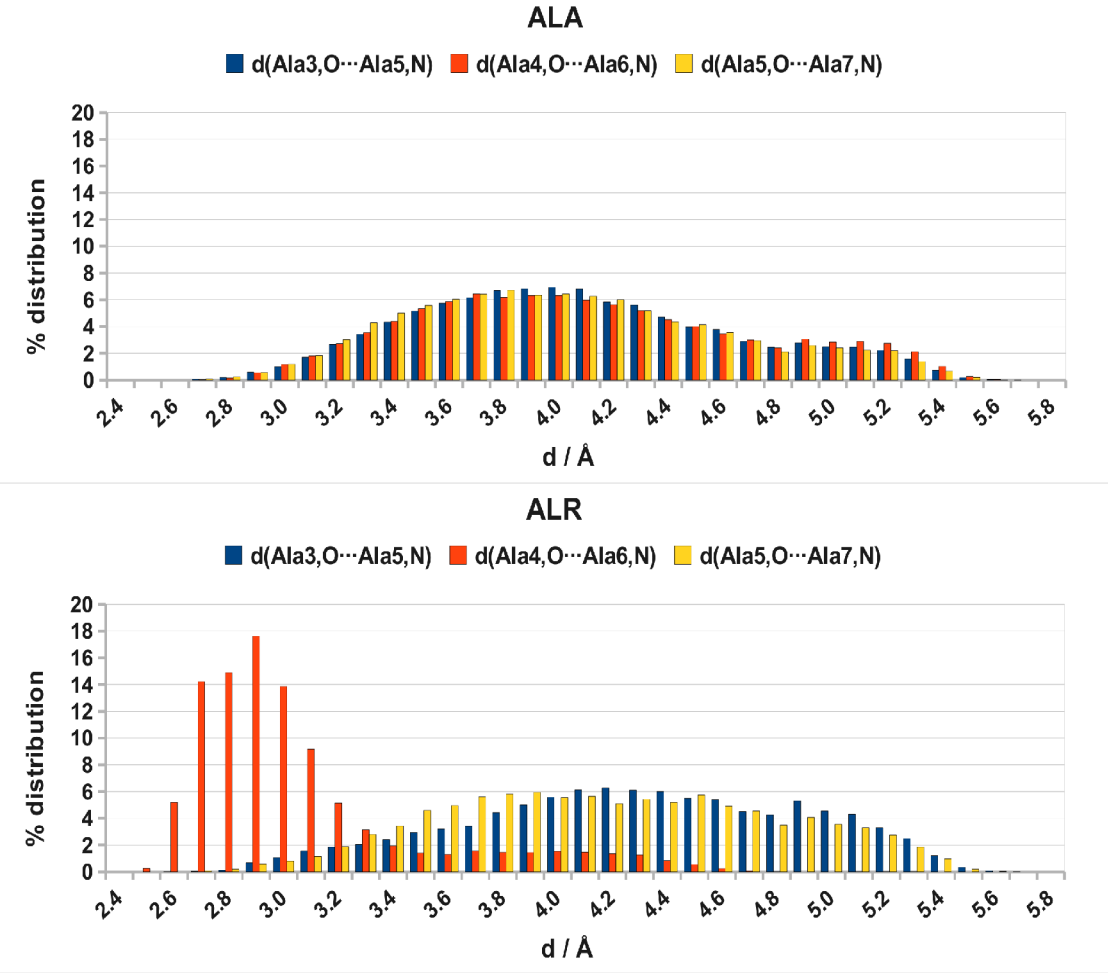

Figure 21. The percentage distribution of the structures according to the measured distance between Ala3,O···Ala5,N, d(Ala4,O···Ala6,N) and (Ala5,O···Ala7,N).

The distribution of the distance between the carbonyl oxygen of Ala_3, Ala_4 and Ala_5 (residue "i") of ALA and the amide hydrogen of its corresponding "i + 2" residue, Ala_5, Ala_6 and Ala_7, respectively, was plotted to determine whether hydrogen bonds between these residue pairs can enable γ-turn formation. The same residue pairs were plotted for the ALR peptide (**Figure 21**). A similar distribution of the inter-atomic distances was shown for ALA and ALR when Ala_5 or Alr_5 was at the residue was the first or third residue of the "i" or at the residue "i + 2" position. These values were most frequently between 3.8 Å and 4.1 Å

in ALA, and between 4.1 Å and 4.4 Å in ALR. However, this distance is reduced to approximately 2.95 Å in ALR when Alr_5 is the central residue "i + 1" of the turn. This distance shortening increased the propensity of hydrogen bonds to to form between the atom pairs, and enabled γ-turns to form in this region of the peptide.

The density Ramachandran map (**Figure 22**) indicates that the most populated region of the Ramachandran space of Ala_5 was when ϕ was between -90° and -60° and when ψ was between -30° and 0°, which contained 13.6% of the structures. The highest populated region occupied Alr_5 was when ϕ was between -30° and 0° and when ψ was between -60° and -30°, which includes 21.7% of the structures. Moreover, the Ramachandran map of Alr_5 shows that the region where ϕ is between -30° and 30° was also highly populated.

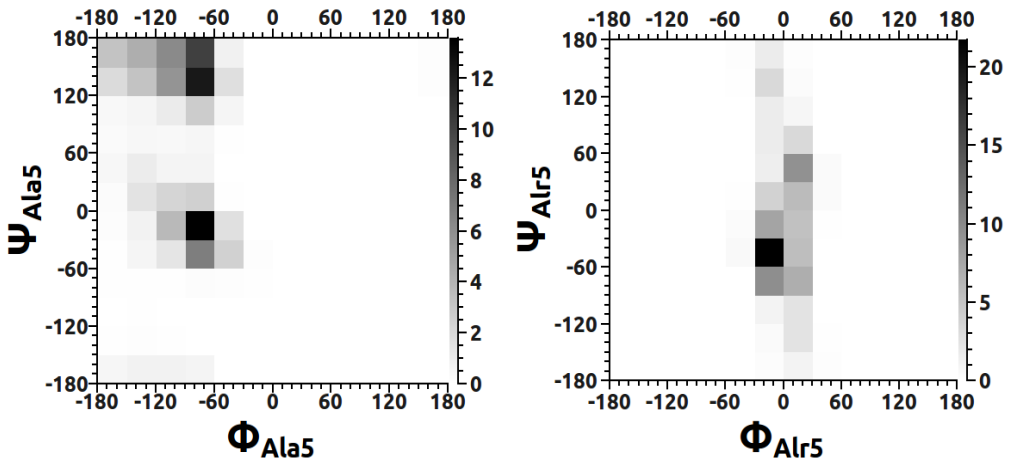

Figure 22. The density (top) and classic (bottom) Ramachandran maps of the central amino acid (Ala5 or Alr5) for ALA (left panel) and ALR (right panel).

5.0 DISCUSSION

5.1 Consequences of C_α Radical Formation on Monopeptide Conformers

The use of the acetyl and *N*-methyl amide groups to protect the N- and C- termini, respectively, helps conserve the electronic environment of the C^α center of amino acid residues since the C^α is between two amide bonds. The methyl carbons of the N- and C-terminal acetyl and *N*-methyl amide groups, respectively, correspond to C^α of the adjacent amino acid residues in an extended polypeptide structure. Thus, the steric interactions between the C^α and the adjacent amide bonds can be taken into consideration and contributions to local C^α structure from other residues in a polypeptide are avoided.[79-81]

The relatively flat potential energy surface of *N*-Ac-Gly-NHMe, matches the characteristic flexibility of Gly in proteins. Conformations in both D and L configuration can easily be accessed by Gly and this is demonstrated by the absence of large energy barriers between the minima. The "flat valleys" between these conformations indicate that the structures are stable but conformations of Gly can inter-convert easily. The PES of the *N*-Ac-Gly$^\bullet$-NHMe was substantially different from that of its closed-shell counterpart. The β_L conformation was the most stable structure on the PES and was surrounded by a high-energy rim, trapping the ϕ and ψ angles in β_L conformation. Furthermore, because the other minima are shallow and a relatively small amount of energy could bring the structure back to the more stable β_L conformation. It is evident that changes in hybridization of the C^α has a large effect on its PES. The sp^3-hybridized C^α of the Gly residue generates three low energy conformations, *gauche*$^+$, *gauche*$^-$ and *anti* (**Figure 9A**). This is displayed in the closed shell

model. With two hydrogen atoms bonded to the C^{α}, however, only the steric hindrance of the amide bonds provides a significant energy barrier. The $\phi = 0^{o}$ line on the PES illustrates this. On the other hand, the sp^2-hybridized C^{α}-centered radical has only two low energy conformations, which indicates the tendency of the C^{α}-centered radical to adopt planar (ϕ and ψ angles of 0^{o} or 180^{o}) conformations. The adoption of planar conformations following radical formation by the Gly residue may facilitate the formation of β-sheets, with H- bonds stabilizing the interactions between β-strands.

5.2 H-Abstraction from Amino Acid Monopeptides

The structures and energies of the Ala and Gly pre-reaction van der Waals complexes, transition states, and post-reaction van der Waals complexes will be discussed in the subsequent sections.

5.2.1 The Pre-Reaction van der Waals Complexes

The difference between the relative energies of the Gly and Ala pre-reaction complexes shows that the Ala side chain could inhibit the formation of the γ_D and α_D pre-reaction complexes. The relative energies of the β_L, γ_D, α_L and α_D pre-reaction complexes of Gly are within 4 kJ mol^{-1} of each other, whereas the γ_L is a slight outlier, which suggests that the pre-reaction complex can form easily from multiple conformations. The distribution of the pre-reaction Ala energy values is similar, however the α_D and γ_D complexes are higher in energy. It is worth noting that the α_D pre-reaction complex is is only 1.4 kJ mol^{-1} lower than the energy at the entrance level. The side chain of the Ala residue destabilizes this complex by hindering the ability of the oxygen atom of the $^{\bullet}OH$ radical to interact with the pro-D

hydrogen of the Ala residue. As a result, the formation energy of the complex in this conformation is 20 – 25 kJ mol^{-1} less than the other conformations. The complex formation energies of all five conformations of Gly and the four (excluding α_D) of Ala indicate that the formation energies of the pre-reaction complexes are sufficient enough to enable the hydrogen abstraction reaction to occur, particularly when the activation energy is close to zero.[82,83] When these nine conformations of the residues are considered, the formation energies of the pre-reaction complexes show that the Ala side chain does not significantly inhibit complex formation. Side chains larger than Ala could further hinder complex formation, and a future study could provide a rationale for this effect.

With the exception of the γ_D conformation of Gly, the ϕ and ψ angles of the Gly and Ala van der Waals complexes are within a few degrees of the ϕ and ψ angles of the respective Gly and Ala residues. Therefore these complexes can form without perturbing the structure of the respective Gly and Ala minima, and the differences in relative energy only depend on the interaction between the $^{\bullet}$OH radical and the respective residues. This can also be expected if explicit water molecules were studied as well, since the $^{\bullet}$OH would occupy a similar place that a structural H_2O molecule would occupy. The lack of conformational change of the residues during complex formation with $^{\bullet}$OH enables the H-abstraction reaction to occur with greater ease.

5.2.2 The Transition State Structures

Both Gly and Ala combine with $^{\bullet}$OH to form six and seven-membered rings in the respective transition state structures (**Figure 11 and Figure 12**). The ϕ and ψ angles of the

Gly transition state structures remain similar to those of the Gly PES, whereas the ψ angle of γ_D becomes more like the ψ angle of Gly•. The change in the β_L conformation of Ala transition state suggests that the capto-dative stabilization of Ala in this conformation is less than that of Gly, and is likely to be the reason for the decreased relative energy of the Ala β_L transition state. It can be concluded that the transition states for each conformation of the Gly and Ala residues except for the γ_D of Gly and β_L of Ala deviate from the geometries of the PES minima by only a few degrees.

Both the Gly and Ala transition states in the β_L conformation are below the entrance level, and the next lowest lying transition states of Gly are the γ_D and α_D conformations, followed by the γ_L and α_L conformations. The ϕ and ψ angles indicate that the β_L conformation is capto-dative stabilized, and is the reason for the low-lying β_L conformation, however the differences between the energy of the other conformations are less significant. After the β_L conformation, the next lowest-lying transition states of Ala are the γ_L and γ_D, followed by the α_L and α_D transition states which are much higher in energy. The Ala side chain has a larger influence on the energy of these conformations, and a distinct conformational effect can be observed in Ala.

5.2.3 The Post-Reaction van der Waals Complexes with H_2O

The relative energy values of the Gly and Ala post-reaction van der Waals (**Table 6**) complexes were similar to those of the respective Gly• and Ala• PES minima shown in **Table 4**. The geometries of the post-reaction complexes only varied from the fully isolated Gly• and Ala• residues by a few degrees, except for the α_L complex of Gly and Ala, which are

not similar to any of the respective Gly$^{\bullet}$ or Ala$^{\bullet}$ conformations. Moreover, the corresponding α_D conformation of Gly$^{\bullet}$ converged to the γ_D, which can be attributed to the absence of the methyl group of the Ala side chain. The post-reaction complexes of the Gly$^{\bullet}$ residue were more planar than the respective Ala$^{\bullet}$ complex, which is probably due to the increased capto-dative stabilization of the Gly residue. The H_2O molecule interacts with the Gly$^{\bullet}$ and Ala$^{\bullet}$ with a hydrogen bond between a hydrogen atom of water and one of the carbonyl oxygen atoms (**Figure 11 and 12**). In the γ_L and α_L complexes of Gly$^{\bullet}$ and the γ_L of Ala$^{\bullet}$ hydrogen bonds form with both carbonyl oxygen atoms, but these complexes are the highest in energy.

The post-reaction complexes of Gly are 120.7 - 159.8 kJ mol^{-1} below the energy of the entrance level, and those of Ala are 137.1 – 156.4 kJ mol^{-1} below the Ala entrance level. This complex is the lowest point of the reaction coordinate for both the Gly and Ala residue, and the stability of these complexes show that their formation is a significant driving force for the progress of the H abstraction reactions. The side chain of Ala does not appear to interact with the H_2O molecule, and the stability of the complex is largely influenced by the hydrogen bond between the water molecule and the residue, and by the ϕ and ψ angles of the residue. This is supported by the observation that these angles remain similar to those of the respective Gly and Ala residues in the absence of the the H_2O molecule. The ϕ and ψ angles of Gly and Ala are expected be similar if this system were to include structural water.

5.2.4 H-Abstraction by Gly$^{\bullet}$ and Ala$^{\bullet}$ Radicals from H_2O_2

To quantify the stability of the C_α-centered radical of Gly$^{\bullet}$ and Ala$^{\bullet}$ we also compared the

reaction coordinates for the hydrogen abstraction from H_2O_2 by Gly$^{\bullet}$ and Ala$^{\bullet}$, in order to form the Gly and Ala residues. H_2O_2 can donate a hydrogen atom and can be found in areas of the body where $^{\bullet}$OH can be found as well. It should be stressed that H_2O_2 is not the only molecule that can play this role, but it has been selected as an example. The β_L conformation of these residues was used as the starting conformation because they are the lowest in energy, as shown in the potential energy surfaces (**Figure 10**). Both the Gly and Ala residues are likely to unfold to the β conformer following hydrogen abstraction from any of the other conformers. The formation energy of the van der Waals complex is the same for both residues, however, the lower lying transition state and subsequent van der Waals complex and separated products of the Ala residue shows that the Ala$^{\bullet}$ would be easier to convert back to Ala, whereas the Gly$^{\bullet}$ would have a higher propensity to remain a C_α radical, as shown in **Figure 21**. A representative scheme of the reaction coordinate for the re-formation of Gly and Ala can be found in **Figure 22**.

Since the energy of the Gly-$^{\bullet}$OH/Gly$^{\bullet}$-H_2O_2 and Ala-$^{\bullet}$OH/Ala$^{\bullet}$-H_2O_2 systems remain below the energy of the entrance level, the re-formation to Gly and Ala by H_2O_2 has enough energy to proceed. Using Gly as an example, it has been shown that the post-reaction complexes contain Gly in the β_L, γ_L and δ_D conformations, whereas the Gly$^{\bullet}$ PES indicated that other Gly$^{\bullet}$ minima are stable. However, the relative energy values of Gly$^{\bullet}$ PES minima indicate that the β_L conformation is approximately 30 kJ mol^{-1} more stable. This can also be said for Ala and presumably for any other residue. This suggests that any rearrangement of the residue will result in the residue converting to the β_L conformation. These results can

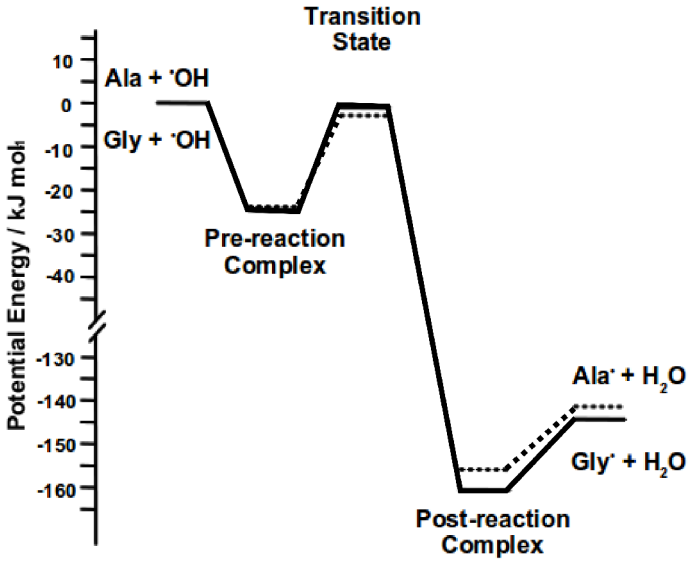

Figure 21. The reaction coordinate diagram showing the E_{pot} of the hydrogen abstraction from Gly and Ala in the β_L conformation by ·OH. The energy of the reactants is used as a reference.

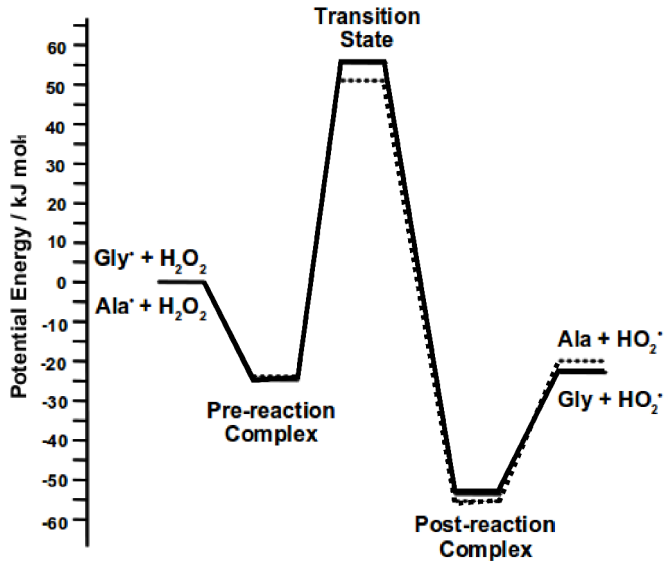

Figure 22. The reaction coordinate diagram showing the E_{pot} of the hydrogen abstraction from H_2O_2 by Gly· and Ala· in the β_L conformation. The energy of the reactants is used as a reference.

help elucidate the mechanism by which •OH initiates protein unfolding, and potential aggregation. It would be interesting to see whether the conversion to the β_L conformer that was shown here can be reproduced using other techniques, particularly molecular dynamics, which enables the time-dependent nature of this unfolding to be observed in larger systems.

5.3. Deviations from the G5 and A5 structures

5.3.1 Structural Perturbations due to C_α H-Abstraction from G5 and A5

The shift towards the β conformation (ϕ, ψ = 180°) is in agreement with that shown in a glycyl diamide model, in which the β conformation was shown to be the most stable.[80] Allyl-type radicals have a higher stability compared to non-delocalized radicals and also favor the planar conformation. This structure has been shown to have a rotational energy barrier of approximately 15 kcal mol^{-1}.[66,84,85] The stability of this conformation can be attributed to the overlap of the semi-occupied π-orbital of the radical with the p-orbitals of the amide nitrogen and carbonyl carbon. This structure stabilizes the C_α radical of G5(C_α•) and A5(C_α•) due to the conjugation between the nitrogen atom of the amide and carbon atom of the carbonyl group, which has also been shown previously in cyclic and amino alkyl compounds.[86,87] Further evidence of the delocalization is the decreased length of the N-C_α and C_α-C bonds, which indicates an increase in double-bond character. The increase in the C_α-C bond length was observed in the extended structure, but not in the helix, indicative of the tendency of the helix to inhibit the delocalization of the unpaired electron. The increased length of the amide bonds between residues "i" and "i - 1" and the amide bond between residues "i" and "i + 1" of both G5 and A5 indicates that these bonds become more like

single bonds, which are weaker and are more susceptible to enzymatic degradation and peptide fragmentation.

The stabilization of the radical by the amide nitrogen of G5(N•)and A5(N•) is twofold, due to the electron-donating properties of the amide nitrogen, and the ability of the amide bond to delocalize the unpaired electron.[88] The stronger C_α• coupling to the amide nitrogen than to the carbonyl carbon is shown in the larger change in bond length in both G5(C_α•) and A5(C_α•). The increased planarity of Ala^3 is shown by the lack of pleats in the extended conformation (**Figure 19**) and ϕ and ψ angles of nearly 180°. An increase in the planarity of the atoms in Gly^3 and Ala^3 was also shown in the helical conformation (**Figures 17 and 20**), with both the ϕ and ψ angles approaching 0° (**Tables 9 and 11**). It can be observed that this effect does not carry over to residue 2 or residue 4 of the G5 and A5 peptides in either the extended or helical conformations.

5.3.2 Structural Perturbations due to Amide Nitrogen H-Abstraction from G5 and A5

Numerous theoretical studies have been done on hydrogen atom abstraction from the free amino group, with some suggesting the that the amino hydrogen is the preferred target by •OH.[44,89,90] However, when the amide nitrogen is derivatized it was shown that reactions at the side chain are always preferred.[91] Although free amino acids and their derivatives can provide a good description of local electronic effects, hydrogen abstraction from the amide bond of model peptides helps determine the effect of long-range interactions and hydrogen bonding. The removal of a hydrogen atom from G5 and A5 showed an increase of the amide bond length with the adjacent carbonyl carbon, along with the an increase in the length of

the C_α-C bond. The N-C_α bond length decreased, which is consistent with the formation of an imine.[92]

The most significant effect of the H-atom abstraction from the amide nitrogen is due to the rearrangement of the hydrogen bonds within the G5 and A5 peptides. Instead of the intra-residue hydrogen bond between the amide nitrogen and carbonyl oxygen of Gly^3 and Ala^3 in the extended conformation, a hydrogen bond formed between the carbonyl oxygen of residue "i – 1" and the amide hydrogen of residue "i +1". It is presumed that this caused the observed deviation in the ϕ and ψ dihedral angles in this structure compared to those of the G5 and A5 extended ϕ and ψ angles. In the helical conformation, the removal of the Gly^3 and Ala^3 amide hydrogen atoms eliminated the hydrogen bonds that were formed with residue 3 and the carbonyl carbon of residue 1. The observed increase in the amide bond length suggests that N•-containing peptides can be more labile than in a peptide without a radical.

5.3.3 Structural Perturbations due to C_β H-Abstraction from A5

The change in length of the amide bond between adjacent residues is indicative of the coupling between the methyl group and the resonance structures of the amide bond.[93] However, compared to the effect of radical formation on the C_α and amide nitrogen on the peptide structures, this coupling is relatively weak. Apart from the length of the C_α- C_β bond, C_β-radical formation had a negligible effect on the bond lengths, dihedral angles, or hydrogen bonds of either the extended or helical A5 peptide. The methyl group of Ala is the β-CH_2 of the other amino acids apart from glycine, and it is expected that radical formation

at this or any other position of the side chain would have negligible inductive effects on the conformation of the peptide backbone. Moreover, the effect on the length of the amide bond is negligible, suggesting that side chain oxidation does not cause the peptide bond to weaken.

The RMSD values indicate that the H abstraction from the C_β did not significantly change the structure of A5. H abstraction from the C_α increased the planarity of the peptide but the secondary structure of the peptide remained intact, whereas H abstraction from the amide nitrogen altered the secondary structure of the peptide.

5.4 Thermodynamic Analysis

5.4.1 H-Abstraction Energy and Stability of Peptide Radicals

It is expected that with the increase in the number of delocalized electrons in the conjugated system the stability of the radical will increase.[94] This phenomenon will contribute to the lower dissociation energy of the C_α-H bond compared to that of the C_β-H and N-H bonds. The lower relative bond dissociation energy of the extended peptide compared to that of the helical conformation is similar to results shown by others, however the secondary structures were mimicked with the use of smaller peptide fragments.[43,64] The use of model pentapeptides enables the inclusion of intra-molecular hydrogen bond effects of the secondary structural elements. The conformational dependence shown in the smaller fragments was shown to be less in the pentapeptides computed herein, suggesting that the diamide models may exclude the stabilization effect of intra-molecular hydrogen bonding. The similarity of the BDE results computed at the 6-31G(d) and 6-311+G(d,p) basis sets

indicate that the inclusion of diffuse functions and polarizable functions on hydrogen did not significantly improve the BDE values. It is possible that capto-dative stabilization and the larger number of delocalized electrons of the G5(C_α) and the A5(C_α) are reasons for the relative stability. These results also agree with experimental results that state that $^{\bullet}$OH attack at the C_α position of Ala peptides are favored over C_β.[44,91]

5.4.2 Helical Unfolding

The use of computational chemistry enables the stability of radicals at specific sites and the relative stability of otherwise transiently stabilized structures to be evaluated. This information can help measure the thermodynamic functions and determine the stability of folding intermediates, which can provide insight into unfolding mechanisms. Here, the ΔG^o values indicate that the unfolding of the G5 and A5 peptides from a 3_{10}-helix to an extended conformation is favorable, but much more so when there is a C_α present on residue 3. The similarity between the ΔG^o for the unfolding of G($N^{\bullet}$), A5($C_\beta^{\bullet}$) and A5($N^{\bullet}$) to that of the respective G5 and A5 peptides suggests that the propensity of these structures to unfold is not significantly greater than that of the G5 or A5 peptides. It has been shown that radical formation on peptides causes peptides and proteins to unfold, and it has been hypothesized as a possible mechanism for the aggregation of amyloid peptides.[95,96] These results indicate that the unfolding of G5 and A5 are more favorable when a C_α radical is present. If a radical was to form at the C_β or amide nitrogen, then a hydrogen transfer reaction is likely to preclude unfolding. According to several experimental studies, intramolecular hydrogen transfer reactions almost exclusively result in the formation of C_α radicals.[97-99] The

unfolding of all investigated peptides results in an increase in entropy, which can also drive peptides and proteins to unfold. The C_β and amide nitrogen peptide radicals do not show a significantly larger propensity than A5 or G5 to unfold. Therefore, radical-initiated unfolding is likely to be a result of the formation of the C_α radical.

5.4.3 Reactions of Pentapeptides with Reactive Oxygen Species

The results in a model peptide indicate that hydrogen abstraction by the $^{\bullet}OH$ radical is favorable from each of the three positions, which is consistent with what was shown in model amides.[100] This study also showed that abstraction from the amide nitrogen was the least favored, which can be attributed to the relative stability of the amide bond. Hydrogen abstraction from the amide nitrogen also had the largest change in entropy when G5 and A5 were in the helical conformation. The smaller gain in entropy can be observed in the extended conformation because the intra-residue hydrogen bond in residue 3 is replaced with a hydrogen bond between the carbonyl oxygen of residue 3 and the amide nitrogen of residue 2. The reaction at the C_α is the most endergonic and is enthalpy driven, due to the stabilization discussed previously. In spite of the large endergonicity the associated gain in entropy of reactions at the C_α is less than at the other sites, though the differences are not significantly different to that measured at the C_β in the case of A5.

The reactivity of $^{\bullet}OH$ can be attributed to the high dissociation energy of the O-H bond in H_2O, which is 499.2 kJ mol^{-1}.[101] Accordingly, reactions with the $^{\bullet}OH$ radical are exergonic at the C_α, C_β and amide nitrogen sites in all conditions calculated herein. Despite being the most endergonic, the largest gain in entropy was measured in the reactions with the $O_2^{-\bullet}$

radical, which, in addition to the ΔH measured directly, indicates that the change in enthalpy was the least favorable in this ROS.

These results indicate that a hydrogen atom from the C_α, C_β and amide nitrogen can be abstracted by $^{\bullet}OH$ but not by $HO_2^{\bullet}$ or $O_2^{-\bullet}$. It is well known that the $^{\bullet}OH$ is the most reactive, but it has also been shown that $^{\bullet}OH$ is more destructive when $HO_2^{\bullet}$ or $O_2^{-\bullet}$ are present. A hypothesis for this phenomenon is discussed in the next section.

5.4.4 Thermodynamic Cycles of H-Abstraction

As discussed previously, the oxidation of proteins has been shown to cause proteins to unfold. Moreover, it has been hypothesized that radical-initiated protein unfolding is the first step in the mechanism that causes the formation of the amyloid plaques, which are hallmarks of Alzheimer's, Creutzfeld-Jakob, and Parkinson's diseases.[102] The results obtained herein allow for quantification of the thermodynamic parameters of this process and enables the comparison of the propensity of $^{\bullet}OH$, $HO_2^{\bullet}$ and $O_2^{-\bullet}$ radicals to initiate this process. The ΔH^o, ΔG^o and ΔS^o for the oxidation of the helical G5 and A5 by $^{\bullet}OH$ are all favorable, whereas oxidation by $HO_2^{\bullet}$ and $O_2^{-\bullet}$ are not favorable. After the endothermic, exergonic and entropically favorable unfolding of $G5_{HEL}^{\bullet}$ and $A5_{HEL}^{\bullet}$, the ΔH^o and ΔG^o for the formation of the reduced and extended G5 and A5 by H_2O_2 and HO_2^- are all negative. Amyloid plaques are not radicals, so in this scheme, the extended G5 and A5 structures best represent the amyloid plaques that have been associated with Alzheimer's disease, and can therefore a suggest a role for H_2O_2 and HO_2^- in the formation of amyloid plaques. This scheme illustrates how each step in the unfolding of G5 and A5 is favorable when $^{\bullet}OH$, H_2O_2

and HO_2^- are present, as shown by Davies et al., in which backbone cleavage and degradation by $^{\bullet}OH$ is exacerbated when H_2O_2 and HO_2^- are also present.[10,20,103] A schematic comparison between the radical-initiated unfolding of G5 and A5 peptides is shown in **Figures 23 and 24**. The radical-initiated unfolding of a helix is more favorable than a mechanism without a radical, which would likely involve less stable intermediates.

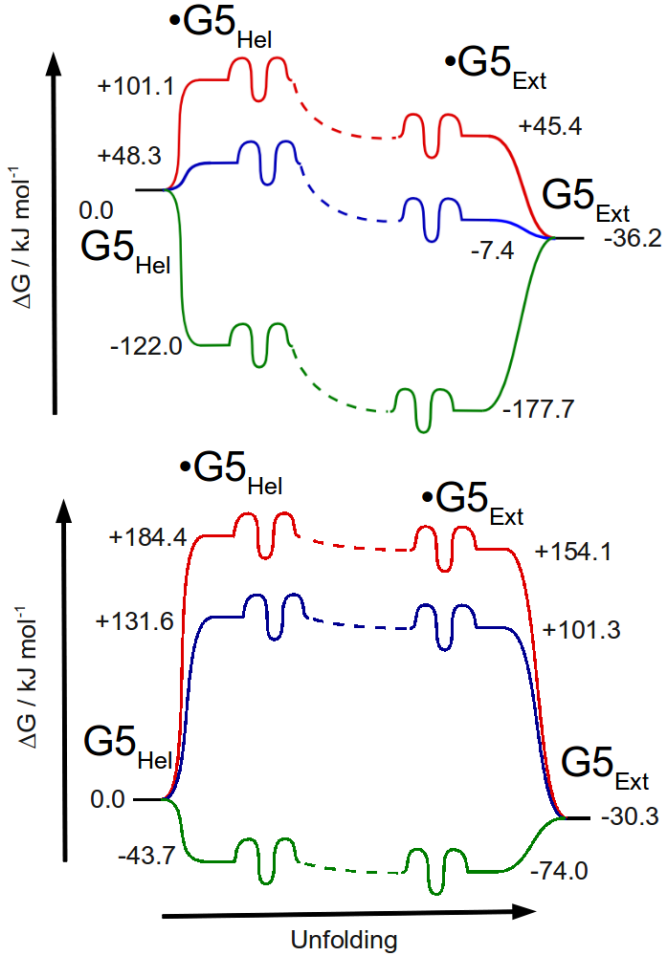

Figure 23. Schematic representations of the ΔG^o associated with the radical-initiated conversion of $A5_{HEL}$ to $A5_{EXT}$ by $^{\bullet}OH$,(green), $HO_2^{\bullet}$ (blue) and $O_2^{-\bullet}$ (red). The top panel shows the ΔG^o for the reaction at the C_α, whereas the the middle and bottom panels show ΔG^o for H abstraction from C_β and the amide N, respectively.

In **Figure 25**, competing mechanisms for the conversion of the helical G5 and A5 to and extended $G5^{\bullet}$ and $A5^{\bullet}$ are shown. The $G5^{\bullet}$ and $A5^{\bullet}$ are the forms in which the oxidized

peptide can propagate, causing new C_α radicalized peptides to form. The ΔG^o values of the unfolding of the peptide radicals show that the $G5^{\bullet}_{EXT}$ and $A5^{\bullet}_{EXT}$ conformations of the peptide radicals are more stable, therefore, with its longer half-life, the extended conformations of the peptide radicals are likely to be more toxic.

Amyloidogenic peptides are generally helix forming. In order to form the extended peptide radicals, the helices must either unfold prior to or after oxidation. As shown in **Figure 25**, the unfolding of the peptides is exergonic for both pathways when oxidized by $^{\bullet}OH$; however, unfolding prior to oxidation is entropy-driven, whereas oxidation prior to

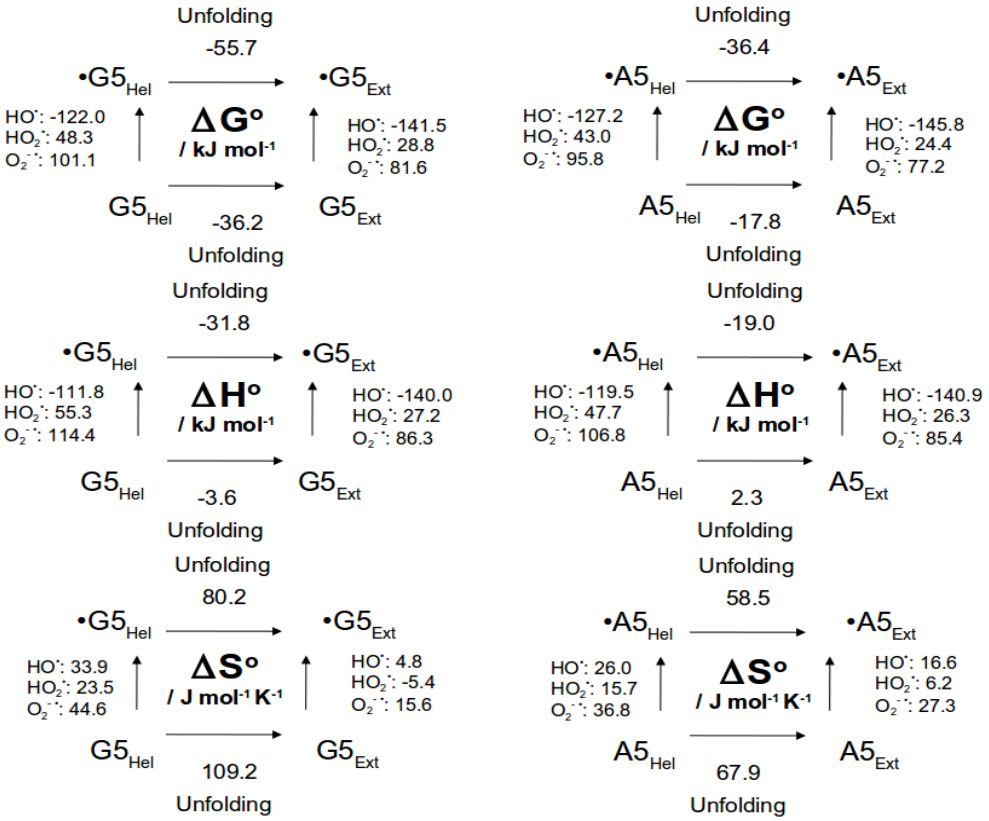

Figure 25. ΔH^o, ΔG^o and ΔS^o for the competing mechanisms of $G5_{HEL}$ (left panel) and $A5_{HEL}$ (right panel) converting to $^{\bullet}G5_{EXT}$ and $^{\bullet}A5_{EXT}$ initiated by H abstraction from the C_α of Gly^3 and Ala^3, respectively, by $^{\bullet}OH$, $HO_2^{\bullet}$ or $O_2^{-\bullet}$. In mechanism one (upwards from $G5_{HEL}$ or $A5_{HEL}$) the H abstraction precedes the unfolding. In mechanism two (to the right from $G5_{HEL}$ or $A5_{HEL}$) the unfolding precedes the H-abstraction.

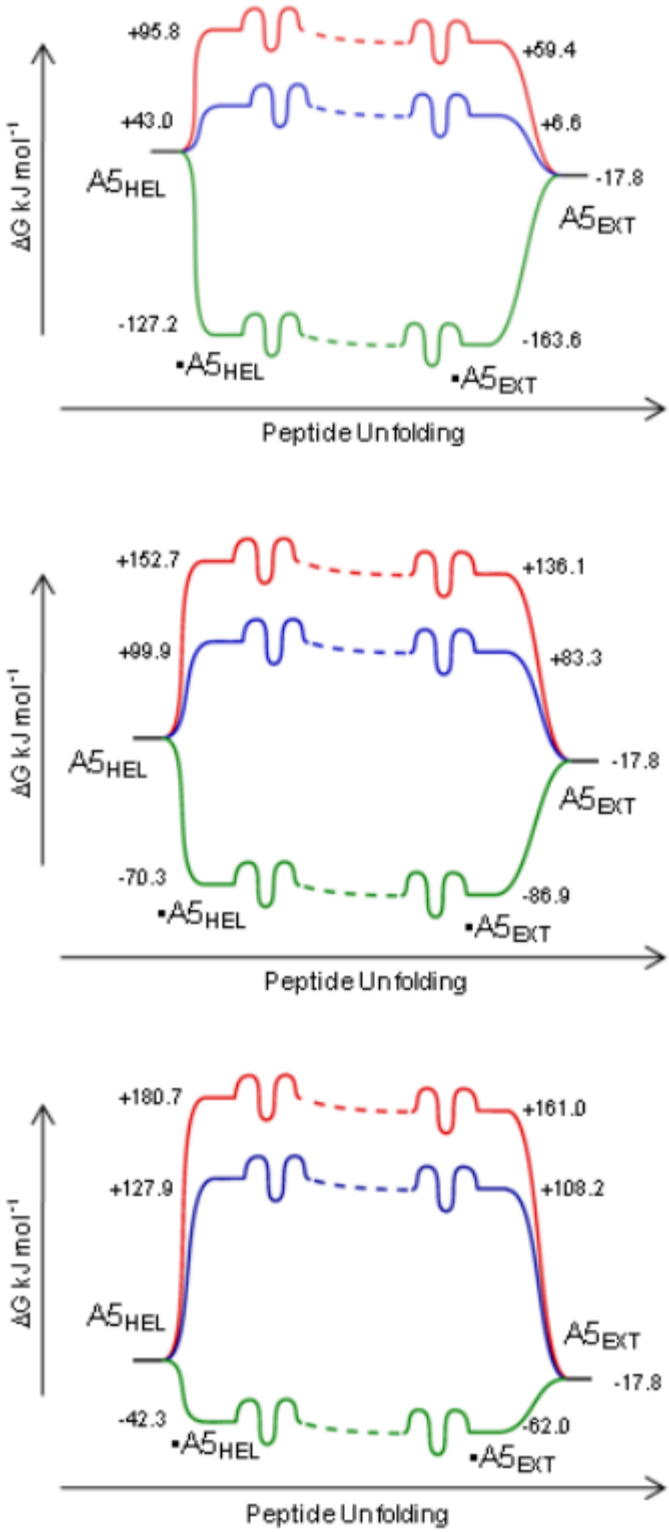

Figure 24. Schematic representations of the ΔG^{o} associated with the radical-initiated conversion of $G5_{HEL}$ to $G5_{EXT}$ by $^{\bullet}OH$,(green), $HO_2^{\bullet}$ (blue) and $O_2^{-\bullet}$ (red). The top panel shows the ΔG^{o} for the reaction at the C_{α}, whereas the bottom panels show ΔG^{o} for H abstraction from the amide nitrogen.

unfolding is enthalpy-driven. In a previous study in which the entropy per residue of homo-oligomeric peptides was measured, it was shown that there is a greater entropy per each residue added in the extended conformation than in the helical conformation.[104] The entropy contribution to the helical to extended equilibrium would favor the extended conformation in native peptides, however it remains to be seen how peptide length will affect this equilibrium when a C_α radical is present.

5.5 Comparison of the Unfolding of G5 to that of A5

5.5.1 Geometric Analysis

A greater decrease in N-C_α and C_α-C=O bond length was shown in the G5 peptide than for the A5 peptide, whereas the latter peptide showed a greater decrease in the length of the C_α-R bond length when a $C_\alpha^\bullet$ radical was formed. The difference between the G5 and A5 peptides is the identity of the R group, which is a hydrogen atom in G5 and a methyl group in A5. Since the sp^3 orbital of the methyl group is larger than the s orbital of hydrogen, it can accommodate the unpaired electron from the C_α to a larger degree than the s orbital of the hydrogen can. This should be the reason for the larger decrease in the length of the C_α-N and C_α-C=O bonds shown in G5. This effect was observed both in the extended and helical peptides in the $C_\alpha^\bullet$-containing peptides, but was not detected in the $N^\bullet$-containing peptides.

The increased delocalization observed after the C_α radical formation caused residue 3 of G5 and A5 to be more planar. Since the $G5_{EXT}$ was already within 1° of planarity, a greater RMSD was observed in the $A5(C_\alpha^\bullet)_{EXT}$ than in the $G5(C_\alpha^\bullet)_{EXT}$ compared to the respective A5 and G5 structures. However, a larger RMSD was shown in $G5(C_\alpha^\bullet)_{HEL}$ than in the

$A5(C_\alpha^\bullet)_{HEL}$, which can be attributed to the changes in the local (around the C_α) electronic environment, as observed in the changes in bond lengths surrounding the C_α. As such, formation of a C_α radical induced larger changes in the structure of $A5_{EXT}$ than that of $G5_{EXT}$, whereas a larger change was observed in the structure of $G5_{HEL}$, than was observed in $A5_{HEL}$.

5.5.2 Thermodynamic Analysis

The dissociation energies of the G5 and A5 H-C_α bonds are within 2 kJ mol^{-1} of each other in the extended conformation, whereas the H-C_α bond of A5 is slightly more labile (by 7 kJ mol^{-1}) than G5 when the peptides are helices. The differences between the H-N dissociation energies of the G5 and A5 peptides were less than 5 kJ mol^{-1}. Both the $A5(C_\alpha^\bullet)$ and $G5(C_\alpha^\bullet)$ peptides released more free energy during unfolding than their respective A5 and G5 peptides, however, the $G5(C_\alpha^\bullet)$ peptide releases 18.4 kJ mol^{-1} more free energy during unfolding than the $A5(C_\alpha^\bullet)$ peptide does. This indicates that a peptide that has a hydrogen abstracted from a Gly residue will have a greater tendency to unfold than when hydrogen is abstracted from an Ala residue. Since this value for the hydrogen abstraction comes from one residue, this ΔG^o value could have a greater significance when multiple residues are considered. Therefore, when considering the hydrogen abstraction from the C_α of peptides and proteins by free radicals, it can be assumed that regions that are rich in glycyl residues would be particularly susceptible to conformational changes.

5.6 Comparing the MD Simulations to the Potential Energy Surfaces

The quantum chemically-derived Ala and $Ala^\bullet$ potential energy surfaces can be compared to the Ramachandran map for the Ala and Alr residues at position 5 of the

pentapeptides. The data points of the PES are the same as shown in Section 3.1.1. However, in **Figure 26**, the IUPAC cut, which goes from -180° to 180° for ϕ and ψ, is used to enable comparisons to the Ramachandran maps to be made.

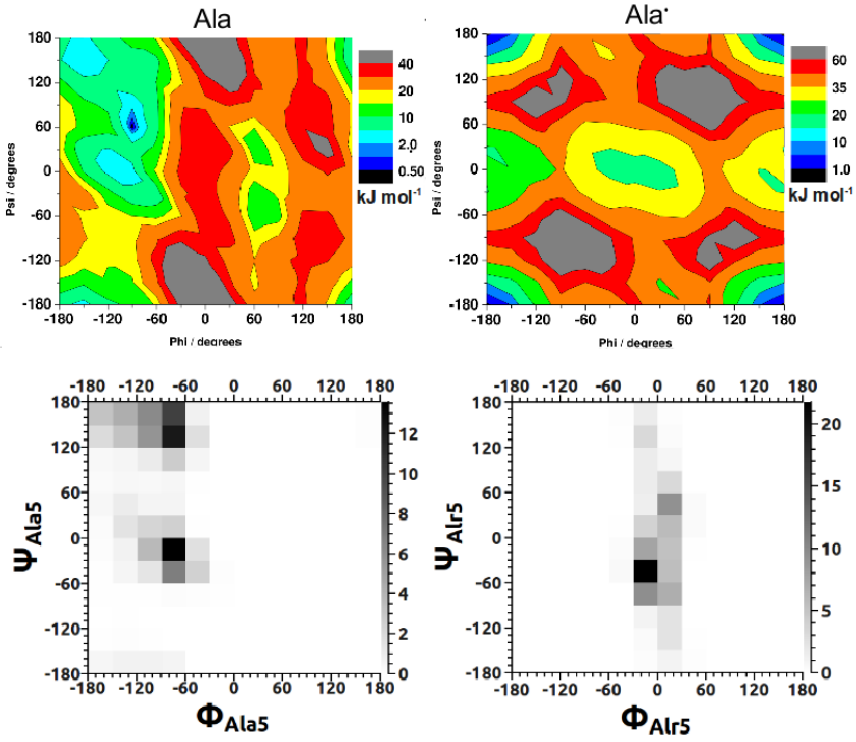

Figure 26. The IUPAC "cut" of the Ala and Ala• potential energy surfaces (top) and the density Ramachandran map of the Ala5 and Alr5 residues.

It can be seen that the ϕ and ψ angles of the most stable conformers of Ala agree well with the highest populated ϕ and ψ angles of the Ala5 structures. The Ramachandran maps and potential energy surfaces show that the L conformational space is both lower in energy and has a larger population of structures than that which can be found in the D conformational space. The agreement between the ϕ and ψ angles of the Ala• potential energy surface and those of the Alr5 Ramachandran map is not as pronounced as those of Ala and Ala5, largely because the global minimum of the Ala• PES has a relatively low population density in the

MD simulations. Instead, the minimum in the ϕ and ψ equal to zero region has a higher population density. Moreover, the distribution of the population density is wider along the ψ axis of the Alr Ramachandran map despite of the fact that the energy is lower along the ϕ axis of the Ala$^{\bullet}$ potential energy surface. These differences can be attributed to the tendency of the peptide to form a turn to enable intra-molecular hydrogen bonding and to reduce the solvent accessible surface area of the peptide. It is possible that the intramolecular hydrogen bonding observed in the peptide is more favorable when the ϕ angle is near zero degrees than when the ψ angle is near zero degrees. However, the delineation of these and other parameters used to compare the ϕ and ψ angles of single amino acids is still under investigation, considering that the solvent and secondary structures can perturb the ideal ϕ and ψ angles of single amino acid residues.[105-107] Both the quantum chemical and MD results presented herein show the conversion of helical ϕ and ψ angles to planar ϕ and ψ angles after hydrogen atom abstraction, which corresponds to the conformations that are also stabilized by the capto-dative effect. Both the potential energy surfaces from *ab initio* methods and the Ramachandran maps from the MD simulations show the consequences of this effect on the structure of the C^{α}-centered peptide radical.

6.0 CONCLUSIONS

The PES for the Gly, Gly$^{\bullet}$ Ala and Ala$^{\bullet}$ structures show the stable conformers for these residues. The Gly and Ala PES each contained 5 minima, which remained similar to the geometries of the respective pre-reaction complexes and transition states in the hydrogen abstraction reaction. Changes to the ϕ and ψ angles were shown upon the formation of the post-reaction complexes, which where similar to the structures of the Gly$^{\bullet}$ and Ala$^{\bullet}$ conformers. The first-order saddle points of the PES showed that the Gly residue loses its flexibility when changed to Gly$^{\bullet}$, whereas the flexibility of Ala and Ala$^{\bullet}$ is similar.

The stability of the β_L conformer of Gly and Ala radicals was shown in transition state and post-reaction van der Waals complex with the $^{\bullet}$OH radical. The β_L conformer of the Gly and Ala radicals is stabilized by resonance and the capto-dative effect and it is suspected that these factors also influence the stability of the transition state and van der Waals complexes. The γ and α conformers of the Gly transition state were of similar energy, whereas the Ala side chain strongly destabilized the α conformers of the transition state structures. This could inhibit the abstraction of hydrogen from residues other than glycine in helical peptides and proteins. Given the similarity between the structures of H_2O and $^{\bullet}$OH, the structure of the complexes found herein should be similar to the structure of these complexes in the presence of structural water.

The unfolded Gly$^{\bullet}$ and Ala$^{\bullet}$ residues can be converted to Gly and Ala by H_2O_2, since the energy of the system remains well-below the pre-$^{\bullet}$OH abstraction entrance. The conversion of Gly and Ala to the β conformer shown in this work reveals a possible mechanism for the

•OH-initiated unfolding of peptides and proteins.

Here it has also been shown how a free radical can initiate the unfolding of a helical peptide. Hydrogen atom abstraction from the C_α of residue 3 of *N*-Ac-GGGGG-NH_2 and *N*-Ac-AAAAA-NH_2 produces a radical that is stabilized by capto-dative and inductive effects, with no effects shown on the structure neighboring residues. The conformation of both Ala^3 and Gly^3 becomes more planar, however, the secondary structural elements are conserved. Hydrogen atom abstraction from the amide nitrogen eliminates the hydrogen bond with Ala^1, but not Gly^1 in the helix and the hydrogen bond within residue 3 in the extended conformation. The structural perturbations of the peptide containing the C_β radical are negligible. An increase in the length of the amide bond is shown when the C_α and amide nitrogen radicals are formed, suggestive of a decrease in bond stability, which is not observed when a radical forms at C_β.

The hydrogen abstraction reaction energies indicate that the C_α radical is the most stable, whereas the radical at the amide nitrogen is the least. The ΔG values for the transition from the 3_{10}-helix to the extended conformation indicated that the unfolding of the peptides with the C_α radical are the most favorable, followed by the those with the radical at the amide nitrogen, whereas the propensity of $A5(C_\beta)_{HEL}$ to unfold is similar to that of $A5_{HEL}$. The secondary structure of a peptide has a strong influence on the H-C_α bond, but not the H-C_β, nor the N-H, which can protect the protein from radical-initiated hydrogen abstraction. Hydrogen abstraction by •OH radical is the most favorable of the ROS studied, followed by HO_2• and O_2•$^-$.

The unfolding of the pentapeptides shown in the quantum chemical calculations was also shown in the MD simulations. The Ramachandran maps of the central residue of the hepta-alynyl peptide in its closed-shell and radical states were similar to the corresponding potential energy surfaces of the Ala and Ala$^{\bullet}$ diamides. These representations showed that planar conformations of the radicals were the most stable and the most abundant in the radical and distinct from the stable and abundant conformations of the closed-shell residue, which populated the more stable $_{L}$ conformations. Long-range interactions that stabilize turn structures are possible reasons for the differences shown between the representations of the radical, however future work could delineate the effect of long range interaction on peptide structures.

The thermodynamic cycles of A5 and G5 indicate that the conversion of the peptide helices to $A5_{EXT}^{\bullet}$ or $G5_{EXT}^{\bullet}$ or are exergonic, exothermic and entropically favorable. Therefore, the radical-initiated unfolding of $A5_{HEL}$ and $G5_{HEL}$ is endothermic when initiated by $^{\bullet}OH$ and terminated by a reducing agent.

This work provides new insight into the unfolding mechanism of peptides in the cellular condition known as oxidative stress.

7.0 REFERENCES

1. Falkowski, P. G. *Science* **2006**, *311*, 1724-1725.
2. Raymond, J.; Segré, D. *Science* **2006**, *311*, 1764-1767.
3. Goldfine, H. *J. Gen. Physiol.* **1965**, *49*, 253-274.
4. Cohen, S. M. *Environ. Health Perspect.* **1983**, *50*, 51-59.
5. Kobliashev, V. A. *Biochemistry (Moscow)* **2010**, *75*, 675-685.
6. Fatehi-Hassanabad, Z.; Chan, C. B.; Furman, B. L. *Eur. J. Pharmacol.* **2010**, *636*, 8-17.
7. Jenner, P. *Ann. Neurol.* **2003**, *53 (Suppl 3)*, S26-S36.
8. Barnham, K. J.; Masters, C. L.; Bush, A. I. *Nat. Rev. Drug Discov.* **2004**, *3*, 205-214.
9. Stadtman, E. R. *Free Radic. Res.* **2006**, *40*, 1250-1258.
10. Davies, K. J. A. *J. Biol. Chem.* **1987**, *262*, 9895-9901.
11. Fridovich, I. *Annu. Rev. Biochem.* **1975**, *44*, 147-159.
12. Halliwell, B.; Gutteridge, M. C. *Biochem. J.* **1984**, *219*, 1-14.
13. Spiteller, G. *Free Radic. Biol. Med.* **2006**, *41*, 362-387.
14. Dizdaroglu, M. *Mutat. Res.* **1992**, *275*, 331-342.
15. Fu, M. X.; Wells-Knecht, K. J.; Blackedge, J. A.; Lyons, T. J.; Thorpe, S. R.; Baynes, J. W. *Diabetes* **1994**, *43*, 676-683.
16. Gebicki, J. M.; Nauser, T.; Domazou, A.; Steinmann, D.; Bounds, P. L.; Koppenol, W. H. *Amino Acids* **2010**, *39*, 1131-1137.
17. Willix, R. L.; Garrison, W.M. *Radiat. Res.* **1967**, *32*, 452-462.
18. Garrison W. M.; Jayco, M. E.; Bennett, W. *Radiat. Res.* **1962**, *17*, 341-352.
19. Levine, R. L. *J. Biol. Chem.* **1983**, *258*, 11823-11827.
20. Davies, K. J. A.; Delsignore, M. E.; Lin, S. W. *J. Biol. Chem.* **1987**, *262*, 9902-9907.
21. Prütz, W. A.; Butler, J.; Land, E. J. *Int. J. Radiat. Biol.* **1983**, *44*, 183-196.
22. Schuessler, H.; Schilling, K. *Int. J. Radiat. Biol.* **1983**, *45*, 267-281.
23. Davies, K. J. A.; Delsignore, M. E. *J. Biol. Chem.* **1987**, *262*, 9908-9913.
24. Barlow, D. J.; Thornton, J. M. *J. Mol. Biol.* **1988**, *201*, 601-619.
25. Biron, Z.; Khare, S.; Samson, A. O.; Hayek, Y.; Naider, F.; Anglister, J. *Biochemistry* **2002**, *41*, 12687-12696.
26. Venkatachalam, C. M. *Biopolymers* **1968**, *6*, 1425-1436.
27. Moretto, A.; Formaggio, F.; Kaptein, B.; Broxterman, Q.B.; Wu, L.; Keiderling, T.A.; Toniolo, C. *Biopolymers* **2008**, *90*, 567-574.
28. Toniolo, C. *CRC Crit. Rev. Biochem.* **1980**, *9*, 1-44.
29. McPhalen, C. A.; Vincent, M. G.; Picot, D.; Jaonsonius, J. N.; Lesk, A. M.; Chothia, C. *J. Mol. Biol.* **1992**, *227*, 197-213.
30. Gertstein, M; Chothia, C. *J. Mol. Biol.* **1991**, *220*, 133-149.
31. Singh, Y.; Sharpe, P. C.; Hoang, H. N.; Lucke, A. J.; McDowall, A. W.; Bottomley, S. P.; Fairlie, D. P. *Chem. Eur. J.* **2011**, *17*, 151-160.
32. Armstrong, D. A.; Yu, D.; Rauk, A. *Can. J. Chem.* **1996**, *74*, 1192-1199.
33. Chass, G. A.; Sahai, M.; Law, J. M. S.; Lovas, S.; Farkas, O.; Perczel, A.; Rivail, J. L.; Czismadia, I. G. *Int. J. Quant. Chem.* **2002**, *90*, 933-968.

34. Jorgensen, W. L.; Maxwell, D. S.; Tirado-Rives, J. *J. Am. Chem. Soc.* **1996,** 118, 11225-11236.
35. Maxwell, D. S.; Tirado-Rives, J.; Jorgensen, W. L. *J. Comp. Chem.* **1995**, 16, 984-1010.
36. Kaminski, G.; Friesner, R. A.; Tirado-Rives J.; Jorgensen, W. L. *J. Phys. Chem. B* **2001**, *105*, 6474-6487.
37. Lifson, S.; Warshel, A. *J. Chem. Phys.* **1968**, *49*, 5116-5129.
38. Szőri, M.; Fittschen, C.; Csizmadia, I. G.; Viskolcz, B. *J. Chem. Theory Comput.* **2006**, *2*, 1575-1586.
39. Sousa, S. F.; Fernandes, P. A.; Ramos, M. J. *J. Phys. Chem. A* **2007**, *111*, 10439-10452.
40. Speck, E. J.; Olson, A.; Zhengshuang, S.; Kallenbach, N. R. *J. Am. Chem. Soc.* **1999**, *121*, 5571-5572.
41. Chou, P. Y.; Fasman, G. D. *J. Mol. Biol.* **1977**, *115*, 135-175.
42. Rauk, A.; Yu, D.; Armstrong, D. A. *J. Am. Chem. Soc.* **1997**, *119*, 208-217.
43. Rauk, A.; Yu, D.; Taylor, J.; Shustov, G.; Block, D.; Armstrong, D. *Biochemistry* **1999**, *39*, 9089-9096.
44. Galano, A.; Alvarez-Idaboy, J. R.; Montero, L. A.; Vivier–Bunge, A. *J. Comput. Chem.* **2001**, *22*, 1138-1153.
45. Galano, A.; Alvarez-Idaboy, J. R.; Bravo-Pérez, G.; Ruiz-Santoyo, M. E. *J. Mol. Struct. (THEOCHEM)* **2002**, *617*, 77-86.
46. Huang, M. L.; Rauk, A. *J. Phys. Org. Chem.* **2004**, *17*, 777-786.
47. Zhu, R.; Lin, M. *J. Phys. Chem. A* **2001**, *105*, 6243-6248.
48. Chersakov, A.; Jonsson, M. *J. Chem. Inf. Comput. Sci.* **2000**, *40*, 1222-1226.
49. MacInnes, I.; Walton, J. C.; Nonhebel, D. C. *J. Chem. Soc. Chem. Commun.* **1985**, 712-713.
50. Viehe, H.-G.; Janousek, Z.; Mirnyi, R; Stella, L. *Acc. Chem. Res.* **1985**, *18*, 148-154.
51. Owen, M. C.; Viskolcz, B.; Csizmadia, I. G. *J. Phys. Chem. B* **2011**, *115*, 8014-8023.
52. Owen, M. C.; Viskolcz, B.; Csizmadia, I. G. *J. Chem. Phys.* **2011**, *135*, 035101.
53. Tannor, D. J.; Marten, B.; Murphy, R.; Friesner, R. A.; Sitkoff, D.; Nicholls, A.; Ringnalda, M.; Goddard III, W. A.; Honig, B. *J. Am. Chem. Soc.* **1994**, *116*, 11875-11882.
54. Marten, B.; Kim, K.; Cortis, C.; Friesner, R. A.; Murphy, R. B.; Ringnalda, M. N.; Sitkoff, D.; Honig, B. *J. Phys. Chem.* **1996**, *100*, 11775-11788.
55. Gaussian 09. Frisch, M. J. et al. Gaussian Inc, Wallingford CT, **2009**.
56. Becke, A. D. *Phys. Rev. A*, **1988**, *38*, 3098-3100.
57. Becke, A. D. *J. Chem. Phys.* **1996**, *104*, 1040-1046.
58. Lee, C.; Yang, W.; Parr, R. G. *Phys. Rev. B* **1988**, *37*, 785-789.
59. Li, X.; Frisch, M. J. *J. Chem. Theory and Comput.* **2006**, *2*, 835-839.
60. Note that BHandHLYP means 0.5 x E_X^{HF} + 0.5 x E_X^{LSDA} + 0.5 x $E_X^{Becke88}$ + E_C^{LYP} functional.
61. Zhao, Y.; González-García, N.; Truhlar, D. G. *J. Phys. Chem. A* **2005**, *109*, 2012-2018.
62. Baboul, A. G.; Curtiss, L. A.; Redfern, P. C.; Raghavachari, K. *J. Chem. Phys.* 110,

1999, 7650-7657.
63. Cossi, M.; Rega, N.; Scalmani, G.; Barone, V. *J. Comput. Chem.* **2002**, *24*, 669-681.
64. Lu, H. -F.; Li, F. -Y.; Lin, S. H. *J. Comp. Chem.* **2007**, *28*, 783-794.
65. Wille, U. *J. Org. Chem.* **2006**, *71*, 4040-4048.
66. Szőri, M.; Abou-Abdo, T.; Fittschen, C.; Csizmadia, I. G.; Viskolcz B. *Phys. Chem. Chem. Phys.* **2007**, *9*, 1931-1940.
67. Janoscheck, R.; Rossi, M. *Int. J. Chem. Kin.* **2002**, *34*, 550-560.
68. Fiser, B.; Szőri, M.; Jójárt, B.; Izsák, R.; Viskolcz, B.; Csizmadia I. G. *J. Phys. Chem. B.* **2011**, *115*, 11269-11277.
69. Cossi, M.; Rega, N.; Scalmani, G.; Barone, V. *J. Comput. Chem.* **2002**, *24*, 669-681.
70. Bayly, C. I.; Cieplak, P.; Cornell, W. D.; and Kollman, P. A. *J. Phys. Chem.* **1993**, *97*, 10269.
71. Cornell, W. D.; Cieplak, P.; Bayly, C. I.; Kollman, P. A. *J. Am. Chem. Soc.* **1993**, *115*, 9620-9631.
72. Cieplak, P.; Cornell, W. D.; Bayly, C.; Kollman, P. A. *J. Comp. Chem.* **1995**, *16*, 1357-1377.
73. Case, D. A. et al. AMBER 8, University of California, San Francisco, **2004**.
74. Maestro, version 9.2, Schrödinger, LLC, New York, NY, **2011**.
75. Jorgensen, W. L.; Chandrasekhar, C.; Madura, J. D.; Impey, R.W.; Klein, M. L. *J. Chem. Phys.* **1983**, *79*, 926-935.
76. Martyna, G. J.; Tobias, D. J.; Klein, M. L. *J. Chem. Phys.* **1994**, *101*, 4177–4189.
77. Darden, T.; York, D.; Pedersen, L. *J. Chem. Phys.* **1993**, *98*, 10089-10092.
78. Chou, K. *Anal Biochem.* **2000**, *286*, 1-16.
79. Rauk, A.; Armstrong, D. A. Fairlie, D. P. *J. Am. Chem. Soc.* **2000**, *122*, 9761-9767.
80. Owen, M. C.; Komáromi, I.; Murphy, R. F.; Lovas, S. *J. Mol. Struct.* **2006**, *759*, 117-124.
81. Zhu, X.; Koenig, P.; Hoffmann, M.; Yethiraj, A.; Cui, Q. *J. Comput. Chem.* **2010**, *31*, 2063-2077.
82. Sekusak, S.; Sabljic, A. *Chem Phys Lett*. **1997**, *272*, 353-360.
83. Alvarez-Idaboy J. R.; Mora-Diez N.; Boyd, R. J.; Vivier-Bunge, A. *J. Am. Chem. Soc.* **2001**, *123*, 2018-2024.
84. Shaik, S. S.; Hiberty, P. C.; Lefour, J. -M.; Ohanessian G. *J. Am. Chem. Soc.* **1987**, *109*, 363-374.
85. Kollmar, H. *J. Am. Chem. Soc.* **1978**, *101*, 4832-4840.
86. Katritzky, A. R.; Soti, F. *J. Chem. Soc., Perkin Trans 1* **1974**, *1*, 1427-1432.
87. MacInnes, I.; Walton, J. C.; Nonhebel, D. C. *J. Chem. Soc., Chem. Commun.* **1985**, 712-713.
88. Bordwell, F. G.; Zhang, X. *J. Org. Chem.* **1990**, *55*, 6078-6079.
89. Stefancic, I.; Bonifacic, M.; Asmus, K.; Armstrong, D.A. *J. Phys. Chem. A* **2001**, *105*, 8681.
90. Leissmann, M. H.; Hansmann, B.; Blachly, P. G.; Francisco, J. S.; Abel, B. *J. Phys. Chem. A* **2009**, *113*, 7570.

91. Hawkins, C. L; Davies, M. J. *J. Chem. Soc., Perkin Trans.* **1998**, *2*, 2617-2622.
92. Garrison, W. M. *Chem. Rev.* **1987**, *87*, 381-398.
93. Plusquellic, D. F.; Pratt, D. W. *J. Phys. Chem. A* **2007**, *111*, 7391-7397.
94. Vystovsky, Y. B.; Bryantsev, V. S. *Int. J. Quant. Chem.* **2004**, *96*, 123-135.
95. Rauk, A. *Chem. Soc. Rev.* **2009**, *38*, 2698-2715.
96. Allsop, D.; Mayes, J.; Moore, S.; Masad, A.; Tabner, B. J. *Biochem. Soc., Perkin Trans 1* **2008**, *36*, 1293-1298.
97. Easton, C. J. *Chem. Rev.* **1997**, *97*, 53-82.
98. Sperling, J.; Elad, D. *J. Am. Chem. Soc.* **1971**, *93*, 3839-3840.
99. Elad, D.; Sinnreich, J. *J. Chem. Soc. Chem. Commun.* **1965**, 471-472.
100. Doan, H. Q.; Davis, A. C.; Francisco, J. S. *J. Phys. Chem. A* **2010**, *114*, 5342-5357.
101. Berkowitz, J.; Ellison, G. B.; Gutman, D. *J. Phys. Chem.* **1994**, *98*, 2744-2765.
102. Eakin, C. M.; Berman, A. J.; Miranker, A. D. *Nat. Struct. Mol. Biol.* **2006**, *13*, 202-208.
103. Kellogg, E. W. 3rd; Fridovich, I. *J. Biol. Chem.* **1975**, *250*, 8812-8817.
104. Viskolcz, B.; Csizmadia, I. G.; Knack Jensen, S. J.; Perczel, A. *Chem. Phys. Lett.* **2010**, *501*, 30-32.
105. Tosatto, S. C.; Battistutta R. *BMC Bioinformatics* **2007**, *8*, 155.
106. Malkov, S. N.; Zivkovic, M. V.; Beljanski, M. V.; Hall, M. B.; Zaric, S. D. *J. Mol. Model.* **2008**, *14*, 769-775.
107. Beck, D. A. C.; Alonso, D. O. V.; Inoyama, D.; Daggett, V. *Proc. Natl. Acad. Sci. U.S.A.* **2008**, *105*, 12259-12264.

8.0 ACKNOWLEDGEMENTS

I thank my supervisor, Professor Béla Viskolcz for giving me the opportunity to earn my PhD in his laboratory. I am grateful for his guidance and encouragement and providing an excellent work environment. I also thank Professor Imre Csizmadia for his guidance and for inspiring me over the course of ten years of studentship. I could not have received two better teachers as mentors, and for this I am very grateful. I also thank Professor Gregory A. Chass for his mentoring during these years.

I thank Professor István Marsi, Dr. Laszló Seres, Dr. Milán Szőri, Dr. Balázs Jójart, Dr. Szilárd Fejer, Béla Fiser, Laszló Müller, Máté Labadi and DongJin Lee for their technical expertise and for welcoming me into their research group.

I thank my past colleagues at Creighton University, Dr. Zsolt Bozsó, Dr. Atilla Borics, Dr. Krisztina Heredi-Szabó, Dr. Shawn Ahmed, Dr. Jeffrey Copps and Dr. Nicholas Palermo.

I thank my parents, Winston Owen and Joyce Owen, my brother, Marlon Owen, and the rest of my family.

I thank Benjamin Currall, Anthony Florita, Kristin Woodley, Marsha Haynes, Andrew Court, Jason Palmer, Joseph Leo, Terry Wortman, Amanda Millemon, and others whom I have not mentioned, for their friendship.

APPENDIX A – PUBLICATION LIST

Publications related to this dissertation

M. C. Owen, I. Komáromi, R. F. Murphy, S. Lovas. The conformational preference of C^{α}-centered radicals in proteins. Journal of Molecular Structure. (Theochem) 759, (2006) 117-124.

M. C. Owen, B. Viskolcz and I. G. Csizmadia. Quantum chemical analysis of the unfolding of a penta-alanyl 3_{10}-helix initiated by $HO^{\bullet}$, $HO_2^{\bullet}$ and $O_2^{-\bullet}$ J. Phys. Chem. B 115, (2011) 8014-8023

M. C. Owen, B. Viskolcz and I. G. Csizmadia Quantum chemical analysis of the unfolding of a penta-glycyl 3_{10}-helix initiated by $HO^{\bullet}$, $HO_2^{\bullet}$ and $O_2^{-\bullet}$ J. Chem. Phys. 135, (2011) 035101.

M. C. Owen, Milán Szőri, Imre G. Csizmadia and Béla Viskolcz. Conformation-Dependent $\bullet OH/H_2O_2$ Hydrogen Abstraction Reaction *Cycles of Gly and Ala Residues: A Comparative Theoretical Study.* J. Phys. Chem. B 2011 DOI: 10.1021/jp2089559.

M. C. Owen, I. Komáromi, B. Jojárt, I. G. Csizmadia and B. Viskolcz. The development of alanyl radical parameters for the OPLS-AA/L force field. J. Chem Theory Comput. (*Submitted*)

Other publications

M. C. Owen, M. Szőri, B. Jojárt, B. Viskolcz, I. G. Csizmadia. Conformational and Thermodynamic Analysis of the COXIB Scaffold Using Quantum Chemical Calculations. International Journal of Quantum Chemistry, (2011). DOI: 10.1002/qua.23049

I. Komáromi, M.C. Owen, R.F. Murphy, S. Lovas. Development of glycyl radical parameters for the OPLS-AA/L force field. Journal of Computational Chemistry 29, (2008) 1999-2009.

N.Y. Palermo, J. Csontos, M.C. Owen, R.F. Murphy, S. Lovas. Aromatic-backbone interactions in model α-helical peptides. Journal of Computational Chemistry 28, (2007) 1208-1214.

T.A. Pecora, M.C. Owen, C.N.J. Marai, D.H. Setiadi, G.A. Chass. Bridging the gap between pure science and the general public: comparison of the informational exchange for these extremities for scientific awareness. Journal of Molecular Structure. (Theochem) 666-667, (2003) 699-706.

ÖSSZEFOGLALÓ

A disszertációban azt mutatjuk meg, hogy peptidekben kialakuló szabadgyök centrum, hogyan befolyásolja a peptidek másodlagos szerkezetét, és milyen szerkezeti változásokat tud indukálni.

Annak eldöntésére, hogy a glicin pro-L hidrogénatomját lehet-e könnyebben leszakítani, mint az ugyanolyan pozícióban lévő alanin hidrogénjét, a reakció kiindulási van der Waals komplexeinek, átmeneti állapotainak és a reakció utáni van der Waals komplexeinek szerkezet és energiáit számítottuk a β_L, γ_L, γ_D, α_L és α_D konformerekre MPWKCIS1K/6-311++G(3df,2p)//BHandHLYP/6-311+G(d,p) elméleti szinten.

A helikális szerkezetek $HO^{\bullet}$, $HO_2^{\bullet}$ és $O_2^{-\bullet}$ gyökök által indukált letekeredésének (unfolding) mechanizmusát (**1. ábra**) a különböző pozíciókból történő hidrogén absztrakciós reakciók segítségével, valamint a reakciók termodinamikájának számolásával derítettük fel. Ehhez modell peptidekben a középső aminosavakból képzett C_α és amid nitrogénen kialakuló gyököket vizsgáltuk a G5 (*N*-Ac-GGGGG-NH_2), valamint a C_α, C_β és amid nitrogénen centrált gyököket az A5 (*N*-Ac-AAAAA-NH_2) esetekben a sűrűségfunkcionál elmélet felhasználásával. A potenciális energia-, standard entalpia-, standard szabadentalpia- és standard entrópiaváltozásokat a reakciók során a B3LYP /6-31G(d) és B3LYP/6-311+G(d,p) elméleti szinteken számoltuk ki a G5 és A5 peptidekre, azok 3_{10}-helikális és teljesen nyújtott struktúráin, követve az absztrakciós reakciót, mind gáz fázisban, mind pedig CPCM implicit vízmodell alkalmazásával.

Ahhoz, hogy az α szénatomon létrejövő szabad gyök hatását hosszabb peptidekben és fehérjékben lehessen szimulálni, hosszabb futási idejű molekula dinamikai (MD) számolásokat alkalmazhatunk. Az Ala-ból képződő szabad gyökre új paramétereket fejlesztettünk ki az OPLS-AA erőtérhez a kvantumkémiai és az OPLS-AA potenciálenergia-hiperfelületek különbségének minimálásával. Ezt az új paraméter készletet használtuk MD szimuláció során, hogy felderítsük az α szénatomon létrejött szabad gyök hatását a hepta-alanin peptid konformációjára. A Gly és Ala konformereiben történő szabadgyök-képződés

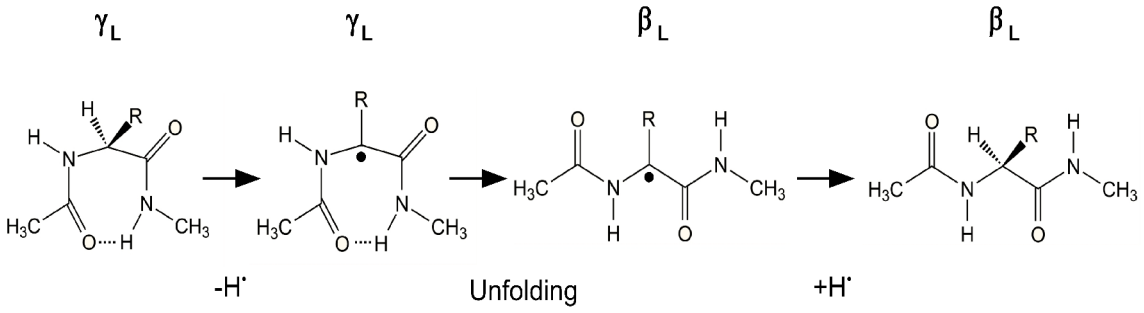

1. ábra. Egy aminosav részegységnek szabad gyök inicializált letekeredése sémája.

során jelentősen megváltozik a konformáció, és ezt a változást mindegyik aminosavegység konformereire követni lehet a legkisebb energiájú úton keresztül (kiszámolva a belső reakciókoordinátát). A H-elvonási reakciókban a Gly és az Ala β_L konformereinek átmeneti állapota (TS) rendelkezik a legkisebb relatív energiával. A TS-ekben az Ala oldallánca jelentősen destabilizálja az α konformereket a γ konformerekhez képest. Lényeges különbség az Ala-tól, hogy a Gly esetében az α és γ konformerek H-elvonási reakcióinak aktiválási energiája nem különbözik jelentősen. Ez a szerkezeti hatás gátolja a fehérjék hélixeiben a királis aminosavakból történő hidrogénelvonási reakciót. A gyökképződést követő H-elvonás átmeneti állapota a H_2O_2 és Ala$^{\bullet}$, ill. Gly$^{\bullet}$ reakciójában is mintegy 90 kJ mol^{-1}-lal alacsonyabban fekszik, a kezdeti lépéshez viszonyítva. Ez azt sugallja, hogy a hidoxil gyök képes $\alpha \rightarrow \beta$ átmenetet okozni egy aminosav szekvenciában, miután a peptidgyök pl. a H_2O_2 segítségével normál peptiddé alakul vissza.

A G5 és A5 pentapeptidek esetén megmutattuk, hogy a H-elvonási reakció az α-szénatomon a legkedvezőbb, majd a β-szénatomon, és utána az amid nitrogénen. A H-C_α kötés disszociációs energiájára nagy hatással van a peptid másodlagos szerkezete, de ez a hatás nem figyelhető meg a H-CH_2 és H-N kötések esetén. A HO$^{\bullet}$ gyök a legerősebb hidrogénelvonó ágens, ezt követi a $HO_2^{\bullet}$ és végül az $O_2^{-\bullet}$. Másodlagos szerkezeti elemek, mint például a hidrogénhidak a 3_{10}-hélixben, védelmet nyújtanak a gyökökkel szemben, gátolva a kialakuló elektron-delokalizációt az α-szénatomon. Ezzel szemben a nyújtott szerkezet a

gyökcentrum és a szomszédos peptidkötések delokalizációját segít elő. Az α-szénatomon létrejött szabad gyökök jelentősen elősegítik a pentapeptidek letekeredését a zárt elektronszerkezetű pentapeptidekkel szemben. Megmutattuk, hogy csak a HO• képes a pentapeptidek nyújtott szerkezetté történő letekeredését inicializálni, és az α-szénatomon létrejött szabad gyökök miatt könnyebben letekeredik a G5 mint az A5.

Az újonnan kifejlesztett OPLS-AA torziós paraméterek jó egyezést mutattak az LMP2-CCpVTZ(-f) hiperfelülettel, míg a kovalens kötés paraméterei elhanyagolható mértékben változtak az illesztés során. Az új paraméterezéssel végzett MD szimulációk azt mutatták, hogy az α-szénatomon levő gyökcentrumot tartalmazó aminosav (Alr) a nyújtott konformációt kedveli, és ezek a konformációk megnövelik a γ-, α- és π-turn-ok (kanyarok) számát, attól függően, hogy a szabad gyök melyik aminosavon található. A magasabb rendű struktúrákat destabilizálja az Alr gyök jelenléte, kivéve, amikor ez az aminosav a 3_{10}-hélix "i + 1"-edik pozíciójában található.

Eredményeink egy új értelmezést adnak a fehérjék hibás felcsavarodási mechanizmusára, amiket a fehérjék részegységeinek α-szénatomról történő hidrogénelvonása idéz elő.